Structure Functions and Final-State Properties in Deeply Inelastic electron-proton Scattering

Hamid Kharraziha

Department of Theoretical Physics
Lund University
Sweden

1997

Structure Functions and Final-State Properties in Deeply Inelastic electron-proton Scattering

Hamid Kharraziha

Department of Theoretical Physics
Lund University, Sweden

Thesis for the degree of Doctor of Philosophy

Thesis Advisors: Bo Andersson & Gösta Gustafson
Faculty Opponent: Yuri Dokshitzer

To be presented, with the permission of the Faculty of Mathematics and Natural Sciences of Lund University, for public criticism in the Auditorium of the Department of Theoretical Physics on Friday 23rd January 1998, at 10.15 a.m.

This thesis is based on the following publications:

I. Bo Andersson, Gösta Gustafson, Hamid Kharraziha, Jim Samuelsson,
Structure Functions and General Final State Properties in the Linked Dipole Chain Model
Zeitschrift für Physik **C 71**, 613-624 (1996).

II. Bo Andersson, Gösta Gustafson and Hamid Kharraziha,
Investigations into the BFKL Mechanism with a Running QCD Coupling
LU-TP 97-29, Submitted to *Physical Review D.*

III. Hamid Kharraziha and Leif Lönnblad,
The Linked Dipole Chain Monte Carlo
LU-TP 97-21.

IV. Hamid Kharraziha and Leif Lönnblad,
LDCMC V1.0
LU-TP 97-34, Submitted to *Computer Physics Communications.*

V. Jari Häkkinen and Hamid Kharraziha,
Colour: A Computer Program for QCD Colour Factor Calculations
Computer Physics Communications **100**, 311-321 (1997).

Introduction

The elementary particles (quarks and gluons) which build up the proton are called partons. The distributions of quarks inside the proton are measured by scattering against electrons and are dependent on the resolution of the scattering process. Knowing the parton distributions at some low resolution scale, not much smaller than the proton size, one can use the laws of Quantum Chromo Dynamics (QCD), the description of quarks and gluons, to derive the parton distributions at a higher resolution and also to evaluate the distribution of jets (hadron showers) produced in the scattering process. This works as a rigid test of QCD, by comparing with experiments, and is the topic of this thesis.

The considerations in this thesis are based on a new model, the Linked Dipole Chain model [1]. This model is based on a leading log approximation formalism developed by M. Ciafaloni, S. Catani, F. Fiorani and G. Marchesini [2] (the CCFM model). In the LDC model one separates possible parton emissions into two sets. The first set is called Initial State Bremsstrahlung and is considered in the determination of the cross-section. The initial partons form a chain of linked colour dipoles [3] from which partons of the second set, the Final State Bremsstrahlung, is emitted.

The LDC model is here used mainly for describing low-x electron-proton scattering but it can in principle also be used for hadronic photon-photon or hadron-hadron scattering. The results are both of a general qualitative type and also, with a set of corrections to the leading log approximation, of a more quantitative type for direct comparison with experiments. The specific experiment that we refer to in this thesis is conducted at the HERA storage ring at Deutsches Elektronen-SYnchrotron (DESY) where 30 GeV positrons or electrons are scattered against 820 GeV protons allowing a study of the proton at a resolution scale of a thousandth of the proton size and a momentum fraction for the probed parton of 0.00001.

In this introduction we will start with a general overview of the DIS process followed by a more technical description of the CCFM model. Finally, a brief description of the publications that this paper is based on, is provided.

1 The Inner Structure of the Proton

The proton has a size of about 10^{-15}m. It consists of three quarks, tightly bound by gluons. In addition, the proton contains a sea of virtual quarks, anti-quarks and gluons (fig. 1). The quarks and anti-quarks inside the proton can be studied by scattering with high energy electrons (or positrons) which interact through the exchange of an electro-weak gauge boson (in the following referred to as “the photon”). The two main parameters for labeling these events are

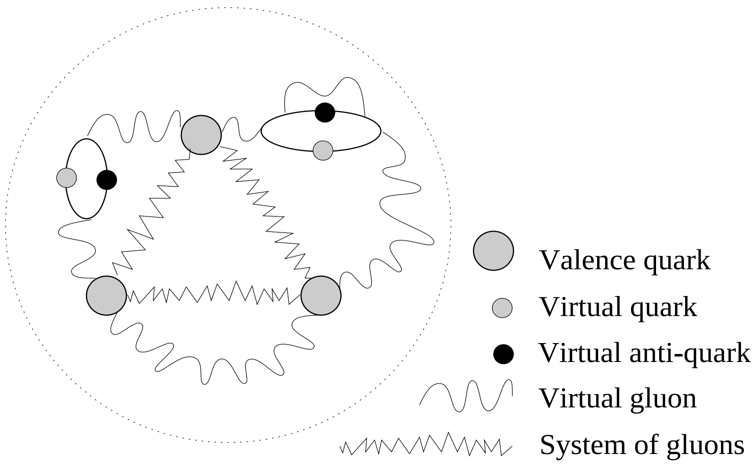

Figure 1: The inner structure of a proton.

the virtuality Q^2 of the exchanged photon and the Bjorken parameter $x \equiv \frac{Q^2}{2Pq}$, where P and q are the four-momenta of the proton and the photon, respectively.

Before the middle of the 60's there was no experimental evidence that the proton consisted of smaller particles. The proton was a solid object with a certain mass and radius (corresponding to a charge distribution) interacting with the rest of the world through all the known forces. At that time, the concept of quarks had already been introduced [4], but since no quarks had been detected (quarks do not exist as free particles), the general view was that the concept of quarks is only good for the systematization of the very many hadron species that had been observed. The first evidence for the structure of the proton was the scattering of electrons against a proton target, conducted at the Stanford Linear Accelerator Center (SLAC) in 1968 [5]. By observing the recoil of the electrons one could deduce that it did not interact with the proton as an object but was scattered against something smaller inside the proton.

To be able to distinguish a quark (from here on, "quark" can mean both quark and anti-quark) from the rest of the proton system, that is, to see that the proton is made of smaller particles, the interaction time of the electron-quark scattering must be smaller than the time it takes for the proton system to react. This means that the virtuality Q of the exchanged photon must be larger than the inverse size of the proton which is about 200 MeV. In the process, the proton is caused to disintegrate into other hadrons. This is called Deeply Inelastic Scattering (DIS) contrary to inelastic scattering, when the proton holds together but is excited to a higher energy level, or elastic scattering when the proton continues with only a change of its momentum.

2 The proton as a bag of real quarks and gluons

For moderately high virtualities, 0.5 GeV $< Q <$ 5 GeV, electron-proton DIS events are consistently described with the assumption that the proton arrives as a bag containing real quarks and gluons moving collinearly and with different fractions of the proton momenta [6, 7]. A quark inside this bag is assumed to interact directly with the electron (fig. 2) and the distribution of quarks can in this way be extracted experimentally. In this model, the momentum distribution of the partons is independent of the photon virtuality. This independence was predicted and is called Bjorken scaling [8]. The bag model worked very well in explaining the observations at SLAC and was an evidence for the validity of the quark model.

Bjorken scaling is only approximately true. Any physically real particle is surrounded by a cloud of virtual particles. These virtual fluctuations are constantly produced, they last during a time inversely proportional to the virtuality and then they recombine with the mother particle and disappear (fig. 3). When the quark and the electron interact, low-virtuality particles in the cloud around the quark may last a longer time than the collision time. In the collision, the quark changes its direction of motion and virtual particles which survive the collision do not fit into the virtual cloud of the quark anymore and are separated from it. In this way low-virtuality particles become real particles that are emitted. These particles are produced before the interaction and, since they carry momentum, the momentum of the quark is decreased prior to the collision, leading to altered conditions for the interaction. For a shorter collision time, that is for a larger virtuality of the photon, fluctuations with higher virtuality can survive. They carry more momentum and the reduction of the momentum of the quark before the collision becomes larger.

This dependence on the photon virtuality, a small disturbance of the Bjorken scaling, was experimentally observed in 1974 [9] and is called scaling violation.

A second scaling violating effect is due to the fact that the virtual cloud can contain quarks (and anti-quarks). If these quarks last long enough, they can actually interact with the electron. For larger photon virtualities, more quarks add in this way to the observed quark distribution of the proton. The first mentioned effect is important for the distribution of quarks with large momentum fractions, while this second effect is more important for low momentum fractions.

The electron is also surrounded by virtual particles but the density of particles in the cloud is lower since the electro-weak force is weaker than the strong force. Whenever a quark or a gluon inside the virtual cloud of the electron interacts directly with the proton it has a significant effect on the jets produced in the collision and makes an experimental signature for these events. These events are called photo production or boson-gluon fusion events. Conventionally they are explained by assigning parton distributions to the photon

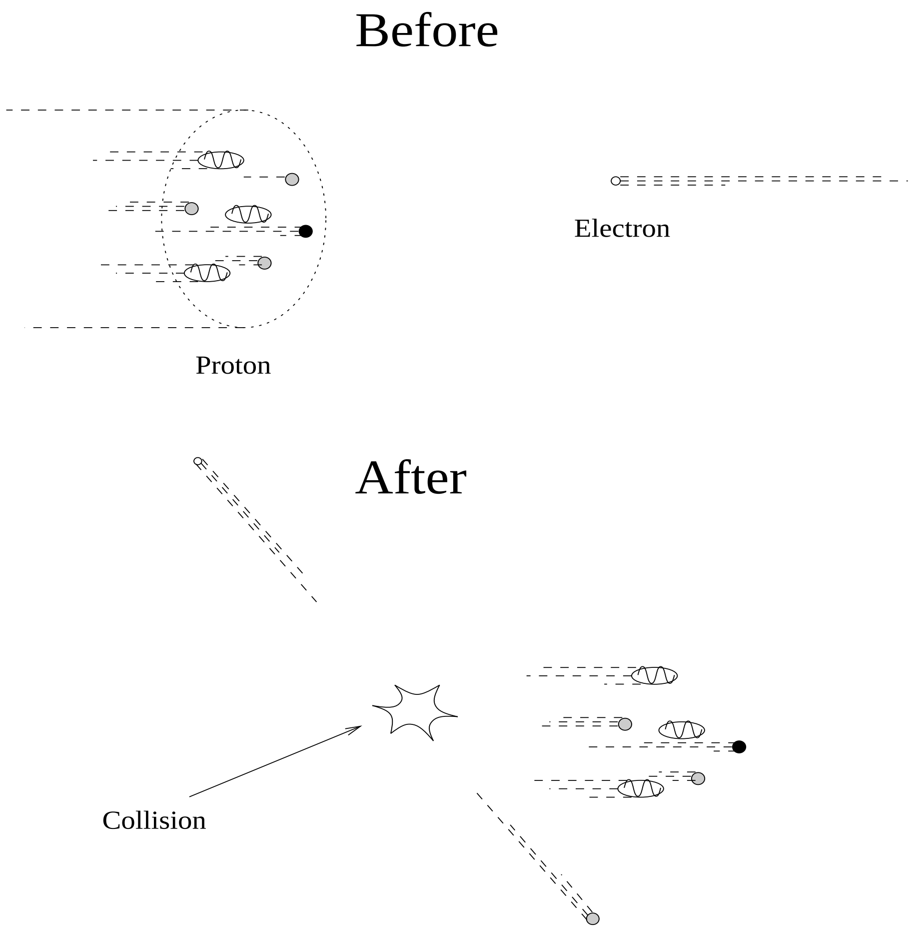

Figure 2: Electron-proton scattering according to the bag model. Note that this is a schematic picture and quark number conservation is not indicated.

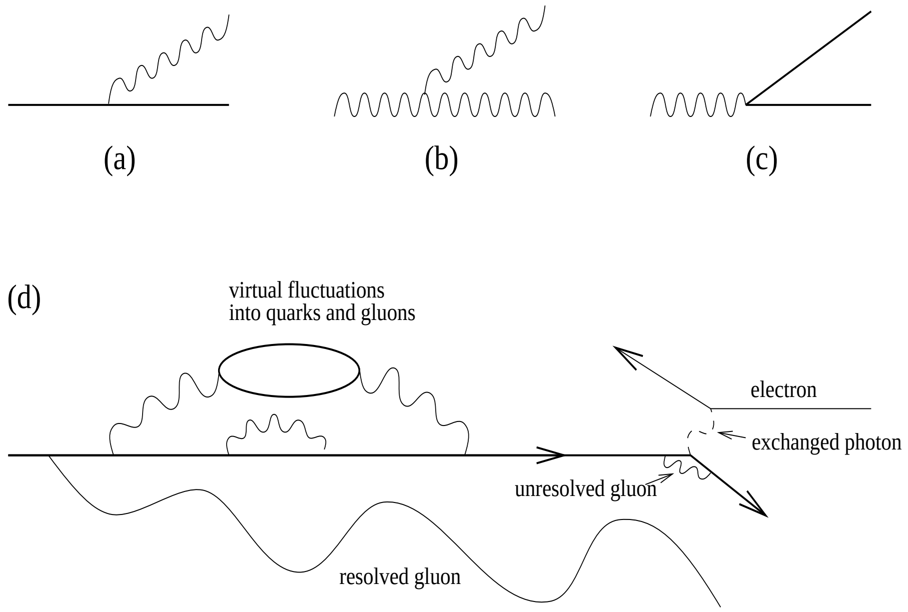

Figure 3: Virtual fluctuations: (a) A quark fluctuates into a quark and a gluon. (b) A gluon fluctuates into two gluons. (c) A gluon fluctuates into a quark and an anti-quark. (d) Virtual fluctuations around a quark prior to scattering. Fluctuations with low virtuality (long wave) survive the collision and are emitted. Fluctuations with high virtuality (short wave) are reabsorbed during the collision.

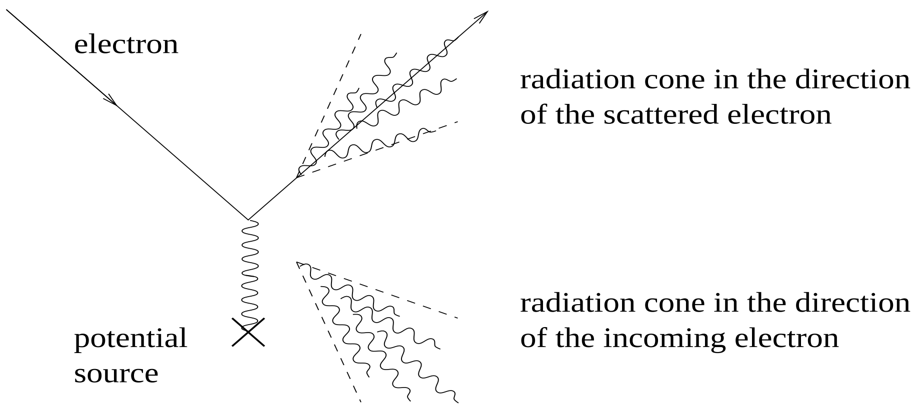

Figure 4: In the scattering process, photons are emitted inside two separate cones centered round the electron direction before and after the scattering.

and describing the scattering process as a strong scattering between one parton from each side.

3 The evolution of the scaling violation

Suppose the quark distributions inside the proton are measured by the exchange of photons with a certain virtuality. Because of the virtual fluctuations, these distributions will be different for measurements at a higher virtuality. Since more virtual particles are resolved, the proton energy is shared by more particles and the energy distribution of the quarks will be shifted to lower values.

To examine the dynamics of the scaling violation we have to take a closer look at the behaviour of the virtual cloud around particles inside the proton. Let us first examine the virtual cloud around an electron. It is a simpler system than the virtual cloud around a quark since it is to a large extent filled only with photons which are produced directly by the electron.

This examination can be done by studying the process of when an electron hit by a virtual photon is caused to radically change its direction of motion. It shakes off some of the photons from its virtual cloud (mainly photons with virtuality smaller than Q) and these photons are transformed into real particles which can be detected. After the scattering, the electron has to replace its lost companions and in this process more real photons are emitted. We get two cones of photon radiation, one centered around the electron direction before the collision and one centered around its direction after the collision (fig. 4). By studying the content of these cones, we get a picture of the virtual cloud of the electron.

The contents in these cones have been measured and it is well known that the distribution of the emitted photons is proportional to the coupling constant α_{QED} and inversely proportional to the energy and the transverse momentum $k_\perp$ relative to the cone center

$$dn_{incone} \propto \alpha_{QED} \frac{dE}{E} \frac{dk_\perp^2}{k_\perp^2}.$$

The transverse momentum corresponds roughly to the virtuality $v \equiv \sqrt{-k^2}$ of the photons in the virtual cloud. If z is the energy fraction carried by a virtual photon, the distribution of photons in the virtual cloud thus becomes

$$dn_{incloud} \propto \alpha_{QED} \frac{dz}{z} \frac{dv}{v}.$$

It is possible to understand why the number of photons with low virtuality is larger. These photons survive a longer time. Those that are present at the collision have been produced during a long time, while photons with larger virtuality that are present at the collision must have been produced a short time before the collision and do not become as large in number.

If the electron itself is in a virtual state with virtuality v', it would start to fill its virtual cloud as soon as it is created and during its life time $1/v'$. Photons with a lower virtuality than the electron survive a longer time and only a few of them recombine with the electron before it falls out of the virtual state. This means that it is the virtuality of the electron which determines their number and we can modify the previous equation to the more general form

$$dn_{incloud} \propto \alpha_{QED} \frac{dz}{z} \frac{dv}{\max(v, v')}.$$

A quark fills its virtual cloud mainly by producing gluons in the same way as the electron produces photons with the difference that the rate is now given by the strong coupling constant α_s. Gluons inside the proton fill their virtual cloud also mainly by producing gluons. They are produced with the same momentum distribution as for quarks producing gluons but roughly with the double rate since gluons are doubly (strongly) charged. They can also split into a virtual quark and anti-quark pair. The splitting process has a lower rate but is important since it is in this way the number of quarks inside the proton is increased.

There is a lower limit $\Lambda \sim 200$ MeV, set by the proton size, on the virtuality of a fluctuation inside the proton. If the virtual particle can not resolve the inner structure of the proton, the strong charge of the emitter is screened by the rest of the proton since the proton in itself is strongly neutral. The distribution of primary (directly) produced virtual gluons from a gluon or a quark can finally be written

$$dn \propto \alpha_s \frac{dz}{z} \frac{dv}{\max(v, v')} \theta(v - \Lambda). \tag{1}$$

The primary produced gluons are only one part of the virtual particles around a gluon or a quark. These gluons can in turn fill the virtual cloud by producing more (secondary) virtual gluons or quarks which in turn can produce more virtual particles and so on. To give a full description of the virtual cloud, we must take all these possibilities into account.

In each step, the new parton must have a shorter life time than its mother parton. This is fulfilled if it has a larger virtuality

$$v > v'.$$

Since the mother parton has more momentum and is a faster moving particle (in a frame where all particles are moving in the same direction) it is slowed down by time dilation with a relative factor $\gamma'/\gamma = v/zv'$. This modifies the ordering condition, which becomes

$$v^2 > zv'^2. \tag{2}$$

In the electron-proton scattering process, where a photon with high virtuality is exchanged, the distribution of quarks that can absorb this photon can be determined by fixing the parton contents at a lower virtuality, and by considering emissions that are visible at the higher virtuality. Formally, the distribution in eq. (1) must be repeatedly integrated in a kinematical region given by the ordering condition in eq. (2) and the result must be convoluted with the parton distributions measured at the lower virtuality. This leads roughly to the evolution equations of the LDC model.

4 The CCFM model

We will here briefly mention some of the ideas behind the CCFM model and state their results.

The method that is used is called soft gluon insertion [10]. By recursively adding a softer (with lower energy) gluon in multi gluon emissions, the distribution of each new emission is approximately determined by an eikonal[1] current J_{eik} stemming from all the harder gluons. The result factorizes between the emissions and is equivalent to classical Bremsstrahlung under certain angular ordering conditions. In low-x DIS where the probed gluon has a momentum fraction x, this approximation is not valid since the inserted gluons are harder

[1] In the triple gluon vertex there is a term which has a similar spin structure as for gluon emission from a quark. This term corresponds to an eikonal emission and gives large contributions for low energies of the emitted gluon.

than the probed one. Therefore non-eikonal emissions are important and the current has to be complemented with a non-eikonal current J_{ne}.

The virtual corrections are determined by the same method. Virtual loops with two eikonal vertices lead to Sudakov form factors which cancel the soft divergence of the gluon splitting function. Virtual loops with one non-eikonal and one eikonal vertex lead to form factors which are referred to as non-Sudakov form factors. This second virtual effect cancels the collinear divergences.

From the possible emissions in a DIS process a subset R is singled out by the requirement that the emitted gluon is not followed in angle (or rapidity) by a harder gluon. Let q_i be the momentum of the i:th (in angle) gluon in R and $y_i = 1 - z_i$ be its energy fraction. By integrating over all possible emissions between q_i and q_{i+1} one gets for the emissions in R a factorized weight distribution given by

$$dw_i = \bar{\alpha} \frac{dq_{\perp i}^2}{q_{\perp i}^2} \frac{dz_i}{z_i} \Delta_{ne} \left(z_i, \vec{k}_{\perp i}, \vec{q}_{\perp i} \right), \tag{3}$$

where $\bar{\alpha} = 3\alpha_s/\pi$, $\vec{q}_{\perp i}$ is the i:th transverse momentum vector, $\vec{k}_{\perp i} \equiv -\sum_1^i \vec{q}_{\perp j}$ and

$$\Delta_{ne} \left(z, \vec{k}_\perp, \vec{q}_\perp \right) = \exp \left[-\bar{\alpha} \log \left(\frac{1}{z} \right) \log \left(\frac{k_\perp^2}{z q_\perp^2} \right) \right]$$

is the remaining form factor referred to as the non-eikonal form factor. A further result is that emissions between q_i and q_{i+1} with a higher transverse momentum than $k_{\perp i}$ are cancelled by virtual emissions.

5 The Papers

The first four papers in this thesis deal with the Linked Dipole Chain model. Papers I and II present some general results of DIS within the leading log approximation. In paper III we describe how the LDC model is developed for achieving quantitative predictions of structure functions and final-state properties in electron-proton DIS and present some results which are compared to data. Paper IV presents a Monte Carlo event generator based on the considerations in Paper III.

The last paper presents a computer program for calculating QCD colour factors.

Paper I

Some qualitative results for the structure function and final-state properties in DIS are presented, using the LDC model. Numerical results are obtained by two different implementations, one integration of MC type and one which is based on a discrete model.

It is found that the LDC model interpolates between DGLAP [7, 11] and BFKL [12] in a smooth way. The emissions along the rapidity axis can be separated into two phases: For rapidities closest to the proton direction there is a steady BFKL-like motion with constant transverse energy flow, but, at a certain distance from the photon end, the transverse momentum of the emissions begins to increase up to the photon virtuality Q^2, as predicted by DGLAP.

For the structure function, a DGLAP behaviour ($e^{const\sqrt{-\log x}}$) is noted for moderate values of x, but for small x-values it has the BFKL $x^{-\lambda}$ behaviour. This is further illustrated by using an approximate formula for the structure function which explicitly interpolates between DGLAP and BFKL.

Using the generality of the LDC model, the relative contribution of different kinds of low-x electron-proton events (normal DIS, boson-gluon fusion, resolved photon) to the cross section, and the dependence on the values of x and Q^2, is evaluated.

Paper II

In this paper, the BFKL mechanism with a running coupling constant is further analyzed and solutions are presented. With a running coupling, the transverse momentum fluctuation ($k_\perp$) along the emission chain is expected to have an exponential fall-off in the variable $\kappa \equiv \log k_\perp$, contrary to a former prediction for a constant coupling that it is Gaussian. Following the argument of a Brownian motion which results in a Gaussian fall-off, it is argued that, with a running coupling, the process resembles a Brownian motion in a gravitational field. This is illustrated with a simple model.

It is found that the evolution equation of the LDC model leads, for the κ dependence of the structure function, to equations similar to the radial part of the hydrogen atom Shrödinger equation. The $x^{-\lambda}$ behaviour of the structure function is confirmed and λ is evaluated by various analytical and numerical methods. It is found that the value of λ significantly depends on the cut-off parameter of the soft region κ_{cut} (but $\lambda \sim 0.5$ in a wide range of κ_{cut}) and also on the hard $z > 0.5$ part of the splitting function, a part which is usually neglected in the leading log approximation.

Paper III

To achieve results which are quantitatively comparable with data, one must include sub-leading effects into the LDC model. This is important particularly for quark parton distributions which are probed in electron-proton scattering. The main steps are to include sub-leading terms of the splitting functions, to conserve energy and to convolute with proton parton distributions at low virtuality. For a description of the final-state properties, final-state emissions are added and a suitable hadronization procedure is used. For many of these corrections no prescription is given by the CCFM model, so other physical arguments, applicable in this field, are used.

The first step is to use the LDC model evolution to fit input parton distributions to the measured structure functions. A crude fit has been done with only four free parameters for the input parton distributions. The result for the fit is quite acceptable and the effect of some of the assumptions on the form of the input parton distributions is shown to be small both for the structure function and for the final-state properties.

For the final-state emissions, the dipole model [3] is used through a modified version of the Ariadne MC [13]. For the hadronization, the Lund fragmentation model [14] is used as implemented in the Jetset MC [15]. The results for the final-state properties are compared with data and reasonable agreement is found. The effect of some of the assumptions for the sub-leading corrections is shown.

Paper IV

The Monte Carlo event generator which is developed in paper III is presented.

Paper V

A computer program for calculating QCD colour factors is presented. A very simple method, based on a work by Cvitanović [16], is used, resulting in a program which is economic both in CPU-time and memory. Also, some colour space projection operators are given as a tool for solving different kinds of multiplicity problems in QCD (or any SU(N) theory).

Acknowledgments

I thank all people at the department for some wonderful times, I thank my supervisors Bo Andersson and Gösta Gustafson for the insight into the world of particles and fenomenology, I thank my co-worker Leif Lönnblad for his commitment to finish our joint work in time, I thank Anders Irbäck, Torbjörn Sjöstrand, Bo Söderberg and others for their patience and help with my strange questions through these years, I thank Jari Häkkinen, Markus Ringnér and Torbjörn Sjöstrand for proof reading the introduction and I apologize to my dear Annika for not giving her as much attention as she deserves, during the time I was completing this thesis.

References

[1] B. Andersson, G. Gustafson, J. Samuelsson, *Nucl. Phys.* **B463** (1996) 217.

[2] M. Ciafaloni, *Nucl. Phys.* **B296** (1988) 49;
S. Catani, F. Fiorani and G. Marchesini, *Phys. Lett.* **B234** (1990) 339, *Nucl. Phys.* **B336** (1990) 18.

[3] G. Gustafson, *Phys. Lett.* **B 175** (1986) 453;
G. Gustafson, U. Petterson, *Nucl. Phys. B* **306** (1988) 746;
B. Andersson, G. Gustafson, L. Lönnblad, *Nucl. Phys.* **B 339** (1990) 393.

[4] M. Gell-Mann, *Phys. Lett.* **13** (1964) 598

[5] E.D. Bloom *et al. Phys. Rev. Lett.* **23** (1969) 930, M. Breidenbach *et al. Phys. Rev. Lett.* **23** (1969) 935.

[6] R.P. Feynman, in *High Energy Collisions*, Proceedings of the Third International Conference, Stony Brook, New York, edited by C.N. Yang *et al.* (Gordon and Breach, New York, 1969).

[7] V.N. Gribov and L.N. Lipatov, *Sov. J. Nucl. Phys.* **15** (1972) 438 and 675.

[8] J.D. Bjorken,*Phys. Rev.* **179** (1969) 1547.

[9] E.M. Riordan *et al. Phys. Lett.* **B52** (1974) 249.

[10] A. Bassetto, M. Chiafaloni and G. Marchesini, *Phys. Rep.* **100** (1983) 1.

[11] G. Altarelli, G. Parisi, *Nucl. Phys.* **B 126** (1977) 298;
Yu.L. Dokshitzer, *Sov. Phys. JETP* **46** (1977) 641.

[12] E.A. Kuraev, L.N. Lipatov and V.S. Fadin, *Zh. Eksp. Teor. Fiz.* **72**, 373 (1977) [*Sov. Phys. JETP* **45**, 199 (1977)];
Ya.Ya. Balitsky and L.N. Lipatov, *Yad. Fiz.* **28**, 1597 (1978) [*Sov. J. Nucl. Phys.* **28**, 822 (1978)]

[13] L. Lönnblad, *Comp. Phys. Comm.* **71** (1992) 15.

[14] B. Andersson, G. Gustafson, G. Ingelman and T. Sjöstrand, *Phys. Rep.* **97** (1983) 31.

[15] T. Sjöstrand, *Comp. Phys. Comm.* **82** (1994) 74.

[16] P. Cvitanović, Group Theory, Nordita Classics Illustrated, 1984

Paper I

LU TP 95-34
December 1995

Structure Functions and General Final State Properties in the Linked Dipole Chain Model

B. Andersson [1], G. Gustafson [2], H. Kharraziha[3], J. Samuelsson [4]

Department of Theoretical Physics
Lund University
Sölvegatan 14A
S-223 62 Lund, Sweden

Zeitschrift für Physik **C 71**, 613-624 (1996)

Abstract

We have in an earlier paper, [1], presented a generalization, the Linked Dipole Chain Model LDC, of the model developed by Ciafaloni-Catani-Fiorani-Marchesini, [2], to describe the structure functions and the states in Deep Inelastic Scattering events. In this paper we would like to present an investigation of a set of general features of the LDC Model, viz the behaviour of the structure functions (we will show how the result interpolates in a precise way in between the well-known DGLAP and BFKL approaches), the average bremsstrahlung emission in the states and finally a partitioning of the structure functions into three different channels: the "ordinary" parton-probe events, where all bremsstrahlung emissions are below the probe Q^2, the boson-gluon fusion events where the last splitting of the parton chains contain transverse momentum above Q^2, and the resolved Rutherford scattering events between the probe and the hadron (where the largest transverse momentum occur somewhere along the emission lines away from the ends).

[1] bo@thep.lu.se (internet)
[2] gosta@thep.lu.se(internet)
[3] hamid@thep.lu.se (internet)
[4] jim@thep.lu.se (internet)

1 Introduction

A major problem in Deep Inelastic Scattering (DIS) is to calculate the flux-factors of the available partons, ie the structure functions of the participating hadron. In a perturbative treatment of QCD this means the summation over a large amount of Feynman graphs relating the constituents, which occur on a certain "initial" scale, to those of the "final" scale, determined by the properties of the probe.

It is not necessary to know all the radiation in the states in order to be able to calculate (this change in) the flux factors. It is perfectly feasible to subdivide the emissions into two sets, "the main emissions", which we conventionally will refer to as the Initial State Bremsstrahlung (ISB) set, and "the remainder" (the Final State Bremsstrahlung, FSB), which is possible to emit in case the ISB is already provided. (In the calculations of the cross-sections the FSB is treated as the contributions from the radiative corrections to the main ISB emissions).

It is possible to make any choice of the ISB set for a particular configuration as long as the FSB can be emitted from this set *in accordance with the coherence conditions of QCD*. (It is, of course, useful to chose the ISB so that the later FSB emissions do not disturb the original configurations very much by recoils and kinematics). For a particular choice of the ISB it is, however, necessary to calculate the corresponding radiative corrections to these real emissions. In the perturbative QCD cascades the results of such calculations exponentiate (at least for the leading contributions, eg in the Leading Log Approximation,LLA) and are known as the corresponding Sudakov factors. It should be recognized, however, that if one changes the ISB set, eg by including some of the "earlier" ISB gluons into the FSB set, then it is also necessary to change the corresponding radiative corrections.

The Sudakov factors obtained by the exponentiation of the radiative corrections can often be interpreted in a probabilistic language. Then they correspond to the probability to not emit anything inside the phase space regions where it should have been dynamically allowed. The perturbative QCD cascades are in general formulated as stochastical processes. There is then an (inclusive) density of emissions in phase space dn, which will lead to an inclusive probability $d\mathcal{P}$ to emit a particular set of partons (the coherence conditions in the QCD radiation are taken into account by introducing an ordering of the process). The semi-inclusive probability to emit just those partons and to emit nothing inside the remaining region, Ω, (allowed by coherence, ie the ordering, and energy-momentum conservation) is then given by the formula

$$d\mathcal{P}\exp(-\int_{\Omega} dn) \tag{1}$$

The exponential factor is just the Sudakov factor, whether it is obtained by calculating the radiative corrections or by general probability arguments. The main point is, of course, that the radiative corrections to a given process often contains the same (inclusive) emission density dn as the "real" emissions.

In conclusion, although the inclusive emission density is the same at any bremsstrahlung vertex, it is necessary to "correct" with the proper Sudakov, depending upon the choice of the ISB gluons. In this way the resulting sum over all the contributions corresponding to the structure functions will be the same.

In an earlier paper, [1], we have presented a generalization and simplification of the model for the states in DIS, which has been developed by Ciafaloni, Catani, Marchesini and Fiorani (the CCFM Model), [2]. In the Linked Dipole Chain (LDC) Model there is a (small) change in the choice of the ISB set of gluons, as compared to the CCFM Model. While the set chosen in the CCFM Model can be described as the most general one possible, if one includes the QCD coherence conditions ("angular ordering") and request energy-momentum conservation at each emission vertex, the set chosen in the LDC Model is restricted to a (large) subset. The emissions which are in this way excluded from the initial state radiation, are instead included in the final state radiation.

In this way we obtain in the LDC Model that, [1]

I The Final State Bremsstrahlung (FSB) can be treated as the emission from a set of color dipoles, spanned by the chosen gluons in the ISB set. Therefore the FSB can be treated directly by means of the Lund Dipole Cascade Model (the DCM), which is implemented in the Monte Carlo simulation program ARIADNE, [3].

II The probabilities (in particular the radiative corrections) for the ISB set of states chosen in the LDC Model are simpler than the results for the CCFM Model. The stochastical process obtained is further explicitly "local" (Markovian) and symmetric with respect to emissions from the hadron end and the probe end. In this way the predictions of the LDC can be easily implemented into Monte Carlo simulation programs to study the particular ISB sets of the model.

III It is possible to incorporate into the formalism both the "ordinary" (perturbative) QCD parton interactions, the Boson-Gluon Fusion interactions and also the resolved (virtual) probe structure functions, including Rutherford interactions between the probe- and the hadron-ends. There is consequently in the LDC no cutoff (besides energy-momentum conservation) necessary for large transverse momenta in the ISB gluon emissions, at the same time as the gluonic bremsstrahlung in a well-defined way also cuts off small transverse momentum (Rutherford) scatterings.

Consequently the LDC Model and the DCM constitute a general method to treat all perturbative QCD interactions along the same lines, in terms of color dipole emissions. This approach directly fits into the final state hadronization model, ie the Lund String Fragmentation Model (as implemented in the Monte Carlo simulation program JETSET, [4])

Both the LDC and the CCFM models interpolate betwen the DGLAP (Dokshitzer-Gribov-Lipatov-Altarelli-Parisi) mechanism, which is relevant for large Q^2- and medium to small x_B-values and the BFKL (Balitsky-Fadin-Kuraev-Lipatov) mechanism, expected to be valid for medium Q^2 and very small x_B. We consider some properties of the models in section 2.

The intention of this note is to present some general results from the LDC Model. We are interested in the qualitative properties of the cascade, and therefore we restrict our study to a purely gluonic cascade without quarks, and we neglect nonsingular terms in the splitting function $P(z)$. We do however study the different results obtained for both a fixed and a running coupling α_s, for which significant differences are obtained. In subsection 4.1 we investigate the following properties by means of two calculational methods (the methods are presented in section 3 and correspond to different approaches to the basic equations):

A The behaviour of the structure functions for different (x_B, Q^2) (to be precise we treat emission from an incoming gluon at $x_{B0} = 1$ at a (small) initial virtuality Q_0^2 up to the probe at (x_B, Q^2); the methods will be extended to the other possible emission processes in future publications). We consider parametrizations of both the DGLAP type, $\propto \exp C\sqrt{\log(1/x_B)}$, and of the BFKL type $\propto x^{-\lambda}$ with C and λ possibly Q^2 dependent.

B The average "road" in the available phase space from (x_{B0}, Q_0^2) to (x_B, Q^2), together with the regions containing roads at most one standard deviation from the mean. At the same time we consider the density of the ISB gluon emission along the roads. We find that besides a small region "in the beginning" (about $3-4$ units in rapidity or $\log(1/x)$), which depends upon the starting-out conditions for the "undisturbed" hadronic wave-function constituents, there is a region in which the main road stays close to small $k_\perp$. Finally there is a region with a size depending upon the value of Q^2, ie the properties of the probe. The latter two regions correspond to contributions expected from a BFKL and a DGLAP treatment of the structure functions, respectively. The larger the total $\log(1/x)$ region is for a given $\log(Q^2)$ the more BFKL and vice versa for the DGLAP mechanism.

Using our findings from A. and B. we present a new general parametrization of the structure functions for small x-values, which in a well-defined way interpolates between the DGLAP and BFKL contributions.

C The contributions to the structure functions from the different channels mentioned above for different (x_B, Q^2). In particular we investigate in some detail the regions where the DGLAP mechanism dominates, where the Boson-Gluon Fusion will provide essential contributions and where the (virtual) probe-hadron interactions contains large Rutherford contributions. In this way we exhibit the regions inside which a cut-off in the ISB gluon transverse momenta, $q_\perp^2$, by eg $q_\perp^2 < Q^2$ will be dangerous according to the LDC.

2 The LDC and the CCFM Models

2.1 Some properties of the CCFM Model

In order to describe the choice of the ISB set of gluon emissions in the CCFM Model we consider the fan diagram shown in Fig 1. This does not correspond to a single Feynman diagram but rather to a collection of such diagrams.

Along the main line from the incoming parton, denoted by the energy-momentum vector P, to the probe, with the vector $q = P_{probe}$, there is a set of initial state emissions called (q_j). Besides these gluons there is another set called (C_j) (the corresponding FSB) of emissions "in between" the q_j and q_{j+1}. There is further a set of "connector vectors", (k_j), between the q_j-emissions. Energy-momentum conservation is imposed for each q_j-emission (justified by chosing the q_j as more "energetic", cf below, than the C_j-gluons):

$$k_j = P - \sum_{m=1}^{j} q_m \quad \text{ie} \quad k_j = k_{j-1} - q_j \tag{2}$$

All emissions are ordered in rapidity which (due to the relation between angle and rapidity) means *angular ordering* along the chain. The CCFM then pick the ISB (q_j) set from the set of all emissions as those which are not followed (in the rapidity ordering variable) by another one with a larger lightcone energy-momentum $q_+ (= q_0 + q_\ell)$, ie in this way the q_j has larger "energy" than the rest. (We will later specify the meaning of the "longitudinal", ℓ, direction).

To be more precise we introduce the variables $(z_j, \vec{q}_{\perp j})$ with $k_{+j} = z_j k_{+(j-1)}$ and $\vec{k}_{\perp j} = \vec{k}_{\perp (j-1)} - \vec{q}_{\perp j}$. In the LLA the CCFM choice for the q_+ will imply $q_{+j} \ll q_{+(j-1)}$ which corresponds to an approximation of the splitting function $P(z) \simeq 1/z$ and the assumption that z is small enough so that $(1-z) \simeq 1$. Further the gluons in the sets (C_j) are in accordance with the LLA treated as soft enough so that the q-vectors can be taken on-shell and massless.

The corresponding propagator vectors k_j are, however, spacelike with the values $k_{+(j-1)} = q_{+j}/(1-z_j) \simeq q_{+j}$. The transverse momentum of the propagators $k_{\perp j}$ are dominated by the $q_\perp$-emissions in the neighbourhood (for a

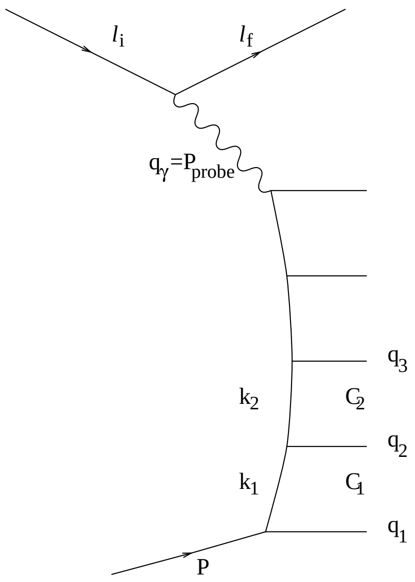

Figure 1: *A DIS fan diagram*

detailed discussion cf Ref [1]). One major kinematical constraint is that

$$k_{\perp j}^2 > z_j q_{\perp j}^2 \tag{3}$$

If this condition is not fulfilled then the "virtuality" of the propagator will in the LLA fulfil $|k^2| \gg k_\perp^2$, which implies strong suppression. Each step in the emission chain will in the CCFM Model be described by the weight

$$\bar{\alpha} \frac{dz_j}{z_j} \frac{dq_{\perp j}^2}{q_{\perp j}^2} \Delta_{ne}(z_j, k_{\perp j}, q_{\perp j}) \tag{4}$$

Here $\bar{\alpha} = 3\alpha_s/\pi$ is the effective coupling (including color factors) and Δ_{ne} is the so-called "non-eikonal formfactor" with

$$\Delta_{ne}(z_j, k_{\perp j}, q_{\perp j}) = \exp(-\bar{\alpha} \log(1/z_j) \log(k_{\perp j}^2 / z_j q_{\perp j}^2)) \tag{5}$$

The major result in the CCFM Model is this non-eikonal formfactor, corresponding to the radiative corrections for the choice of the ISB set defined above. We note in particular that due to the properties of the non-eikonal formfactor small values of z_j and $q_{\perp j}$ in Eq (4) are effectively cut-off in case we assume $k_\perp$ is finite.

2.2 The Properties of the LDC Model

In Ref [1] the results in Eqs (4) and (5) are analysed and reformulated. It is shown that the non-eikonal formfactor actually can be considered as an "ordinary" Sudakov formfactor, in the probability sense we described in section 1. The negative exponent is besides the $\bar{\alpha}$-factor a region excluded for gluon emission by the particular choice of the ISB $\{q_j\}$ in the CCFM Model.

In the LDC Model there is a restriction of the (q_j) states such that those gluons for which $q_{\perp j} < \min(k_{\perp j}, k_{\perp (j-1)})$ are included in the final state emission. This means that the remaining gluons satisfy the relation

$$q_{\perp j} \approx \max(k_{\perp j}, k_{\perp (j-1)}) \tag{6}$$

In this way we obtain in the LDC *that the weights in the q_j emissions are given by Eq (4) but with the non-eikonal formfactor Δ_{ne} exchanged for* 1. What is shown in Ref [1] is that *if we include into the FSB the gluons which in the CCFM belong to the IBS-set, but do not fulfil Eq (6), then the sum over the states containing such gluons, with the appropriate non-eikonal weights, will provide just the factor* 1.

This evidently corresponds to a major simplification and the weight in the LDC can be written solely in terms of the connectors (k_j). Integrating over the angle between $\vec{k}_{\perp j}$ and $\vec{k}_{\perp (j-1)}$ we obtain
(remember that $\vec{q}_{\perp j} = \vec{k}_{\perp (j-1)} - \vec{k}_{\perp j}$)

$$\int \frac{d\phi dk_{\perp j}^2}{q_{\perp j}^2} = \frac{dk_{\perp j}^2}{\max(k_{\perp j}^2, k_{\perp (j-1)}^2)} \cdot h(k_{\perp j}^2 / k_{\perp (j-1)}^2) \tag{7}$$

where the function $h(a)$ is given by

$$\left\{ \begin{array}{l} h(a) = \frac{1}{1-a}\left[1 - \frac{2}{\pi} arctan\left(\frac{1+\sqrt{a}}{1-\sqrt{a}}\sqrt{\frac{2\sqrt{a}-1}{2\sqrt{a}+1}}\right)\theta(a-\frac{1}{4})\right] \quad ; 0 < a < 1 \\ h(a) = h(1/a) \end{array} \right. \tag{8}$$

In leading approximation $\log(k_{\perp j}^2 / k_{\perp (j-1)}^2)$ is not close to 0, and we have $h \approx 1$ which implies

$$\bar{\alpha}\frac{dz_j}{z_j}\int \frac{d\phi}{2\pi}\frac{dk_{\perp j}^2}{q_{\perp j}^2} \approx \left\{ \begin{array}{ll} \bar{\alpha} d\ln(1/z_j) d\kappa_j & \text{if } \kappa_j > \kappa_{j-1} \\ \bar{\alpha} d\ln(1/z_j) d\kappa_j \exp(\kappa_j - \kappa_{j-1}) & \text{otherwise} \end{array} \right. \tag{9}$$

(the last factor stems from the requirement in Eq (6) and obviously corresponds to a "local" statement, ie a comparison of the sizes of two neighboring connector vectors).

Before we continue we will make a few comments on the time-like dipole cascades. We note that for a dipole bremsstrahlung emission (from eg a gluon-gluon (g_0, g_0') state) of a gluon g_1 with transverse momentum $q_{\perp 1}$ and rapidity

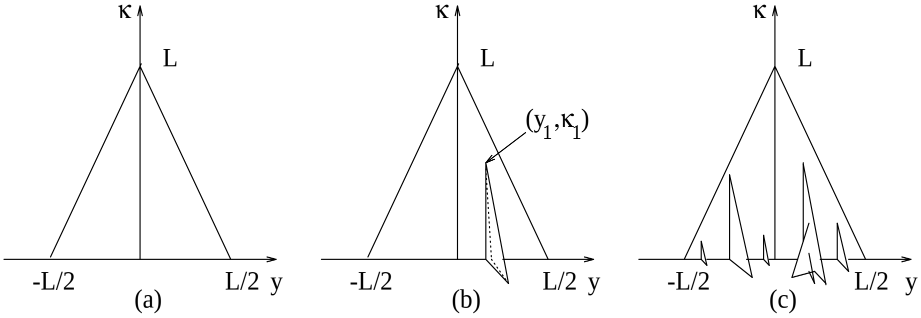

Figure 2: *The phase-space available for gluon emission from a dipole is a triangle in the (y, κ)-plane (a); in case one gluon is emitted at (y_1, κ_1) then the phase-space for a second (softer) gluon is the the area of the folded surface (below kappa$_1$) (b); each emitted gluon increases the phase-space for softer gluons and is represented by this many-facetted surface*

y_1 the inclusive density dn_1 is in the LLA

$$dn_1((g_0, g_0') \to (g_0, g_1, g_0')) \equiv dn_1((g_0, g_1, g_0')) = \bar{\alpha} dy_1 \frac{dq_{\perp 1}^2}{q_{\perp 1}^2} \tag{10}$$

The phase space for such an emission from a dipole with mass W is in the dipole cms:

$$q_\perp \cosh(y) \leq W/2 \tag{11}$$

This relation can be conveniently approximated in the $(y, \log(q_\perp^2))$-plane, cf Fig 2, as the inside of a triangle

$$|y| \leq (L - \kappa)/2 \quad \text{with} \quad (L, \kappa) = (\log(W^2), \log(q_\perp^2)) \tag{12}$$

We note that in case we consider the corresponding inclusive density to emit two gluons at $(q_{\perp j}, y_j)$, $j = 1, 2$ then the density is factorisable so that (this is shown to be good to about 99% all over phase space in Ref [6])

$$\begin{aligned} dn_2((g_0, g_0') &\to (g_0, g_1, g_2, g_0')) = \\ &= dn_1((g_0, g_1, g_0'))(dn_1((g_0, g_2, g_1)) + dn_1((g_1, g_2, g_0')) \end{aligned} \tag{13}$$

in case $q_{\perp 1} > q_{\perp 2}$ (or else the indices have to be exchanged in Eq (13)). Thus "the original dipole" with (the basement) "length" L in accordance with Fig 2 is subdivided into two with the corresponding lengths $\pm y_1 + (L + \kappa_1)/2$. Each dipole can independently emit the gluon indexed 2 as shown in Fig 2. The requirement that $\kappa_2 < \kappa_1$ means that the two new dipole triangles are cut-off at the "height" κ_1. In this way we may define the notion of "virtuality" (as $\log(k_{\perp 1}^2) = \kappa_1$) for the newly produced dipoles.

In the Lund Dipole Cascade Model (DCM) this time-like cascade process is then continued in an obvious way into more and more gluon emissions with smaller and smaller dipoles. The main point is the ordering in $\kappa = \log(k_\perp^2)$ (which is the correspondence to the strong angular ordering, ie to the coherence conditions in the QCD radiation). This implies that any "new" emission at κ_j in a dipole is limited by the earlier "virtuality" of the dipole, ie $\kappa_{j-1} > \kappa_j$.

We also note that in the "geometry" of the triangular phase space, all points with a fixed value of $q_+ = q_{+j}$ ($q_- = q_{-j}$) are placed along lines parallell to the triangular side(s) because $\log(q_{\pm j}) = \pm y_j + \kappa_j/2$. In this way an on-shell (mass-less) gluon emission can be described either in terms of (q_{+j}, q_{-j}) or (what amounts to the crossing point of the two (logarithmic) "lightcone-lines") in terms of the coordinates (y_j, κ_j).

In order to interprete the results of the LDC and CCFM Models into the dipole phase space we note that there is in the fan diagram in Fig 1 in principle a large color "dipole". It is spanned between the incoming parton P (which we parametrize to be on the mass-shell with the positive lightcone energy-momentum P_+; in that way "the front lightcone line" corresponds to $\log(P_+)$) and the parton "kicked out" by the probe q (the probe is not on the mass-shell but provides the negative lightcone energy-momentum Q_- to the parton, ie the "backward lightcone line" corresponds to $-\log(Q_-)$). The essential ISB emissions, $\{q_j\}$, as well as the connector vectors, $\{k_j\}$, can be exhibited in this phase space triangle in the following way for the LDC:

LDCa. the q_j-vectors are onshell and massless and are therefore shown as extended triangular folds, just as we describe the emissions of the gluons in the time-like dipole cascade above

LDCb. the connector vectors k_j are not on the mass-shell but as we have mentioned before the component $k_{+j} = q_{+(j+1)}$ and (due to the necessary symmetry between the hadron and probe end) the component $k_{-j} = q_{-j}$. Finally the requirement in Eq (6) means that the transverse momentum $\log(k_{\perp j}^2)$ is fixed by the q_j emission (or vice versa). Therefore the k_j can be described by an extended line between the $q_{+(j+1)}$ and the q_{-j} at the appropriate height $\log(k_{\perp j}^2)$. (Note that in this way, cf also Eq (3), the "true" virtuality $-k_j^2 \simeq k_{\perp j}^2$)

Thus we obtain the picture in Fig 3 with a set of connected ISB dipoles spanned between the adjacent $\{q_j\}$ with the virtualities given by the corresponding connectors $\{\log(-k_j^2) \simeq \log(k_{\perp j}^2)\}$. The situation is obviously symmetric between the hadron and probe ends so that in Eq (9) we may interprete the splitting function z-pole either as the positive lightcone fraction

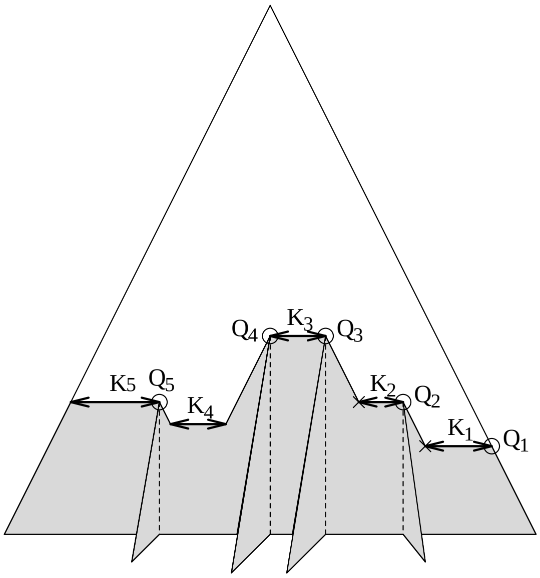

Figure 3: *A gluon-chain in the LDC Model described in the triangular phase-space. The extended folds correspond to on-the-mass-shell gluons and the arrows to the connector propagators*

$z = k_{+j}/k_{+(j-1)}(= q_{+(j+1)}/q_{+j})$ or the negative lightcone fraction $z \equiv z_- = k_{-j}/k_{-(j+1)}(= q_{-j}/q_{-(j+1)})$ (in case we would describe the process instead from the probe end).

In the CCFM Model more gluons are included in the essential ISB set. In particular when the requirement in Eq (6) is lifted the model no longer provides complete dipoles but also "parts of dipoles" as described in Ref [1]. We note one very important requirement, however. *In the FSB of the LDC Model (and this is the same for the CCFM Model) there can be no emission between the q_j and q_{j+1} with transverse momenta exceeding the virtuality of the connector $-k_j^2 \simeq k_{\perp j}^2$.*

The dynamical reason is that the gluon currents from the pair (q_j, q_{j+1}) due to the existence of the connector k_j "starts out" from two different space-time points. Therefore there is an "effective" (due to Lorentz contraction essentially transverse) distance between these emission points equal to $b \simeq 1/\sqrt{-k_j^2} \simeq 1/k_{\perp j}$. It is well-known that an "antenna" of the size b is not well-suited to emit radiation with the wave-length $\lambda < b$ (for smaller wave-length, ie larger transverse momenta, there will in general be a form-factor suppression). *The*

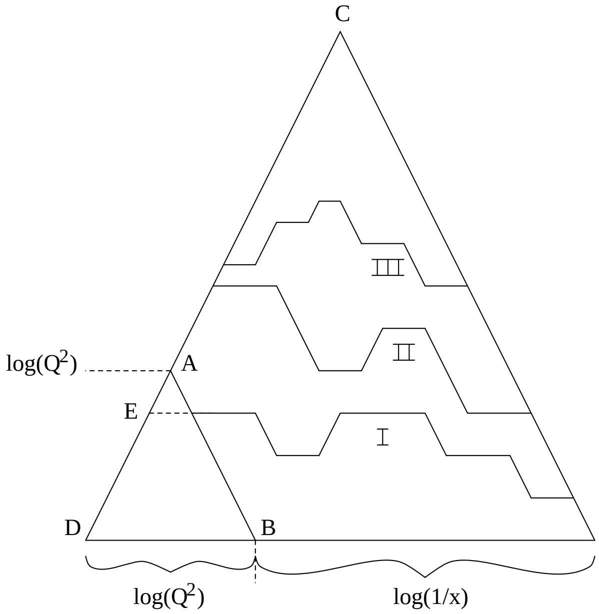

Figure 4: The different kinds of gluon chains. As the probe $Q_+ = xP_+$, cf text, the baseline rapidity region is divided into $(-\log(Q_-), \log(Q_+))$ and $(\log(Q_+), \log(P_+))$ with the marked out lengths $\log(Q^2)$ and $\log(1/x)$, respectively.

corresponding major result from the valiant CCFM Model calculations is that the dipole produced between q_j and q_{j+1} can emit no FSB bremsstrahlung with transverse momentum larger than the virtuality $-k_j^2 \simeq k_{\perp j}^2$. There is a cancellation between the virtual and real corrections for the emission region above the transverse momentum $k_{\perp j}$ in between the gluons q_j and q_{j+1}.

2.3 The Different Channels in Deep Inelastic Scattering

We end this section with a subdivision into three different channels of the contributions from the dipole chains in the LDC. Firstly we note that the Bjorken x_B-variable is in this language $x_B = Q^2/2(pq) = Q_+Q_-/P_+Q_- = Q_+/P_+$. We have in Fig 4 shown both a description of the variables $\log(1/x_B)$ and $\log(Q^2)$, (note that the latter one occurs both as a rapidity region in the "big" dipole phase space triangle and as a measure of virtuality $\kappa_Q = \log(Q^2)$).

In Fig 4 we have shown three possible "chain-roads" and they correspond to, respectively

I a “normal” quark-parton model interaction, in which the largest virtuality along the chain is given by Q^2. The chain may after n emissions end anywhere along the line $\kappa_n < \log(Q^2) \equiv L_Q$ with a parton with $\prod^n z_j = x_B$. Depending upon the coordinate frame we consider (cf for more details Ref [1]) the parton will after the interaction with the probe end up at the point, denoted A at $(\log(1/x_B), \kappa = L_Q)$ (this would be in a Lorentz frame corresponding to the lepton-hadron cms) or at the point denoted E along the line with $\log(k_{-n}) = \log(Q_-)$ at the appropriate “incoming” virtuality κ_n (this is the probe-hadron cms frame, where the transverse momentum of the kicked-out parton is provided solely by the cascade).

II a “Boson-Gluon Fusion” event, in which the (final) splitting transverse momentum variable exceeds the probe virtuality $\kappa_n(\simeq \log(q_{\perp n}^2)) > L_Q$. Then the final parton ends on the line $\log(Q_-)$ above the value L_Q, ie for $\kappa > L_Q$, due to this final (large virtuality) splitting. According to the way the structure function is defined we obtain from the weight factors of Eq (9) an extra “going-down” factor $Q^2/k_{\perp n}^2$. We call these events boson-gluon fusion events, although in the present study we have only gluons and no quarks, whereas in a real DIS event with γ, Z or W exchange the last parton in the chain has to be a quark.

III a Rutherford scattering between a remnant of the probe, which although it starts out at the probe virtuality L_Q splits up into a set of emissions $L_Q < \kappa_n < \kappa_{n-1} < ... < \kappa_{max}$ to “meet” the corresponding hadron remnant chain with $\kappa_1 < \kappa_2 < ... < \kappa_{max}$. In accordance with Eq (9) we will in this case obtain a factor (in the way we have defined it $\kappa_{max} = \log(k_{\perp max}^2)$ is the only maximum in transverse momentum along the chain)

$$\prod_1^n d\kappa_j \frac{Q^2 k_{\perp n}^2 k_{\perp(n-1)}^2 \cdots}{k_{\perp n}^2 k_{\perp(n-1)}^2 \cdots k_{\perp max}^2} = \prod_1^n d\kappa_j \frac{Q^2}{k_{\perp max}^2} \tag{14}$$

(We note that although the factor is described in the language of going from the hadron to the probe end, the result would be the same in case we would have used the opposite direction. We also note that this is a direct generalization of the going-down factor obtained in the case II described above).

The main point is, however, that in Eq (14) we obtain a factor $d\kappa_j = dk_{\perp j}^2/k_{\perp j}^2$ for all bremsstrahlung gluons but the factor $dk_{\perp max}^2/k_{\perp max}^4$ for the largest transverse momentum, which is characteristical for Rutherford scattering with $k_{\perp Ruth} = k_{\perp max}$. In Ref [1] it is shown that the correct Rutherford scattering behaviour occurs both when the propagator corresponds to a gluonic and when it is a quark(anti-quark) exchange.

Note that in this way (as we have mentioned before, [1], [7]) *the major momentum transfer in a chain diagram always corresponds to a Rutherford scattering* with (coherent) bremsstrahlung contributions describing both the "going-up" and "going-down" sides but all of them with $k_{\perp brems} < k_{\perp Ruth}$. *This means that the (largest) transverse momentum of the bremsstrahlung gluons always provide a lowest cut-off of a (possible) Rutherford scattering.*

3 Two Methods to Implement the LDC Model Equations

As we are interested in the qualitative features we are disregarding contributions from quarks, and we keep only the pole term $1/z$ in the gluonic splitting function. We have used two different ways, cf the subsections 3.1 and 3.2 to implement the LDC process. They are both based upon an integral equation.

It is useful to define "the non-integrated structure function", $\mathcal{F}$, instead of the structure function $F(x_B, Q^2)$ of the impinging hadron, by means of the equation

$$F(x_B, Q^2) = \int \frac{dk_\perp^2}{k_\perp^2} \mathcal{F}(\hat{\ell}, \kappa) \tag{15}$$

$$\text{with} \quad \hat{\ell} = \begin{cases} \log(1/x_B) \equiv \ell & \text{if } Q^2 > k_\perp^2 \\ \log(Q^2/x_B k_\perp^2) \cdot \frac{Q^2}{k_\perp^2} & \text{if } Q^2 < k_\perp^2 \end{cases}$$

In terms of the non-integrated structure function $\mathcal{F}$ we may write the following integral equation, corresponding to three contributions, $\mathcal{I}_j$:

$$\mathcal{F}(\ell, \kappa) = \sum_{j=1}^{3} \mathcal{I}_j \tag{16}$$

The contributions are in turn

- $\mathcal{I}_1$ the possibility $\mathcal{I}_1 = \bar{\alpha}$ to take a single step from the starting point $(\ell_0 \equiv \log(1/x_0), L_{Q_0} \equiv \log(Q_0^2))$ all the way to the final point $(\ell \equiv \log(1/x_B), \log(k_\perp^2) \equiv \kappa)$ (this is a "boundary term"). (We often think of the parameter values $(\ell_0 = 0, L_{Q_0} = 0)$, which define both the properties of the starting-point and the scale of the coupling.)

- $\mathcal{I}_2$ the possibility to be at a "point" (κ', ℓ') "below" κ, ie with $(L_{Q_0} < \kappa' \equiv \log(k_\perp'^2) < \kappa$ and $\ell_0 < \ell' \equiv \log(1/x') < \ell = \log(1/x_B))$, and to take the final step "upwards" in transverse momentum and "onwards" in ℓ. (This is the DGLAP mechanism.) We obtain

$$\mathcal{I}_2 = \int_{L_{Q_0}=0}^{\kappa} \bar{\alpha} d\kappa' \int_{\ell_0=0}^{\ell} d\ell' \mathcal{F}(\ell', \kappa') \cdot h(exp(\kappa - \kappa')) \tag{17}$$

where $h \approx 1$ is defined in Eq (8).

$\mathcal{I}_3$ the possibility to be at a point κ' "above" κ and to take a step "downwards" to κ (note that this step is "upwards" in transverse momentum from the probe side and therefore we have to compensate with the change $\ell' \to \ell' + \kappa - \kappa'$, cf also Eq (9)):

$$\int_{\kappa}^{\ell} \bar{\alpha} d\kappa' \exp(\kappa - \kappa') \int_{0}^{\ell+\kappa-\kappa'} d\ell' \mathcal{F}(\ell', \kappa') \cdot h(exp(\kappa' - \kappa)) \tag{18}$$

We note that the factor h implies a suppression if we "stay" in the last step close to $\kappa \simeq \kappa'$, ie in case the emitted gluon transverse momentum is very small, $q_\perp \simeq 0$. This case has been treated extensively both inside the CCFM Model, [2] and the LDC, [1]. In CCFM it is noted that if the upper ℓ'-integral limit in Eq (18) is changed $\ell + \kappa - \kappa' \to \ell$ the integral equation obtained from Eqs (17) and (18) can be treated along the BFKL methods. After suitable rearrangements (with the non-eikonal form-factor regularising the singularity at $q_\perp = 0$) it also provides the well-known BFKL contribution.

Thus, in terms of the anomalous dimension equation, with the structure function $\mathcal{F}$ behaving like

$$\mathcal{F} \sim x^{-(N-1)} (k_\perp^2)^\gamma \tag{19}$$

one obtains in BFKL the result (written in the conventional form):

$$1 = \frac{\bar{\alpha}}{N-1} (g(\gamma) + g(1-\gamma)) \quad \text{with} \quad g(\gamma) = \psi(1) - \psi(\gamma) \tag{20}$$

In case the "correct" integral limit in $\mathcal{I}_3$ is retained there is a change in the argument of the second g-function $g(1-\gamma) \to g(N-\gamma)$. Therefore the change provides in the ordinary QCD language a contribution which is subleading in $\log(1/x)$, ie it is non-singular at the $(N-1)$-pole. We note, however, that this change at the same time provides a very large correction.

To see that we note that the two integral equations are symmetrical around $\gamma = 1/2$ and $\gamma = N/2$, respectively, and that the major contribution to the x-behaviour (the celebrated BFKL-exponent λ) comes for that value of N where there is "pinch" singularity in the inverse Mellin transform. For the case with $g(1-\gamma)$ this correspond to $\lambda \equiv N - 1 = 4\bar{\alpha}\log(2) \simeq 0.56$ (for $\alpha = 0.2$), but for the case with $g(N-\gamma)$ it is changed to $N - 1 \simeq 0.31$ (again for $\alpha = 0.2$).

If we introduce the restriction of the LDC Model in Eq (6) then the result will be similar to Eq (20) but the function g given for the BFKL case is slightly changed. The use of the precise LDC contribution provides another change to the BFKL result $N-1 \simeq 0.41$ but we note that this change is smaller than the earlier one.

If we combine the experience obtained above from the different possible treatments of the small $q_\perp$-region with the arguments of Ref [1] that it is necessary to restrict the integration region in each z-step in order to conserve energy-momentum we may conclude:

- the results of taking all orders in transverse momentum fluctuations provide a rather stable result
- but there are large changes in the exponent λ describing the structure function from the different possible treatments of the small x-behaviour.

It has been known for a long time that there are corrections (principally of the order $\bar{\alpha}^2$ with a constant coupling) to the BFKL treatment. The fact that they are very large means that it is worthwhile trying to retain at least some of them. In this note we also will treat the consequences of introducing a running coupling.

3.1 A MC solution to the Integral Equation for LDC

We will here describe how we solve Eq (16) by first generating events evenly in an extended phase space, and afterwards multiply by appropriate weights. For all partons there is a cut $\kappa > 0$, corresponding to $p_\perp > \Lambda_{QCD}$. For running coupling constant we also have a cutoff such that $\bar{\alpha} \propto 1/\kappa$ for $\kappa > \kappa_{cut}$ ($= 2$ for the results presented below) and $\bar{\alpha} = $ constant for $\kappa < \kappa_{cut}$.

Suppose that we introduce the variables (for the case of a constant effective coupling $\bar{\alpha}$):

$$\begin{aligned} X &\equiv \sqrt{\bar{\alpha}} \log(Q/k_-) = \sqrt{\bar{\alpha}}(y - (\kappa - L_Q)/2) \\ Y &\equiv \sqrt{\bar{\alpha}} \log(k_+/Q) = \sqrt{\bar{\alpha}}(y + (\kappa - L_Q)/2) \end{aligned} \tag{21}$$

then the results of producing an ISB dipole (starting at some value (κ', y') and going to the point (κ, y)) is inclusively given by, cf Eq (9) (where we neglect the possible exponential "going-down" factor for the moment):

$$\bar{\alpha} dy d\kappa = dX dY \tag{22}$$

Further suppose that we introduce the following phase space, which is easily seen to be enlarged compared to the ordinary triangular dipole space:

$$\begin{aligned} 0 \leq X \leq a &\equiv \sqrt{\bar{\alpha}}(\log(Q^2) + \log(1/x)) \\ 0 \leq Y \leq b &\equiv \sqrt{\bar{\alpha}} \log(1/x) \end{aligned} \tag{23}$$

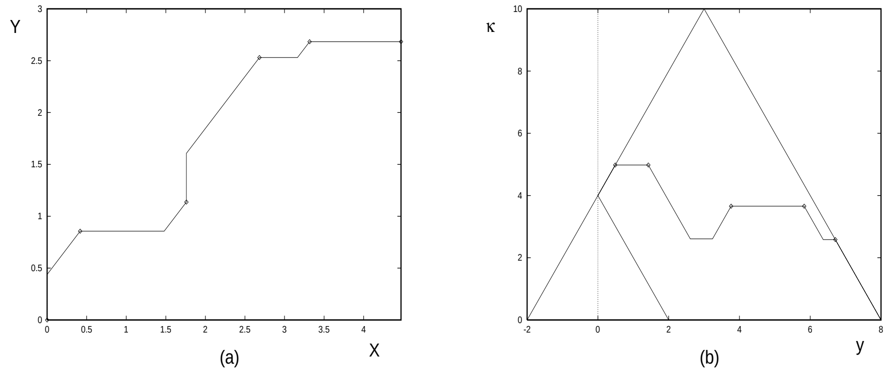

Figure 5: *An event, described in the variables (X,Y) and (y,κ), in (a) and (b) respectively.*

In order to exhibit the relationship between the variables (κ, y) in the triangular dipole phase space and the variables (X, Y) we show in Fig 5 a typical road (this time corresponding to a boson-gluon fusion event as described above).

We will now consider a stochastical process in the (X, Y)-plane, Eq (23), which is an approximation to the solution of the integral equation in Eq (16). Afterwards we will obtain the "correct" solution by introducing a weighting procedure for the steps.

The first step, which corresponds to emitting the first $q = q_1$-vector will always be placed along the right hand edge of the triangular phase space. In the LLA this corresponds to $q_{+1} \simeq P_+$, ie the step is along $Y = b$. In each of the following steps we will decide upon the position of the right end of the (next) propagator so that in the last step we end at the photon propagator. We then note that for every step there is a set of paths from "the starting-point" to the photon end. By our choice we will choose a subset of these paths. It is then necessary to weight every step by means of the available "remaining" possibilities, ie the remaining possible paths.

In the approximate process the weights for a path is given by $\prod dX_j dY_j$. Further we may introduce an ordering so that $a > X_1 > ... > X_n = 0$ and $b = Y_1 > ... > Y_n = 0$. This means that the total weight for all paths, $f_0(X, Y)$, from any point (X, Y) to the end point $(0, 0)$ is given by the integral over all the (ordered) $(X_j Y_j)$-variables and the sum over all partitionings:

$$f_0(X, Y) = I_0(2\sqrt{XY}) \tag{24}$$

with I_0 the modified Besselfunction of the first kind. In order to find the weight, f_1, for all paths given the size of the parameters (a, b) we must integrate f_0 for $0 < X < a$ and $Y = b$. In this way we obtain as a first approximation to the structure function $f(x, Q^2)$ (this is straightfoward Bessel-function machinery):

$$f_1 = \sqrt{\frac{a}{b}} I_1(2\sqrt{ab}) = \frac{\partial f_0(a,b)}{\partial b} \quad \text{with} \quad \sqrt{\bar{\alpha}} f_1(a,b) \leftrightarrow \frac{\partial f}{\partial \log(Q^2)} \tag{25}$$

At the same time we conclude that the (normalized) probability to find the point (X', Y'), starting at (X, Y) is given by

$$dP(X', Y') = \frac{I_0(2\sqrt{X'Y'}) + \delta(X')\delta(Y')}{I_0(2\sqrt{XY})} dX'dY' \tag{26}$$

Given this approximate process we will now define the precise solution to the integral equation, Eq (16), for the non-integrated structure function. We will do that by introducing a weight for each particular road so that we may incorporate those features of the integral equation which are not taken into account for the solution in Eq (25). There are four such corrections and each will provide a weightfactor ρ_j so that the total weight for any road is given by $\rho = \prod_1^4 \rho_j$:

- ρ_1 The first weight is either $\rho_1 = 1$ or $\rho_1 = 0$ depending upon whether the road stays inside the "right" triangular phase space, ie whether all parts of the road is above $\kappa = 0$ or if any part is below that line, respectively.

- ρ_2 The second weight is composed of a (possible) product of subfactors, ie every time we chose a "new" $\kappa_{j+1} \equiv \log(k_{\perp j+1}^2)$ which is smaller than the previous one, ie $\kappa_j > \kappa_{j+1}$ then there should be a factor $\exp(\kappa_{j+1} - \kappa_j)$ according to Eq (9).

- ρ_3 The third factor is the weight function $h(k_{\perp j}^2 / k_{\perp (j-1)}^2)$ defined in Eq (8).

- ρ_4 In order to introduce a running coupling $\bar{\alpha} \propto 1/\kappa$ it is possible to introduce at every vertex a correction factor $\bar{\alpha}(\kappa)/\bar{\alpha}$ (with $\bar{\alpha}$ the constant coupling considered before). It is, however, necessary to introduce some cut-off procedure to avoid values of $\kappa \simeq 0$. In this paper we only consider the choice $\bar{\alpha}(\kappa) \propto 1/\kappa$ if $\kappa > \kappa_{cut}$ and $\bar{\alpha} = constant$ elsewhere but we will in future publications consider the general question of infrared stability.

The product weight we define in this way is for a typical size of the phase space on the percentage level on the average but there are some interesting fluctuations. The average level, $< \rho >$, nevertheless contains the "normalization" of the precise solution to the appoximate solution we obtained in Eq (25). The final result for the structure function is consequently

$$\frac{\partial f(x, Q^2)}{\partial \log(Q^2)} = < \rho > \sqrt{\bar{\alpha}} f_1(a, b) \tag{27}$$

Inside this scheme it is evidently possible to compute not only the contribution from "the average road" but also the fluctuations around it and in particular to construct in a Monte Carlo simulation way "any" possible road. We will come back to the results of this approximate treatment both in the last section and in future publications.

3.2 A Discrete Model

We will in this subsection consider a different approach to the integral equations in Eq (16). In this approach all integrals will be exchanged for sums over a set of discrete values. The basic ideas stem from the approximate treatment of the (time-like) QCD cascades, which are presented in Ref [8]. It turns out that the density of "effective" gluons is very low in the triangular dipole phase space. The reason is three-fold (and actually corresponds to (an extension of) the Modified Leading Log Approximation, MLLA, in QCD, [5]).

The first two reasons are that there are corrections to the bremsstrahlung emission in the triangular phase space, cf Eq (10). There is eg a spin-correlation factor, which is neglected above and there are also recoil corrections in the neighbourhood of any "hard" emission. It is easy to estimate the spin-correlation corrections and also to understand the physics behind them. It is a nice surprise that these corrections also are sufficient to take into account the recoil corrections, at least in the time-like cascades as we have shown in Ref [8].

The estimate from the spin-correlation is a distance in rapidity of $\delta y = 11/6$, which is a large number. It is, however, necessary to understand that in case there is an emission of a hard gluon, a new region in phase space is opened up. This hard gluon is split into many subjets, all with approximately the same rapidity with respect to the original main axis (the thrust axis). The subjets are separated in rapidity *along the parent gluon direction* by distances δy. They contain in their turn sub-sub-jets etc. Thus within one rapidity bin δy, as measured along the thrust axis, there can be a lot of structure.

The third reason for the discretization is related to the properties of the running coupling in QCD. In Ref [8] we have exhibited that those next-order corrections (the "dielectricity of the vacuum" ie the vertex and self-energy Feynman graph corrections) which constitute the change from a constant to a running coupling actually corresponds to the requirement that if two gluons are emitted too close in rapidity then they are again reabsorbed. It turns out that it is again the same "effective" rapidity difference (as we have defined it above) of 11/6, which occurs. (We are then as before neclecting the gluon splitting process $g \to (q\bar{q})$).

Without going into the detailed arguments provided in Ref [8] we note that this number stems from the well-known formula for the effective coupling in gluon emission (with the number of flavors $N_f = 0$)

$$\bar{\alpha} \equiv \frac{N_c \alpha_s}{2\pi} = 3\frac{12\pi}{2\pi 33\kappa} = \frac{6}{11\kappa} \tag{28}$$

which will occur in the dipole emission formula according to Eq (10):

$$\bar{\alpha} d\kappa dy = \frac{6dy}{11}\frac{d\kappa}{\kappa} \tag{29}$$

From this result it is evident that with a discretization of the gluon emission rapidity steps to $\delta y = 11/6$ we obtain the (inclusive) emission density $d\kappa/\kappa$ inside each such rapidity "step". To obtain the probability to obtain a particular κ-value it is necessary to introduce a Sudakov factor. In this case the Sudakov factor becomes, [8], κ/κ_m with κ_m the largest κ-value allowed in that rapidity bin. Consequently the probability to emit an effective gluon is $d\kappa/\kappa_m$, ie it is the same for any κ-value!

We must further remember that each gluon emission corresponds to an extended phase-space fold as described in Fig 2, ie that the "extra" rapidity region obtained along the emitted gluon rapidity is given by $2\kappa/2 = \kappa$. Therefore we find in Ref [8] that it is also necessary to discretize the κ-variable into steps $\delta\kappa = 2\delta y$ in order to be able to accomodate those "collinear gluons".

The result is that the total phase space is subdivided into a set of "effective" gluon emissions and that if we discretize the rapidity region into δy-steps we are forced to discretize the corresponding κ-regions into $\delta\kappa = 2\delta y$ steps as it is shown in Fig 6. We will now introduce this same prescription into the DIS production process of dipoles.

There is a small difference in the procedure, however, because the earlier argument was only related to the emission along a single original color line (a $q\bar{q}$ dipole). Although we have not been particularly precise in connection with the effective color factors it is evident that in case we consider a gluon process $g \to (gg)$ then we are actually considering a process along two color lines. It is then possible to use either the argument that there are two independently emitting color lines with the emission difference δy along each or to say that there is effectively a single emission line with the distance $\delta y/2$. We will in the spirit of the LLA keep to this latter description and therefore exchange $\delta y \to \delta y/2 \equiv \delta = 11/12$.

If we apply this scheme to the LDC Model it implies that the "links" in Fig 3 will have the property that the length of all of them is an integer times ("this new") δ and that the height is an even integer ($\neq 0$) multiplying δ. The result of a step is shown in Fig 7. This means that all real emission q-vectors will be on-shell "above" $\kappa = 0$ but it is also in this scheme possible to reach a "propagator" for which $\log(k_\perp^2)$ is zero.

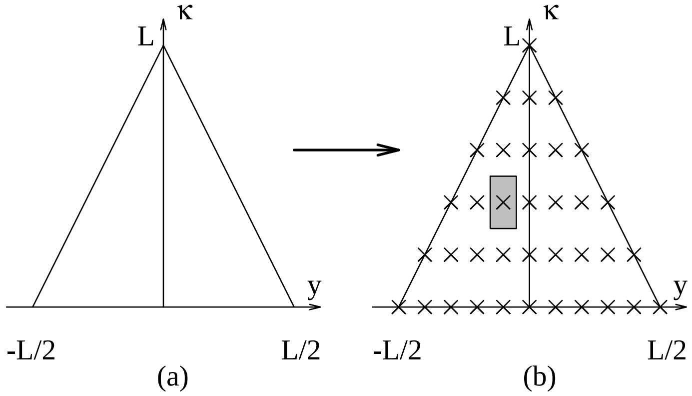

Figure 6: *(a) The continuous phase space triangle for gluon emission in* e^+e^-*-annihilation. (b) Emission points for "effective gluons" in the discretized phase space. One such gluon represents all emission that is taking place in side its cell, shaded area.*

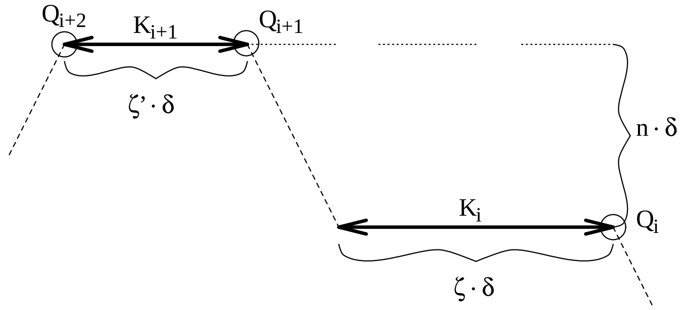

Figure 7: *Illustration of the separation conditions for propagators (arrows) and real gluons (circles) in the discretized logarithmic phase space.* ζ *and* ζ' *are integers and* n *is always an even integer.*

The result is that inside this approach there is a finite number of chain-roads available. In each step we will obtain a weight w_i:

$$w_i = \bar{\alpha}\frac{dz_i}{z_i}d\kappa_i \equiv \bar{\alpha}2(\delta)^2 \exp(n_i - \max(n_i, n_{i-1})) \tag{30}$$

For a running coupling we may write the corresponding weight

$$w_i = \frac{2}{\max(n_i, n_{i-1})} \exp \delta(n_i - \max(n_i, n_{i-1})) \tag{31}$$

The contribution from each chain is the product of all the "step-weights" and

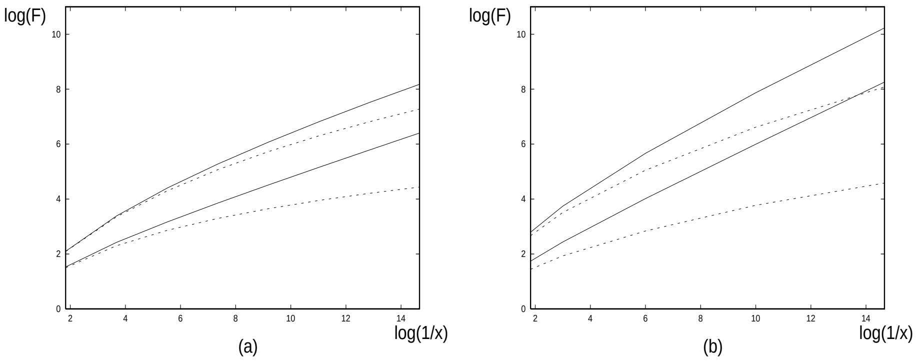

Figure 8: *The* $\log(1/x)$ *dependence for the logarithm of the structure function F, when the coupling is running. Dashed lines (lower:* $\log(Q^2) \approx 4$*, upper:* $\log(Q^2) \approx 12$*) denote the DGLAP contribution and solid lines (lower:* $\log(Q^2) \approx 4$*, upper:* $\log(Q^2) \approx 12$*) all contributions. (a) The discrete model. (b) The continuous calculation.*

the structure function will in this scenarium be the sum over all the allowed roads (r)with their respective weights w_{ir} for each step i:

$$F(x, Q^2) = \sum_r \prod_i w_{ir} \tag{32}$$

4 Some General Results from the LDC Model

4.1 The Behaviour of the Structure Functions

In fig 8 we show some results for the x-dependence of the structure function. It is possible to consider only the "true" DGLAP contribution to the unintegrated structure function $\mathcal{F}$, ie the case when the transverse momenta of the connector vectors are ordered, $k_{\perp 1}^2 < k_{\perp 2}^2 < ... < Q^2$. This contribution is described above by $\mathcal{I}_2$ with the same boundary value $\mathcal{I}_1$. It is shown for the two different models, according to subsections 3.2 and 3.1, in Figs 8a and 8b, respectively, as the dashed lines, corresponding to different values of $L_Q = \log(Q^2)$.

On the other hand the total integral equation solution, also including $\mathcal{I}_j, j = 3, 4$ is shown as full lines in each of the plots. There is evidently no large differences between the results from the two methods for the DGLAP contribution, but there are noticable differences in case we include the terms $\mathcal{I}_j, j = 3, 4$ both in shape and in normalization. In order to see the difference between a running and fixed coupling we show in Fig 9 a few examples for the total $\mathcal{F}$. In this case we find just as expected essential differences. The results presented

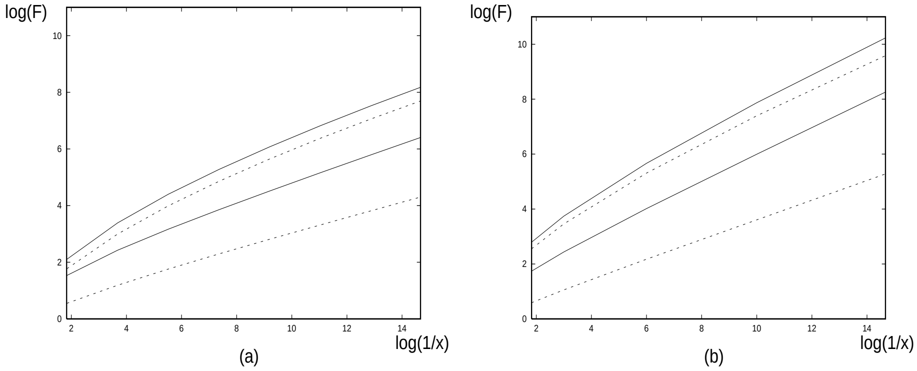

Figure 9: *The* $\log(1/x)$ *dependence for the logarithm of the structure function* F*, when all contributions are included. Dashed lines (lower:* $\log(Q^2) \approx 4$*, upper:* $\log(Q^2) \approx 12$*) denote the result for constant coupling and solid lines (lower:* $\log(Q^2) \approx 4$*, upper:* $\log(Q^2) \approx 12$ *) denote running coupling. (a) The discrete model. (b) The continuous calculation.*

here are similar to the corresponding results in ref [9] obtained in the CCFM formalism.

In Figs 10a and b we show the main path, as described by the average value of the $\kappa = \log(k_\perp^2)$ (for fixed y) for the connector vectors, from the starting-point to the final point for a "small" and a "large" value of L_Q. (We are from now on considering the total $\mathcal{F}$). We also show in the same triangular phase space the values of the connector κ-values (for fixed rapidity), which are one standard deviation above and below the average path. In both cases we have used the continuous approximation to the integral equation and a running coupling as described in subsection 3.1. In Fig 11 we show the corresponding density of emitted gluon $\log(q_\perp^2)$, this time both for a fixed and a running coupling.

We conclude from the main path-contributions that (besides a (small) $\ell = \log(1/x)$-region, ℓ_0, close to $\ell = 0$, which depends upon the way we "start out") the results can be described so that there is firstly a region ℓ_1 in which there is basically a small κ for all emissions. This corresponds to a "going-up and going-down" in a narrow region around $\kappa \simeq L_{Q0} = 0$. This is particularly so for a running coupling, which favors small κ-values. At some point it is, however, necessary to "go up" in order to end on the chosen κ, and this corresponds to a region ℓ_2. Evidently the size ℓ_2 depends upon the final "height", κ. The two regions correspond to the expected behaviour for BFKL-(ℓ_1) and DGLAP-(ℓ_2)dominance, respectively, and we will now consider the results of an approximation, based upon such a "partitioning".

From the results of Figs 8a and 8b these conclusions are confirmed because

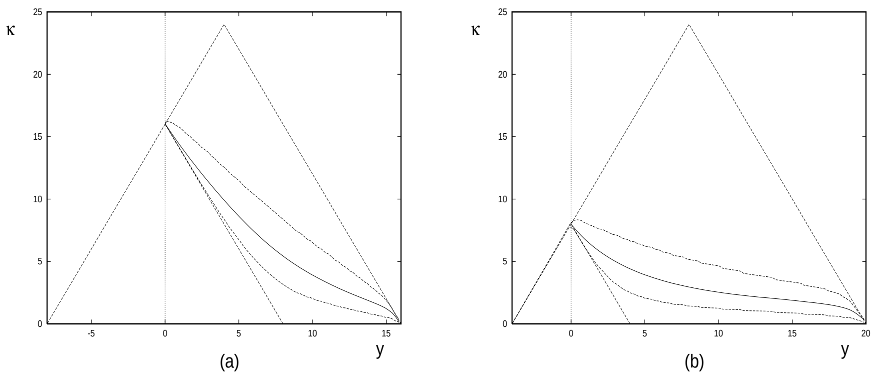

Figure 10: *The mean path and deviations from it, described in the phase space for (a)* $\log(Q^2) = 16$, $\log(1/x) = 8$ *and (b)* $\log(Q^2) = 8$, $\log(1/x) = 16$

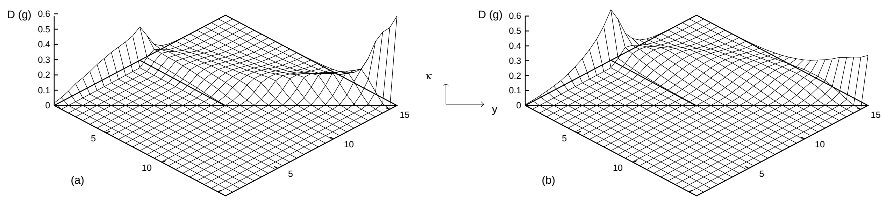

Figure 11: *The density of initial state gluons (q_i), $D(g) = \frac{\partial^2 n}{\partial\kappa\partial y}$, in the triangular phase space with* $\log(Q^2) = 8$ *and* $\log(1/x) = 8$*. (a): running coupling, (b): constant coupling. Inside the triangle, we have a two-dimensional distribution, while on the edges there is a one-dimensional contribution, which is sticking up.*

for small values of the variable $\ell = \log(1/x)$ there is in both cases a "typical", DGLAP growth like $\log(\mathcal{F}) \simeq 2C(k_\perp^2)\sqrt{\log(1/x_B)}$ with a slow κ-dependence of the variable $C(k_\perp^2) \simeq \sqrt{\log(\kappa)}$ (valid for running α_s). (Note that inside an analytic DGLAP-approximation we obtain the behaviour $C(k_\perp^2) = \sqrt{11/12\log(\kappa)}$ for the case when we neglect n_f, the number of flavors). For larger values of ℓ, however, a basically linear behaviour of $\log(\mathcal{F})$ will dominate the amount of available paths. This is typical for the BFKL behaviour $\log(\mathcal{F}) \simeq \lambda\log(1/x)$.

The combined contribution is then (if we neglect the ℓ_0-region)

$$\begin{aligned} \mathcal{F} &= \int \exp\left[2C(k_\perp^2)\sqrt{\ell_1} + \lambda \ell_2\right] d\ell_1 d\ell_2 \delta(\ell_1 + \ell_2 - \ell) \\ &\simeq \exp(\lambda\ell + [C(k_\perp^2)]^2/\lambda) \end{aligned} \tag{33}$$

The result stems from a saddle-point approximation which is valid if the saddle point is inside the integration region, ie if $\ell_1 \equiv \tilde{\ell_1} = [C(k_\perp^2)]^2/\lambda^2 \leq \ell$. It turns out that if we consider an approximation of the form $\log(\mathcal{F}) = a\ell + b[C(k_\perp^2)]^2 + c$, using large values of κ and ℓ from the solution to the integral equation (with $[C(k_\perp^2)]^2 \simeq \log(\kappa)$) then we always obtain results with the fitted parameters obeying $ab \simeq 1$ as expected from these considerations. The value of the λ-parameter is then $\lambda \simeq 0.4$.

On the other hand for smaller values of $\ell \leq \tilde{\ell_1}$ the DGLAP contributions will win out and dominate the results. It is possible to estimate the place where the quantity $\tilde{\ell_1} = [C(k_\perp^2)]^2/\lambda^2 = \ell$, and rough estimates will tell us that for $x \simeq 10^{-5}$ this will occur for $Q^2 \simeq 100\ GeV^2$ (and due to the slow change of C, $x \simeq 10^{-4}$ for $Q^2 \simeq 10\ GeV^2$).

4.2 The Contributions to the Structure Function from the Different Interaction Channels

In this subsection we would like to describe the contributions from the different channels which were described in subsection 2.3. We note in particular the boson-gluon-fusion events, which are defined so that the largest transverse momentum occurs at the last propagator link and also is larger than the momentum transfer Q. Further the Rutherford events in which one (or more) propagator links (away from the last one) have transverse momenta above Q. They correspond to hard scattering events between a resolved probe and a hadron.

The remaining events, in which no propagator transverse momenta is above Q, correspond to what we called the "normal" contribution above. (This is eg the contribution studied in ref [10] and in most situations it is the dominating term.)

In Fig 12a and b we show the contributions from these different event groups as a function of $\log(1/x)$ for two different values of $L_Q = \log(Q^2)$. We find that for a large L_Q the Marchesini-Webber events will dominate but in case we consider a small L_Q we find that the neglect of the other two groups will significantly change the result for the structure functions.

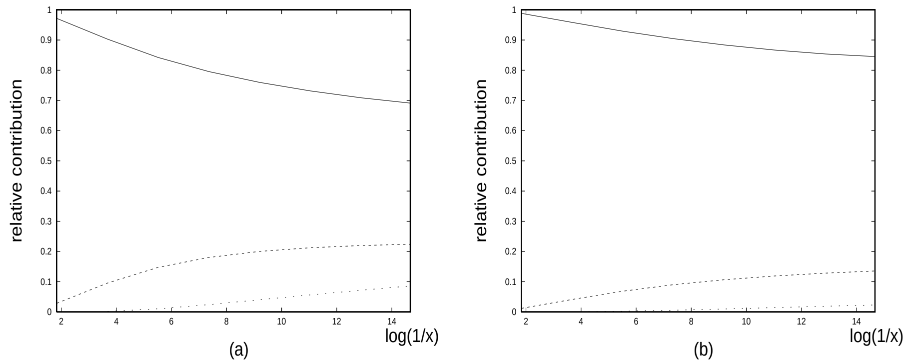

Figure 12: *The relative contributions from the different channels, determined by the discrete method. Solid lines denote Marchesini-Webber events, dashed lines boson-gluon fusion events and dotted lines Rutherford events. (a)* $\log(Q^2) = 5 \cdot \delta \approx 4.6$ *(b)* $\log(Q^2) = 9 \cdot \delta \approx 8.3$

5 Summary

We have studied the behaviour of the structure function and the transverse energy flow in the Linked Dipole Chain model. In this paper we analyse only a purely gluonic cascade. In addition to a direct solution we have also studied a discretized version of the model. The result interpolates smoothly between the DGLAP region, which is applicable for $\log(1/x) \lesssim \tilde{\ell}_1 \equiv \log[\log(Q^2)]$ (This result is applicable for a running coupling, and x is the scaling variable for the perturbative cascade only.) and the BFKL region for larger values of $\log(1/x)$. In the latter case there is first one part of the cascade with length $\log(1/x) - \tilde{\ell}_1$, in which the transverse momenta are limited. This region is followed by a region of length $\tilde{\ell}_1$ in which the transverse momenta are growing towards the virtuality of the probe, Q. We finally study the separation of the events into normal events (where all transverse momenta are smaller than Q), boson-gluon fusion events and hard resolved photon-hadron scattering events.

Acknowledgements

This work is supported in part by the EU Programme "Human Capital and Mobility", Network "Physics at High Energy Colliders", contract CHRX-CT93-0357 (DG 12 COMA).

References

[1] B. Andersson, G. Gustafson, J. Samuelsson, *Nucl. Phys.* **B467** (1996) 443.

[2] M. Ciafaloni, Nucl. Phys. B296 (1988) 49
S. Catani, F. Fiorani and G. Marchesini, Phys. Lett. B234 (1990) 339; Nucl. Phys. B336 (1990) 18

[3] L. Lönnblad, Comput. Phys. Commun. 71 (1992) 15

[4] T. Sjöstrand, M. Bengtsson, Comp. Phys. Comm. 43 (1987) 367
T. Sjöstrand, JETSET 7.4, program and manual

[5] For a review, see Yu.L. Dokshitzer, V.A. Khoze, A.H. Mueller and S.I. Troyan, Basics of Perturbative QCD (Editions Frontières, Gif-sur-Yvette, 1991)

[6] B. Andersson, G. Gustafson and C. Sjögren, Nucl. Phys. B380 (1992) 391

[7] B. Andersson, G. Gustafson and Hong Pi, Z.Phys. C57 (1993) 485

[8] B. Andersson, G. Gustafson, J. Samuelsson, *Nucl. Phys.* **B463** (1996) 217.

[9] J. Kwieciński, A.D. Martin and P.J. Sutton, Durham preprint, DTP/95/22

[10] G. Marchesini and B.R. Webber, Nucl. Phys. B238 (1984) 1;
B.R. Webber, Nucl. Phys. B238 (1984) 492

Paper II

LU-TP 97-29
November 1997

Investigations into the BFKL Mechanism with a Running QCD Coupling

B. Andersson [1], G. Gustafson [2], H. Kharraziha [3]

Department of Theoretical Physics
University of Lund
Sölvegatan 14A
S-223 62 Lund, Sweden

Abstract

We present approximations of varying degree of sophistication to the integral equations for the (gluon) structure functions of a hadron ("the partonic flux factor") in a model valid in the Leading Log Approximation with a running coupling constant. The results are all of the BFKL-type, i.e. a power in the Bjorken variable $x_B^{-\lambda}$ with the parameter λ determined from the size α_0 of the "effective" running coupling $\bar{\alpha} \equiv 3\alpha_s/\pi = \alpha_0/\log(k_\perp^2)$ and varying depending upon the treatment of the transverse momentum pole. We also consider the implications for the transverse momentum ($k_\perp$) fluctuations along the emission chains and we obtain an exponential falloff in the relevant $\kappa \equiv \log(k_\perp^2)$-variable, i.e. an inverse power $(k_\perp^2)^{-(2+\lambda)}$ with the same parameter λ. This is different from the BFKL-result for a fixed coupling, where the distributions are Gaussian in the κ-variable with a width as in a Brownian motion determined by "the length" of the emission chains, i.e. $\log(1/x_B)$. The results are verified by a realistic Monte Carlo simulation and we provide a simple physics motivation for the change.

[1] bo@thep.lu.se
[2] gosta@thep.lu.se
[3] hamid@thep.lu.se

1 Introduction

1.1 The Contents of this Note

In an earlier paper, [1], we have presented the Linked Dipole Chain (LDC) model as a generalization of the well-known CCFM model (for Ciafaloni-Catani-Fiorani-Marchesini), [2], to describe the hadronic structure functions in Deep Inelastic Scattering (DIS) events. We have further in [3] described a set of results from the model. In this note we would like to continue the investigations and in particular *describe the solutions to the equations for the structure functions when a running coupling is introduced.* We will find power-solutions in the Bjorken-variable, i.e. the (gluon) structure function behaves as $x_B^{-\lambda}$ in the same way as for the BFKL-solutions [4] for a fixed coupling.

The power λ is determined by the strength α_0 in the effective running coupling $\bar{\alpha} \equiv 3\alpha_s/\pi = \alpha_0/\ln(k_\perp^2)$ (In a pure Yang-Mills theory we have used the value $\alpha_0 = 12/11$.) and the treatment of the transverse momentum pole, i.e. the small virtualities in our equations. Actually, it will turn out that the equations become unstable in the sense that the value of the parameter λ is sensitive to the approximate treatment of the running coupling in the soft region where $\ln(k_\perp^2)$ is small.

If we introduce a cutoff in the $\ln(k_\perp^2)$-variable we obtain, however, inside a large region, very stable results for an isolated largest eigenvalue λ. One major finding is that the LDC model in itself contains a suppression of the soft region close to the pole of the coupling constant, and thus contributes significantly to this stabilization (This stems from the averaging over the azimuthal angles). Our result is then for the value of the isolated largest power λ that it is about $\lambda \sim (0.3 - 0.4)\alpha_0$ within a realistic cut-off region.

For the transverse momentum dependence of the structure function we will find the asymptotic solution $(\ln(k_\perp^2))^{\alpha_0/\lambda}$. Further, the transverse energy distribution along the chain will not, as for the BFKL case with a constant coupling, be Gaussian in $\log(k_\perp^2)$ with a width determined, as in a Brownian motion, from the "length" of the emission chains, i.e. $\log(1/x_B)$ [5]. Instead it will be a (negative) exponential in $\log(k_\perp^2)$, i.e. it will behave as an inverse power in the transverse momentum $k_\perp^{-2(2+\lambda)}$ with the same λ-value as above. (Note that the Rutherford parton scattering will behave as $k_\perp^{-4}$. The extra factor $k_\perp^{-2\lambda}$ is due to the larger x_B-values needed for higher $k_\perp$.) This is also born out by a Monte Carlo simulation.

It is a well-known property of diffusion equations with a force (in this case stemming from the running coupling which favours small $k_\perp$-values) that there are on the short time scale (for small $\log(1/x_B)$-values) an erratic behaviour, which can easily be mistaken for a stochastic Brownian motion, before the process reaches its long-time stable distribution. Our estimates of the scales in this case unfortunately indicate that the HERA range is too small for a

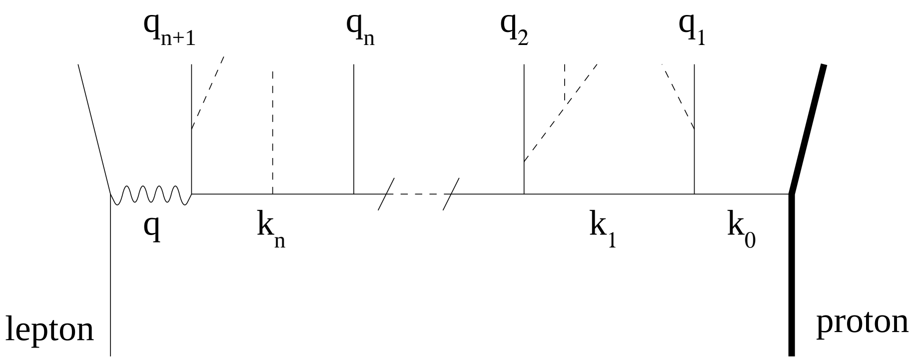

Figure 1: Fan diagram for a DIS event. q_i denote the emitted ISB partons, k_i denote the propagators and the dashed lines are the FSB partons.

noticeable change to the above-mentioned power behaviour in $k_\perp$.

We will end this note with a set of simple examples to show the way the model interpolates between the DGLAP [6] and the BFKL mechanisms, the reasons why and the mechanisms by which the stable distributions in transverse momentum emerge.

1.2 The CCFM- and the LDC-Models

To introduce the models we note that it is always possible to subdivide the radiation in the states into one part, the Initial State Bremsstrahlung (ISB) (denoted by the vectors q_j in Fig 1) and another part, the Final State Bremsstrahlung (FSB) (the dashed lines in Fig 1). The main requirement is that the FSB partons should be possible to emit in accordance with the QCD coherence conditions and with negligible recoils, if the ISB partons are already emitted. The observable emission weights are given by

$$dw = \sum_I dw^{(0)}(I)\Delta(I) \tag{1}$$

i.e. by the sum over the chosen ISB sets (I) with the basic weight $dw^{(0)}(I)$ to emit these particular partons and a form factor $\Delta(I)$ stemming from the radiative corrections from the choice. To be precise each (I)-state contains a sum over all the exclusive states, containing these ISB partons and any other FSB partons. The FSB should have the property that the corresponding form factors $Sud(F)$ are of the Sudakov type, meaning that, for each fixed (I)-state, the sum over all possible exclusive final states F becomes unity $\sum_F d\omega_I(F)Sud(F) = 1$.

If we ask for a particular value of the observables (Q^2, x_B), i.e. the (squared) "inverse wave-length characteristics of the probe" and the scaled energy-momentum, the Bjorken variable x_B, then we should in Eq (1) sum over the ISB sets, which end on such a configuration.

The choice of the ISB set in the CCFM model is to order all emissions in rapidity (due to the relation between angle and rapidity this means angular ordering, a well-known formulation of the QCD coherence conditions). Then CCFM chose as ISB the emissions with the property that there is no emission further along the rapidity ordering with a larger light-cone energy momentum q_{j+}. The ordering is done from the target-hadron side, i.e. the target is supposed to have a (large) positive light-cone energy-momentum $P \equiv (P_+, P_- \simeq 0, \vec{0}_\perp)$. In the probe-hadron cms the probe (with $-q^2 = Q^2$) has a large energy-momentum along the negative light-cone $q \equiv (-q_+, q_-, \vec{0}_\perp)$. This choice of the ISB is then consistent with QCD coherence but not with the fact that there should be symmetry between the hadron and the probe directions, [7].

Assuming that the recoils can be neglected, the ISB partons with momenta q_j are on their mass shells. Energy-momentum conservation at every ISB vertex implies that the connector vectors ("the propagators") k_j, cf. Fig 1, fulfill

$$k_j = P - \sum_1^j q_j \quad \text{ie} \quad k_j = k_{j-1} - q_j \tag{2}$$

CCFM introduce the variables $(z_j, \vec{q}_{\perp j})$ such that $k_{+j} = z_j k_{+(j-1)}$ and $\vec{k}_{\perp j} = \vec{k}_{\perp(j-1)} - \vec{q}_{\perp j}$. In the Leading Log Approximation (LLA), relevant for the CCFM model calculations, the fractional variables should fulfill $z_j \ll 1$, i.e. the splitting functions are approximated by $P(z) \sim 1/z$. While the emitted gluons along the fan diagram in Fig 1 are treated as mass less, the connector vectors k_j are space like with $-k_j^2 \simeq \vec{k}_{\perp j}^2$. This relation is satisfied provided

$$k_{\perp j}^2 > z_j q_{\perp j}^2 \tag{3}$$

while smaller $k_\perp$-values are suppressed. Then the weight and the form factor in Eq (1) is in the CCFM model

$$\bar{\alpha} \frac{dz}{z} \frac{dq_\perp^2}{q_\perp^2} \Delta_{ne}(z, k_\perp, q_\perp) \tag{4}$$

with the effective coupling $\bar{\alpha} = 3\alpha_s/\pi$ and the non-eikonal form factor

$$\Delta_{ne} = \exp(-\bar{\alpha} \ln(1/z) \ln(k_\perp^2 / z q_\perp^2)) \tag{5}$$

The LDC model choice in Ref [1] is to restrict the ISB emissions in the CCFM model to those which also fulfill

$$q_{\perp j} \geq \min(k_{\perp j}, k_{\perp(j-1)}) \tag{6}$$

Gluons which do not satisfy this constraint can be included in the FSB set causing only small recoils. If the ISB set is restricted in this way, and we sum over the corresponding weights and form factors it is in Ref [1] shown that we obtain *the same weight as in Eq (4) but with the non-eikonal factor exchanged for* 1. This is obviously a major simplification in order to calculate the cross sections according to Eq (1).

The second simplification comes with respect to the emission of the FSB radiation. *The FSB gluons are emitted as dipole radiation with the "original" dipoles spanned between the color-adjacent ISB gluons* (q_j, q_{j+1}) *and with the largest allowed FSB transverse momentum determined by the propagator virtuality* $-k_j^2 \simeq k_{\perp j}^2$. This means that we may for the FSB radiation make use of the well-known Lund Dipole Cascade model [8], as it is implemented in the Monte Carlo simulation program ARIADNE, [9].

The transverse momentum restrictions for the FSB emissions, i.e. that the allowed FSB transverse momentum is limited by the propagator $-k_j^2 \simeq k_{\perp j}^2$, occur also in the CCFM model and is a major result from their very complicated calculations, [2]. Physically it means that the two color adjacent gluon currents from the "dipole pair" (q_j, q_{j+1}) in the LDC model do not stem from the same space-time point. There is a distance, which due to Lorenz contraction is essentially transverse, $b_\perp \sim 1/\sqrt{-k_j^2}$. The constraint then stems from the difficulty to emit FSB radiation with a wave-length $\lambda \simeq 1/q_\perp < b$, i.e. smaller than the "antenna size". In other words there should be a form factor, which if it is e.g. an inverse power in $k_\perp$ is exponentially falling in the relevant $\ln(k_\perp^2)$-variable and therefore leads to negligible contributions to the LLA outside this region.

After azimuthal (ϕ) averaging for fixed $|\vec{k}_{\perp j-1}|$ and $|\vec{k}_{\perp j}|$ over the transverse pole in $\vec{q}_{\perp j}^{\,2} = (\vec{k}_{\perp j} - \vec{k}_{\perp (j-1)})^2$ we obtain with the constraint in Eq (6) (see Fig 2a) the LDC weights

$$\begin{aligned} dw(LDC) &= \bar{\alpha}\frac{dz_j}{z_j}\int \frac{d\phi dk_{\perp j}^2}{4\pi \vec{q}_{\perp j}^{\,2}}\theta\left(q_{\perp j} - \min\left(k_{\perp j}, k_{\perp (j-1)}\right)\right) \\ &= \bar{\alpha}\frac{dz_j}{z_j}\frac{dk_{\perp j}^2}{\max(k_{\perp j}^2, k_{\perp (j-1)}^2)} h(k_{\perp j}^2/k_{\perp (j-1)}^2) \end{aligned} \tag{7}$$

The function $h(a)$, which is obtained from the azimuthal integration, is given by (see Fig 2b)

$$\begin{aligned} h(a) &= \frac{(1 - \frac{2}{\pi}\arctan\left(\frac{1+\sqrt{a}}{1-\sqrt{a}}\sqrt{\frac{2\sqrt{a}-1}{2\sqrt{a}+1}}\right)\theta(a - 1/4))}{1-a}; \quad 0 < a < 1 \\ h(a) &= h(1/a) \end{aligned} \tag{8}$$

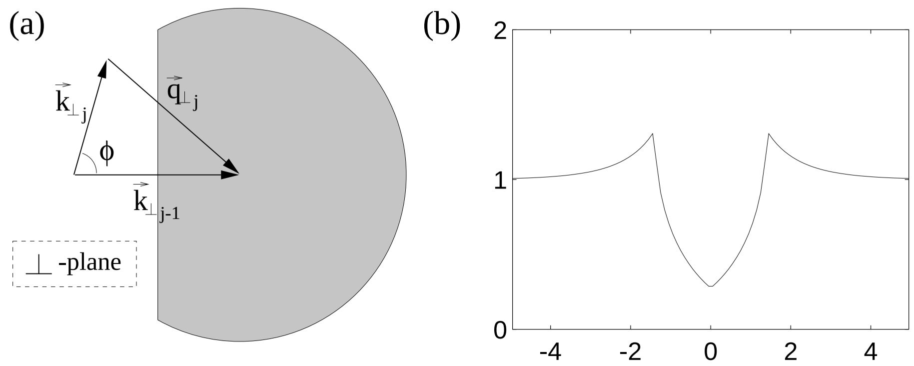

Figure 2: (a) The shaded area denotes the forbidden region for $\vec{k}_{\perp j}$ where $q_\perp < \min(\mathrm{k}_{\perp \mathrm{j}}, \mathrm{k}_{\perp \mathrm{j}-1})$. For $0.5 < k_{\perp j}/k_{\perp j-1} < 2$, the ϕ-integral is limited to a restricted region. (b) The azimuthal average h as a function of $\ln(k^2_{\perp j}/k^2_{\perp(j-1)})$.

As $dz_j/z_j = dy_j$, with y_j equal to the rapidity, we see that the expression in Eq. (7) is *completely symmetric, and the chain could equally well be generated from the probe end towards the target.* We also note that in the LLA in general $\ln(k^2_{\perp j}/k^2_{\perp(j-1)})$ is not close to 0 and then $h(a) \simeq 1$ (although we note that "at the pole" there is a dip $h(1) = \sqrt{3}/2\pi \simeq 0.28$). Thus in the LLA approximation (using $\kappa = \ln(k^2_\perp)$ and $\ell = \ln(1/z)$)

$$dw(LDC) \simeq \begin{cases} \bar{\alpha} d\ell_j d\kappa_j & \text{if } \kappa_j > \kappa_{j-1} \\ \bar{\alpha} d\ell_j d\kappa_j \exp(\kappa_j - \kappa_{j-1}) & \text{otherwise} \end{cases} \tag{9}$$

Therefore we obtain in the LDC model from Eqs (7) and (9) that *the weight distributions are local* (i.e. we may define a Markovian stochastic process). The locality property in particular implies that the process is simple to implement in a Monte Carlo generation program which simultaneously describes *both the structure functions and the final state properties.* Such a general program [10] is now available and is linked to ARIADNE and JETSET [11].

The above-mentioned symmetry implies that we may use either the fractional variable z_{+j} (from the target side) or z_{-j} (from the probe side) as variable in the Monte Carlo generation. In Refs [1] and [3] we have discussed the possibility to extend the scenario outside the LLA. The result is that it is necessary to choose the direction, i.e. to use z_+- or z_--generation, in accordance with the direction of increase in transverse momentum, i.e. in the virtuality, of the propagator. Then the use of the splitting functions in the proper light-cone fraction should contain many of the non-leading contributions to the structure function. The exact results for the radiative corrections are, however, not known in this case. Nevertheless the simplicity and symmetry of the result, i.e. the chain of linked dipoles (containing the FSB and then leading to hadronization in a

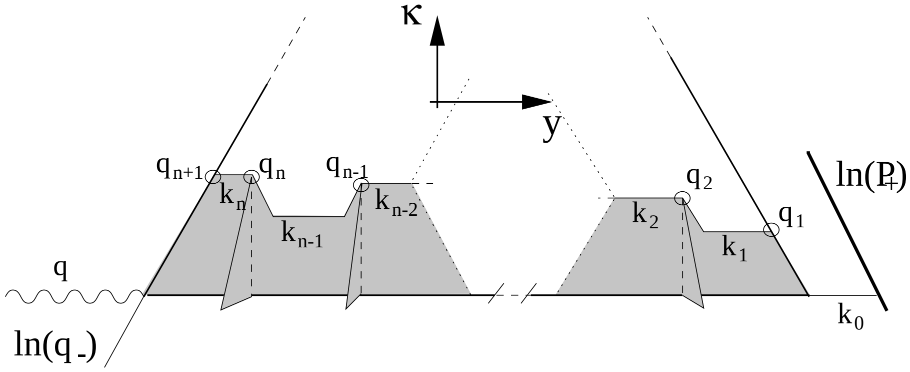

Figure 3: The Dipole phase space in DIS. The shaded area is the phase space for FSB.

similar way as in e^+e^--annihilation events) with the restriction of no emission above the corresponding propagator virtuality, seems physically appealing and stable.

In Fig 3 the fan diagram emissions in Fig 1 are described in the well-known Lund dipole phase space (which for any dipole is a triangle in (y, κ) with y the rapidity and with the height and the base-line size given by $\ln(M^2_{dipole})$). The whole fan emission must occur in between the lines corresponding to $\ln(P_+)$ for the target and $\ln(q_-)$ for the probe (fixed values of the light-cone energy momenta $\ln(k_\pm) = 1/2 \ln(k_\perp^2) \pm y$ correspond to straight lines in the triangle). The emitted gluons are described as extended triangular folds, starting at the (y, κ)-value of the on-shell gluon. The dipoles are spanned between the "tips" of these adjacent gluon folds, i.e. they again correspond to triangles (the two sides of the triangular folds correspond to the colour and anti-colour of the gluon, which are connected each to the two dipoles around the gluon corner). The emission region of each such dipole is limited by the maximum virtuality, which corresponds to the propagator $\ln(-k^2) \simeq \ln(k_\perp^2)$.

A propagator in this plot is specified by a horizontal line indicating its κ-value (transverse momentum) and with the "starting point" (right) given by the rapidity value $y_- \equiv \ln(-k_\perp/k_-)$ and the "end point" (left) given by $y_+ \equiv \ln(k_+/k_\perp)$. This means that the difference δy between the "endpoint" of one propagator and the "starting point" of the next is

$$0 \leq \delta y = \ln(k^2_{\perp max}) - \ln(k^2_{\perp min}) \tag{10}$$

For completeness we mention that inside the LDC model it is possible, Ref [1], to consider different sub-processes in DIS. Besides the "ordinary" parton model description with Q^2 exceeding all the other momentum transfers in the chains, there is the boson-gluon fusion process, where the the last splitting exceeds Q^2 and all the other ones. Finally in a Rutherford parton scattering process the largest momentum transfer, $k_{\perp max}^2$, will occur somewhere in the middle of the chain. Then we may consider the result of the dipole chain generation as the convolution of the target and the probe structure functions (each developed to the virtuality $-k_{max}^2$ with the Bjorken variables $x_\pm$, respectively) and multiplied by the well-known Rutherford transverse momentum pole $(k_{max}^2)^{-2}$. This also implies that such a Rutherford scattering $k_\perp$ must always be larger than all bremsstrahlung $k_\perp$ in the event. This constraint produces an effective cut-off for small $k_\perp$ Rutherford scattering.

2 The LDC Evolution Equations

2.1 Integral Equations

We study in this paper only purely gluonic chains, and we let the gluonic structure function $F(x, Q^2)$ denote the gluon density in $\ln(1/x)$. (Thus F/x is the density in x.) In this section we will treat the LDC evolution equation for the "non-integrated" structure function, $\mathcal{F}(x, k_\perp^2)$ defined by

$$F(x, Q^2) = \int_{k_{\perp cut}^2}^{Q^2} \frac{dk_\perp^2}{k_\perp^2} \mathcal{F}(x, k_\perp^2) + \int_{Q^2}^{Q^2/x} \frac{dk_\perp^2}{k_\perp^2} \frac{Q^2}{k_\perp^2} \mathcal{F}(x\frac{k_\perp^2}{Q^2}, k_\perp^2). \tag{11}$$

Here $k_\perp$ is the transverse momentum of the last link in the chain. We note that the contribution from chains with $k_\perp^2 > Q^2$ is suppressed by the factor $Q^2/k_\perp^2$, which makes it sub-leading. We also note the modified argument, $x \to x \cdot k_\perp^2/Q^2$, obtained for this term within the LDC model. Although less important this modification further suppresses this term.

From the weights in Eq (7) we find a recursive relation for $\mathcal{F}$, and in [1] we derived the following evolution equation:

$$\begin{aligned} \frac{\partial \mathcal{F}}{\partial \ell}(\ell, \kappa) &= \int_{\kappa_{cut}}^{\kappa} d\kappa' \bar{\alpha}(\kappa) h(\kappa - \kappa') \mathcal{F}(\ell, \kappa') \\ &+ \int_{\kappa} d\kappa' \bar{\alpha}(\kappa') h(\kappa' - \kappa) \exp[-(\kappa' - \kappa)] \mathcal{F}(\ell + \kappa - \kappa', \kappa') \end{aligned} \tag{12}$$

We have here used the variables $\ell = \ln(1/x)$ and $\kappa = \ln(k_\perp^2)$, introduced in the previous section. The function h defined in Eq (8) originates from the azimuthal integration in Eq (7). From now on we express h in the logarithmic variables κ and κ', and note that it depends only on the difference $|\kappa - \kappa'|$. (Note that in the LLA we can put $h = 1$. The argument of $\mathcal{F}$ in the second integral is explained in Eq (10)).

The first integral in Eq (12) corresponds to chains, where the last step is upwards in transverse momentum from κ' to κ, and the second integral, where κ' is larger than κ, to chains with a final step downwards. For the scale in the running coupling we have taken the largest virtuality in each vertex. Thus in the first integral we have $\bar{\alpha}(\kappa)$, while in the second term we have $\bar{\alpha}(\kappa')$.

With a running α_s the result will (as we will see in the following) be rather sensitive to the behaviour in the soft region for small $k_\perp$. Naturally a perturbative calculation cannot be trusted when α_s becomes very large. Lacking a good understanding of the soft region, some kind of cut-off is necessary, and in this paper we have studied the results obtained assuming a lower cut-off, $k_{\perp cut}$ or $\kappa_{cut} = \ln(k_{\perp cut}^2/\Lambda^2)$, in Eqs (11) and (12), while keeping the form $\bar{\alpha} = \alpha_0/\kappa$ for the coupling constant. (Another possibility would be to study the result assuming that α_s saturates for $k_\perp$-values below some cut.)

After a Mellin transform in x_B, which corresponds to a Laplace transform in ℓ with

$$f_\lambda(\kappa) = \int d\ell \exp(-\lambda\ell)\mathcal{F}(\ell,\kappa) \tag{13}$$

we obtain (we will in general neglect the index λ on f from now on)

$$\begin{aligned}\lambda f(\kappa) \;&=\; \int^{\kappa} d\kappa' \bar{\alpha}(\kappa) h(\kappa-\kappa') f(\kappa') \\ &+\; \int_{\kappa} d\kappa' \bar{\alpha}(\kappa') h(\kappa'-\kappa) \exp[-(\lambda+1)(\kappa'-\kappa)] f(\kappa') \end{aligned} \tag{14}$$

It is sometimes useful (cf section 4) to introduce a symmetric non-integrated structure function $\mathcal{F}_s$ by the definition

$$\mathcal{F}_s(\ell,\kappa) = \mathcal{F}(\ell,\kappa)\exp(-\kappa/2) \tag{15}$$

In that way the exponential suppression factor $\exp -(\kappa'-\kappa)$ in the second integral of Eq (12), which is "paid" only "for going down" in κ, is changed so that "we pay the same amount for going up as for going down" in κ.

2.2 The Case of a Fixed Coupling $\bar{\alpha}$

The case of a fixed coupling has been treated in Ref [1] (and also at many other places) and we will only briefly describe (some of) the results for future reference. We perform a Laplace transform with respect to κ, and define $\hat{f}$ by

$$\hat{f}(\gamma) = \int d\kappa \exp(-\gamma\kappa) f(\kappa) \tag{16}$$

As h is a function of $\kappa - \kappa'$, we actually work with a convolution integral, and pole-singularities are obtained in $\hat{f}$ at the γ-values (the "anomalous dimensions" for given λ) which satisfy

$$\lambda = \bar{\alpha}[g(\gamma) + g(\lambda + 1 - \gamma)] \quad \text{with} \quad g(\gamma) = \int_0^\infty d\Delta \exp(-\gamma\Delta) h(\Delta) \quad (17)$$

The two g-contributions stem from the two integrals in Eq (14), respectively. and $h(\Delta)$ is here interpreted as a function of the logarithmic variable $\Delta = \kappa - \kappa'$.

There are different levels of approximations possible to apply in the treatment of the Eqs (12), (14) and (17). The simplest one is to make use of the approximation in Eq (9) and to replace h by 1, which gives $g \approx 1/\gamma$. The function h deviates from 1 around the singular point $\ln(\kappa_j^2/\kappa_{j-1}^2) = 0$, and in an improved treatment we can describe this deviation by a δ-subtraction (cf ref [1]):

$$h \simeq \hat{h} = [1 - A\delta(\kappa - \kappa')] \quad (18)$$

Inserted into Eq (17) this gives

$$g(\gamma) \simeq \bar{\alpha}\,[1/\gamma - A/2] \;\Rightarrow\; \lambda \simeq \bar{\alpha}\,[\frac{1}{\gamma} + \frac{1}{\lambda + 1 - \gamma} - A] \quad (19)$$

If we fix A by the condition $\int(\hat{h}(\Delta) - 1)d\Delta = \int(h(\Delta) - 1)d\Delta$ we find $A \approx 0.65$. In g also other moments of h are important, and in ref [1] it was found that for $A \approx 0.8$ the same λ-value was obtained from the original h and the approximation $\hat{h}$.

We note that the BFKL result corresponds to a neglect of the λ-dependence in the second g-term in Eq (17). Although this is a sub-leading term, it is numerically not small, as discussed in Ref [1]. (There is also in BFKL a different method to regularize the singularity at $\ln(\kappa_j/\kappa_{j-1}) \sim 0$.)

In [1] we also pointed out another important non-leading effect. For consistency it is necessary that "the steps" in $\ln(1/z)$ really are large, but it turns out that there are essential contributions to the BFKL-integrals from eg $z > 1/2$. We return to this problem in section 3.2.

The x_B-dependence is then determined by the inverse Mellin (or Laplace) transform. The leading behaviour stems from a pinch singularity at $\lambda = \lambda_s$, when the two symmetrical solutions to Eq (17) coincide, i.e. when $\gamma = (1 + \lambda_s)/2$ (or $\gamma = 1/2$ if the λ-dependence in $g(\lambda + 1 - \gamma)$ is neglected.) From Eq (19) we find e.g. for $\bar{\alpha} = 0.2$ and $A = 0.8$ the result $\lambda_s \approx 0.41$ (neglecting the λ-dependence in g, we would instead obtain $\lambda_s \approx 0.64$), with the corresponding low-x_B behaviour $\sim x_B^{-\lambda_s}$.

When the inverse Laplace(Mellin)-transform is performed one also obtains the dependence on $k_\perp$ (or rather on $\kappa = \ln(k_\perp^2)$) by a saddle-point approximation around the pinch singularity. The result (besides essentially trivial kinematic factors) is a Gaussian in κ with a width $\sim\sqrt{\ln(1/x)}$, a result which can be interpreted as a kind of random walk in κ-space [5].

2.3 The Case of a Running Coupling $\bar{\alpha}$

For a running coupling, chains with larger κ-values are disfavoured by the smallness of α_s. This will imply that $<\kappa>$ does not increase beyond any bound as in the case with a fixed coupling. Instead the κ-distribution saturates, and for small x, $\mathcal{F}(x, k_\perp^2)$ approaches asymptotically a factorizing form

$$\mathcal{F}(x,\kappa) = x^{-\lambda} f(\kappa). \tag{20}$$

The result appears to be similar to the type of random walk an atmospheric molecule follows in the earth's gravitational field. In this case, when the molecules are constantly pulled downwards, an equilibrium is obtained for an exponentially decreasing density (see also the discussion in Appendix C). As discussed in section 3.3, also in our model with a running α_s the asymptotic $k_\perp$-distribution is an exponential in $\kappa = \ln k_\perp^2$. Inserting the asymptotic form in Eq (20) into Eq (12) implies that $f(\kappa)$ must satisfy Eq (14) above, now with $\bar{\alpha}(\kappa) = \alpha_0/\kappa$, where $\alpha_0 = 12/11$ if we study a purely gluonic situation with no quarks. The solution to this equation will be studied in the following section.

3 The Solution for Running Coupling

We have not been able to find an exact analytic solution to the integral equation (14). Instead we have solved it numerically, using Chebyshev polynomials to convert it to a matrix equation. This method was also used in ref [12], and is discussed further in appendix A. The x-dependence for small x-values is determined by the largest eigenvalue λ to this matrix equation.

In order to better understand the properties of the model we have also studied a set of approximations, which all agree with the original Eq (14) to leading logarithmic accuracy:

a) by using κ instead of κ' for the argument of $\bar{\alpha}$ in the second integral of Eq (14)

b) by using the approximation $h \approx (1 - A\delta(\kappa - \kappa'))$ in Eq (18). A special case (called b') with $A = 0$ corresponds to $h \to 1$.

c) with both of the approximations a) and b) (cf section 3.1). (Case c') corresponds to both approximations a) and b').)

The cases b') and c) can be studied analytically. Case b') is discussed in appendix B, and the simpler case c) will be discussed in section 3.1.

3.1 Qualitative properties

In order to understand the qualitative features of Eq (14) we start by investigating the approximation called c) above, which is obtained when $\bar{\alpha}(\kappa')$ is replaced by $\bar{\alpha}(\kappa)$ in the last integral of Eq (14), and the variation of h is approximated by a δ-function according to Eq (18). We note that both these approximations are of non-leading order, and the solution has properties similar to the solution of the original Eq (14). With these approximations the integral equation in Eq (14) can be transformed by straightforward differentiations into the second-order differential equation

$$u\frac{d^2f}{du^2} = [(\lambda+1)u - 2]\frac{df}{du} + (\lambda+1)(1-\mu)f \tag{21}$$

where $u = \kappa + \mu A$ and $\mu = \alpha_0/\lambda$. This is equivalent to (the radial part of) the Schroedinger equation for the hydrogen atom with the angular momentum variable $\ell = 0$. To see that, we introduce the function ψ defined by

$$f = \exp[(\lambda+1)/2)u]\psi(u) \tag{22}$$

We obtain by straightforward calculations

$$-\frac{1}{2}\frac{d^2(u\psi)}{udu^2} - \frac{\mu(\lambda+1)\psi}{2u} = -\frac{(\lambda+1)^2\psi}{8} \tag{23}$$

Thus the "mass"-value is unity and the (squared) "charge" equal to $\mu(\lambda+1)/2$.

For large values of κ (large values of u) the second term in Eq (23) can be neglected, and the solution behaves as $u\psi \sim \exp[\pm(1+\lambda)\kappa/2]$. Here the physical solution must correspond to the minus sign. From Eq (22) this implies that f varies as a power of κ for large κ-values. From the behaviour of eq. (21) for large u, ie large κ, we find

$$f \propto \kappa^{\frac{\alpha_0}{\lambda}-1}; \quad \kappa \text{ large} \tag{24}$$

The value of λ is determined by the boundary condition for small κ, which can be derived from the integral equation (14). (With the present approximation we find $f'(\kappa_{cut}) = [1+\lambda-1/(\kappa_{cut}+\mu A)]f(\kappa_{cut})$.) This implies that we have solutions for a discrete set of eigenvalues λ. The asymptotic behaviour of the solution is determined by the largest of these eigenvalues, which corresponds to a solution ψ with no zeros between κ_{cut} and ∞.

We note that since λ is fixed by the boundary condition, the result is sensitive to the value of κ_{cut}, i e it is sensitive to the soft region. When κ_{cut}

increases, the value of λ decreases continuously. Note, however, that if we include the correction term in h then this sensitivity to κ_{cut} is strongly reduced. As $\kappa = \kappa_{cut}$ implies $u_{cut} = \kappa_{cut} + \mu A$ we keep away from the singular point $u = 0$ in Eq (23), even when κ_{cut} approaches 0. This stabilizing effect of h will be further discussed in the following subsection.

For a *fixed* coupling we can from Eq (14) derive a differential equation similar to Eq (21). This equation does not, however, contain the factors u in front of d^2f/du^2 and df/du. Therefore this equation has two exponentially growing solutions, which implies that in this case the dependence of $\mathcal{F}$ upon x and κ does not factorize.

Summarizing we have found that the asymptotic behaviour of $\mathcal{F}$ is given by the form

$$\mathcal{F} \propto x^{-\lambda} \cdot \kappa^{\frac{\alpha_0}{\lambda}-1} \equiv x^{-\lambda} \cdot (\ln k_\perp^2)^{\frac{\alpha_0}{\lambda}-1}; \quad \ln(1/x) \gg \kappa \gg 1 \tag{25}$$

where the power λ is an eigenvalue determined by the boundary conditions. It turns out that these qualitative features do not rely on the approximations used in this subsection, but are also relevant for the solution to the original equation (14).

3.2 The x-dependence

We will now study the numerical solution to Eq (14). As the second integral is sub-leading, we see that for $\bar{\alpha} = \alpha_0/\kappa$ the eigenvalue λ will to first approximation be proportional to α_0. Since we are here studying only purely gluonic chains, and are not including quark links, it may be most consistent to use a value of α_0 which corresponds to a pure Yang-Mills theory. From the relation $\alpha_0 = 36/(33 - 2n_f)$ we find for a pure Yang-Mills $\alpha_0 = 12/11$ as compared to e.g. $\alpha_0 = 4/3$ for $n_f = 3$.

As we have not studied the influence from the quarks we present results for the more stable quantity λ/α_0. Thus in Fig (4) we show how λ/α_0 depends on the value of κ_{cut} in the range $0.01 < \kappa_{cut} < 2$ (To be exact the results presented correspond to $\alpha_0 = 12/11$ and for $\alpha_0 = 4/3$ they are about 4% smaller). Results are presented for the original equation (14) and also for the approximations a), b') and c') defined above. We see that the result is sensitive to both the soft cut-off, κ_{cut}, and to the non-leading modifications in the different approximations. We note, however, that the factor h in the LDC model provides a very strong stabilizing effect. Thus for the original non-approximated equation, the result is fairly stable in a range $0.5 < \kappa_{cut} < 2.0$, which ought to contain realistic values for κ_{cut}. In this range we find $0.3\,\alpha_0 < \lambda < 0.5\,\alpha_0$.

In the LLA the energy fractions z_i are assumed to be small compared to 1, and in ref [1] we pointed out that quantitatively significant contributions arise from large z-values. We here show that this is true also with a running

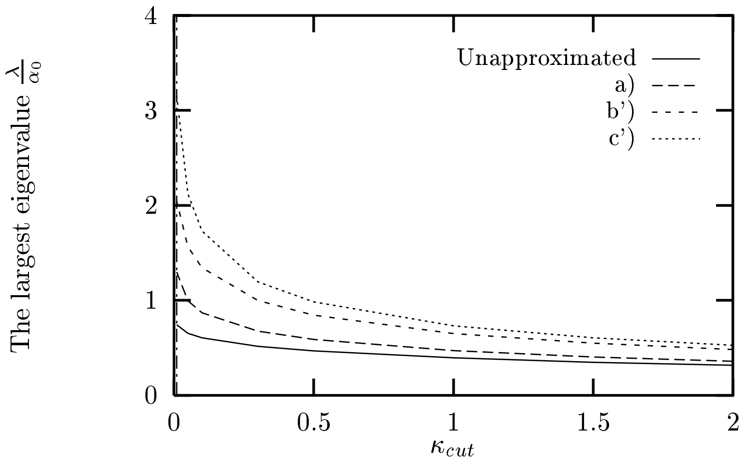

Figure 4: The dependence of λ/α_0 on κ_{cut}. The solid line is from eq. (14) without approximations. The other lines are for the approximations a, b' and c' from down and up. As the calculations do not include quarks we have presented results for the more stable ratio λ/α_0, where $\alpha_0 = 12/11$ for $n_f = 0$ and $\alpha_0 = 4/3$ for $n_f = 3$.

coupling. For the splitting function, we have in the weights in Eq (7) used $P(z) \propto 1/z$, which is correct within the leading log approximation. The full splitting function without regularization for $z = 1$ reads

$$P(z) = 2N_c \left\{ \frac{1-z}{z} + \frac{z}{1-z} + z(1-z) \right\} \tag{26}$$

If inserted in an evolution equation, the pole at $z = 1$ has to be regularized. Virtual corrections imply that this pole does not contribute to the increase of the cross section (ie the structure functions) for increasing Q^2. One way to interpret this is to note that in the gluon splitting process the "old" gluon disappears and is replaced by two "new" gluons. Thus only one new extra gluon is produced, and values of z close to the pole $1/(1-z)$ corresponds to the original gluon losing some of its energy. Thus this contribution does not increase the cross section, but only "shifts it" to slightly smaller x-values.

In the LLA the energy fraction z, which corresponds to the "new" gluon, is assumed to be small. If we want to reduce recoils as much as possible, we can say that the "new" gluon by definition is the one with least energy, which must imply that $z < 0.5$ (c.f. ref.). Therefore it might be sensible to replace the factor $1/z$ in the weight in Eq (7) by $(1/2N_c)P(z)\theta(0.5-z)$. To get some estimate of this effect we note that $P(z)/2N_c$ is smaller than $1/z$ in

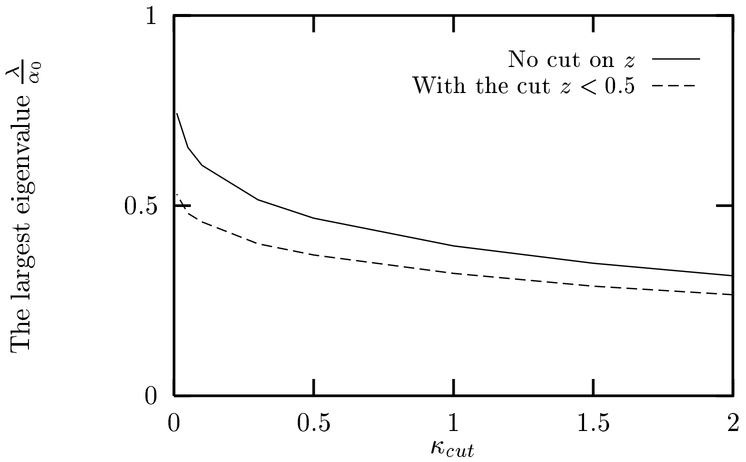

Figure 5: The dependence of λ/α_0 on κ_{cut}. The solid line is for the default splitting function. The dashed line is for $P(z > 0.5) = 0$. As in Fig (4) we present results for the more stable ratio λ/α_0.

most of the region $0 < z < 0.5$. (Actually $P(z)/2N_c - 1/z$ is positive only for $z > 0.43$, and also here it is fairly small.) Therefore to estimate qualitatively the consequence of this non-leading effect, we have studied the changes obtained from the replacement $1/z \to 1/z \cdot \theta(0.5 - z)$. It is straightforward to show that this change will give an extra factor 2^λ to the left hand side of Eq (14), which means that λf will be replaced by $2^\lambda \lambda f$. Apparently, this leads to smaller values of λ with an approximate factor $2^{-\lambda} \approx 1/\sqrt{2}$. In Fig 5, we compare $\lambda(\kappa_{cut})$ for the two alternative splitting functions. This non-leading correction is clearly significant, reducing λ by 20-25%.

We have also checked that the largest eigenvalue is well separated from the smaller ones (see Fig 6). Thus for $\kappa_{cut} = 1$ we find for the largest and the second largest eigenvalue the values $0.4\ \alpha_0$ and $0.2\ \alpha_0$. Thus for $\ln(1/x) \gtrsim 5$ the non-leading contribution should be supressed by a factor e^{-1} (and for $\ln(1/x) \gtrsim 10$ by a factor e^{-2}).

3.3 Transverse Momentum Dependence

In Fig 7 we show the solution to the original equation (14) together with approximation b'), which corresponds to the replacement $h \to 1$. It is easy to demonstrate that in all cases $f(\kappa)$ and $\mathcal{F}$ have asymptotically the same powerlike behaviour as the simpler approximation studied in section 3.1, Eqs (24) and (25).

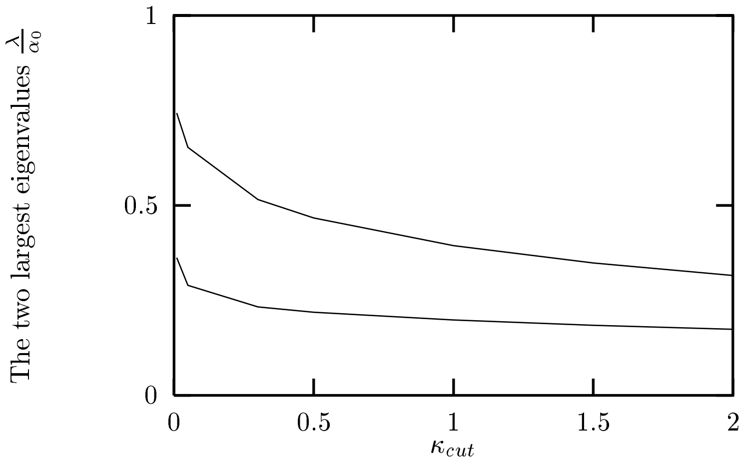

Figure 6: The two largest eigenvalues, as a function of κ_{cut}

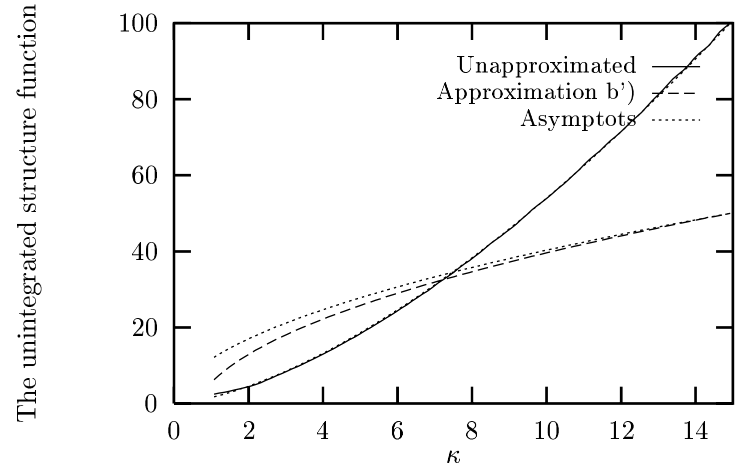

Figure 7: The solution $f(\kappa)$ to the integral eqaution (14) (solid line) and for the approximation b') (dashed line) together with the asymptotic forms.

We note, however, that the parameter λ takes on different values in the different approximations. If we calculate the first correction term to f in an expansion in $1/\kappa$

$$f(\kappa) \propto \kappa^{\frac{\alpha_0}{\lambda}-1}\left(1 + b\kappa^{-1} + \mathcal{O}(\kappa^{-2})\right) \tag{27}$$

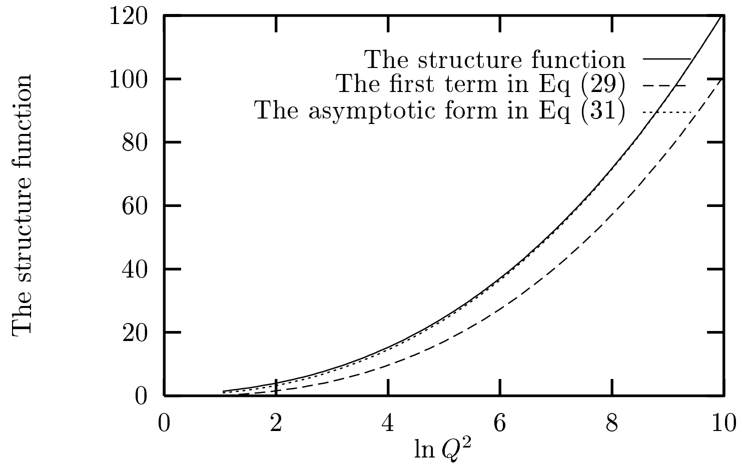

Figure 8: The $\ln Q^2$-dependence of the structure function. The dashed line is the contribution from the first term in Eq. (29). The dotted line is the contribution from the two first terms in the power expansion in Eq (31).

we obtain

$$b = -\frac{\alpha_0(\alpha_0 - \lambda)}{\lambda}\left[\frac{1}{1+\lambda} - \mathcal{A}\right] \quad \text{where} \quad \mathcal{A} = \int (1 - h(\Delta))d\Delta \approx 0.65 \tag{28}$$

For $\lambda \approx 0.4$, b is very small, and from Fig 7 we see that the single power in Eq (24) is a surprisingly good approximation in the whole κ-range. (For the approximation b') with $h \to 1$, we have $\mathcal{A} = 0$, and the correction term becomes much larger, as is also seen in Fig 7.)

We note that the powerlike dependence on κ for f and $\mathcal{F}$ implies a similar power dependence also for the original "integrated" structure function F. For small x we have from Eqs (20) and (11)

$$\begin{aligned} F &= x^{-\lambda}\tilde{F}(\ln Q^2) \\ \tilde{F} = \int_{\kappa_{cut}}^{\ln(Q^2)} f(\kappa)d\kappa &+ \int_{\ln(Q^2)} e^{(1+\lambda)(\ln(Q^2)-\kappa)} f(\kappa)d\kappa \end{aligned} \tag{29}$$

The result is presented in Fig 8, which also shows the separate contributions in Eq (29). These contributions correspond to chains with $k_\perp^2 < Q^2$ and $k_\perp^2 > Q^2$ respectively, where $k_\perp$ is the transverse momentum of the last link in the chain.

Inserting the asymptotic expression in Eq (27) we find for large Q^2

$$F \propto x^{-\lambda}(\ln Q^2)^{\alpha_0/\lambda}; \quad \ln(1/x) \gg \ln(Q^2) \gg 1 \tag{30}$$

For large Q^2 the first integral in eq (29) dominates, and for this term the single power in Eq (30) is a good approximation. The second integral is suppressed by the factor $\frac{\alpha_0}{\lambda(1+\lambda)} \cdot \frac{1}{\kappa}$, which for $\ln Q^2 = 10$ is about 20% , but becomes relatively more important for smaller Q^2. Thus, if we use the power expansion of f in Eq (27), we get for $b \approx 0$ the better estimate

$$\tilde{F} \propto (\ln Q^2)^{\frac{\alpha_0}{\lambda}} \left[1 + \frac{\alpha_0}{\lambda(1+\lambda)} \cdot \frac{1}{\ln Q^2} + \mathcal{O}\left((\ln Q^2)^{-2}\right)\right] \tag{31}$$

To better illustrate the $k_\perp$-dependence of the chain, we have studied a very long chain in order to find out where this chain passes the central line $y = 0$. It is straight forward to show that the density ρ (in the (y,κ)-plane) of all the right hand endpoints of the horizontal lines in the diagram in Fig 3, is given by the expression

$$\rho = F(\ell_1, \kappa) \cdot \mathcal{F}(\ell_2, \kappa) \cdot \exp(-\kappa) \tag{32}$$

where $\ell_1 = \ln W - \kappa/2 + y$, $\ell_2 = \ln W - \kappa/2 - y$ and W equals the total cms energy of the chain. The non-integrated function $\mathcal{F}(\ell_2, \kappa)$ describes the weight for the chains coming from left in Fig 3 to the point (y, κ), while the normal structure function $F(\ell_1, \kappa)$ adds up the contributions from links with all possible values of κ', both those larger than κ and those smaller than κ. Inserting the asymptotic expressions in Eqs (25) and (30) we find the following result (the factor $\exp(-\lambda\kappa)$ comes from the κ-dependences of ℓ_1 and ℓ_2)

$$\rho \sim \kappa^{\frac{2\alpha_0}{\lambda} - 1} e^{-(1+\lambda)\kappa}; \;\; W \,\text{and}\, \kappa \;\text{large} \tag{33}$$

In Fig 9 we present the results from a Monte Carlo simulation for different energies W of the quantity ρ in Eq (32). We note that the distribution has the expected approximate exponential fall off $\sim \exp[-(1+\lambda)\kappa]$, in accordance with Eq (33) and this corresponds to a (negative) power dependence in $k_\perp$ for the density ρ. Further the curve has the same slope independent of the total energy W, consistent with an asymptotically factorizing dependence on x and $k_\perp$, i.e. there is no sign of the expected BFKL diffusion in κ. The dashed line in Fig 9 shows the asymptotic form in Eq (33).

For comparison we also show in Fig 9 the result for a constant coupling $\bar{\alpha} = 0.2$. Here we find a Gaussian distribution with a width increasing with the energy ($\sim \sqrt{\ln 1/x}$), as expected from a random walk.

4 Dominating Paths in Transverse Momentum

The result in Eq (30) is particularly interesting if we compare to a result obtained in [3], where we study the mean paths of the initial state cascade in the

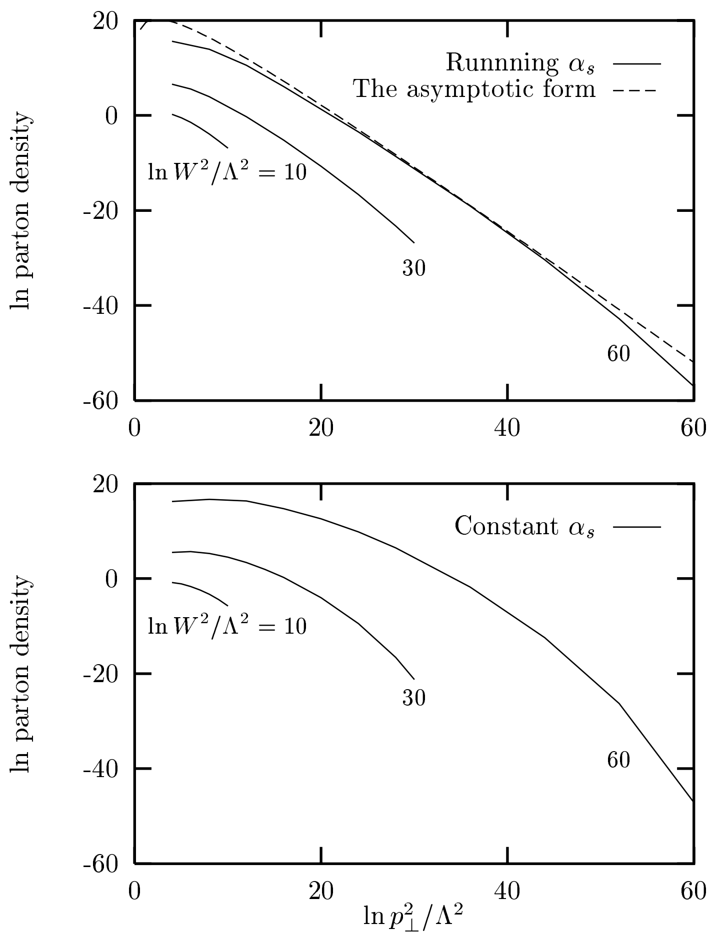

Figure 9: Transverse momentum distributions in the centre of a long chain for different values of hadronic central mass W for running vs. fixed α_s.

(ℓ, κ)-plane. We find that due to the running coupling the region covered by the major contributions (nowadays known as the "Bartel cigar") corresponds to one part, length ℓ_1, with small κ-values and with a BFKL-like contribution, $\simeq\exp(\lambda\ell_1)$ and a second part, length $\ell_2 = \ell - \ell_1$, corresponding to increasing κ-values up to the final $\kappa_Q \equiv \ln(Q^2)$. This second part is a DGLAP contribution, $\simeq\exp(2\sqrt{\alpha_0\ell_2\chi_Q})$, where $\chi_Q = \ln(\kappa_Q)$. Using a saddle-point approximation we demonstrated that the combination of the two parts corresponds for

$\lambda\ell > \alpha_0\chi_Q/\lambda$ to

$$\mathcal{F} \sim \exp(\lambda\ell + \alpha_0\chi_Q/\lambda) \tag{34}$$

which is identical to our result from Eq (30).

For $\lambda\ell < \alpha_0\chi_Q/\lambda$ the DGLAP chains dominate, because in this case the saddle-point is not within the the allowed integration region. We note that this result implies that the BFKL behaviour is relevant only for rather small x-values, $x \sim 10^{-5}$ for $Q^2 \sim 100$ GeV^2.

We will end by showing that for small x-values the very construction of the LDC chains leads to a simple result of the BFKL kind. In the LDC model it is possible to go "up" and "down" in κ along the chains, and thus the total chain can be divided into "cells", where each cell contains a set of up-steps followed by another set of down-steps. Let us study one such cell, which starts in the point at (y_1, κ_1), goes up to a maximum point (y', κ'), and then goes down to the endpoint (y_2, κ_2). We note that this second part corresponds to up-steps from the probe side, and therefore both pieces correspond to "DGLAP-chains".

To describe the path we generalize the structure function $\mathcal{F}$ to a function $\mathcal{F}(\ell, \kappa_2, \kappa_1)$, which describes the sum of all paths, which start at a virtuality given by κ_1 (which may now be different from κ_{cut}) and end at κ_2. It is also convenient to include the exponential factor in Eq (32) into the structure function, and define a "symmetrized structure function" $\mathcal{F}_s$ by the relation

$$\mathcal{F}_s(\ell, \kappa_2, \kappa_1) = e^{-(\kappa_2-\kappa_1)/2}\mathcal{F} \tag{35}$$

If expressed in the rapidity separation between the two endpoints, $\delta y = \ell + (\kappa_2 - \kappa_1)/2$, this function is fully symmetric with respect to the direction of the chain. The result for a long chain is also the direct product of the separate pieces.

Inserting the DGLAP-result for the two sections in the cell, and integrating over possible intermediate points (y', κ') we find

$$\begin{aligned}
&\mathcal{F}_{s,cell}(\delta y = y_2 - y_1, \kappa_2, \kappa_1) \\
&\approx e^{-(\kappa_2-\kappa_1)/2} \int d\kappa' dy' e^{-(\kappa'-\kappa)} \mathcal{F}_{DGLAP}(\ell_1, \kappa', \kappa_1)\mathcal{F}_{DGLAP}(\ell_2, \kappa', \kappa_2) \\
&where\ \ \ell_1 = y' - y_1 - (\kappa' - \kappa_1)/2; \ \ \ell_2 = y - y' - (\kappa' - \kappa_2)/2
\end{aligned} \tag{36}$$

We start by considering the simpler case with a fixed coupling $\bar{\alpha}$, for which we have

$$\mathcal{F}_{DGLAP}(\ell, \kappa', \kappa_1) \simeq exp(2\sqrt{\bar{\alpha}\ell(\kappa' - \kappa_1)}) \tag{37}$$

Inserted into Eq (36) this gives

$$\begin{aligned}\mathcal{F}_{s,cell} &\approx \int dy' d\kappa' \times \\ &\times \quad \exp[2\sqrt{\bar{\alpha}\ell_1(\kappa'-\kappa_1)} + 2\sqrt{\bar{\alpha}\ell_2(\kappa'-\kappa_2)} - \kappa' + \kappa_2/2 + \kappa_1/2]\end{aligned} \tag{38}$$

where ℓ_1 and ℓ_2 are given by Eq (36). This integral can be solved by stationary-phase methods, i.e. we look for the saddle-point in the integrand exponent. After a little algebra we find the surprisingly simple result that

$$\mathcal{F}_{s,cell} \simeq \exp[(R-1)\delta y/2] \quad \text{with} \quad R = \sqrt{1+8\bar{\alpha}} \text{ and } \delta y = y_2 - y_1 \tag{39}$$

Thus the contribution from one cell depends only upon the rapidity difference between the starting point and the endpoint. This also means that this result can be easily generalized to any number of cells.

A closer examination tells us, however, that the maximum is only obtained within the integration region if δy is large compared to $\delta\kappa = \kappa_2 - \kappa_1$. There will be a dividing line with

$$\delta\kappa = \frac{R-1}{R}\delta y \tag{40}$$

(where R is defined in Eq (39)) with the property that for smaller κ-values there is a saddle-point but for larger κ the main contribution is a single DGLAP-motion always directed upwards in κ. For κ below the line the result is obviously of the BFKL kind, i.e. there is (besides the symmetrical κ-dependence) an effective $x^{-\lambda_e}$ behaviour, but this time with $\lambda_e = (R-1)/2 \simeq 0.3$ for our "conventional" value of $\bar{\alpha} \simeq 3/\pi \times 0.2$.

For a running coupling, cells which go very high up in κ are suppressed. Therefore the cells will have limited sizes, both in κ and in y, and for very small x the number of cells will be proportional to the total rapidity range, $\ln(1/x)$. The result becomes a BFKL-like power-dependence on $1/x$ but a saturating distribution in κ, which is described by the limited κ-distribution in a single cell, a behaviour which is in agreement with our results in section 3. The dividing line in Eq (40) will be relevant in the region not too far from the target end, before the κ-distribution saturates for very large rapidity separations.

5 Conclusions

We have shown that if we introduce a running coupling $\bar{\alpha} = \alpha_0/\kappa$ into the integral equations for the gluon structure function in the LDC model then

- for the non-integrated structure function $\mathcal{F}(\ell \equiv \ln(1/x), \kappa \equiv \ln(k_\perp^2))$ we obtain a factorizing BFKL-like behaviour

$$\mathcal{F}(\ell, \kappa) \simeq \exp(\lambda_m \ell) f_{\lambda_m}(\kappa) \tag{41}$$

where the largest eigenvalue λ_m is isolated. It depends upon the soft cutoff κ_c but takes on stable values $\lambda_m \simeq 0.4\,\alpha_0$ for $0.5 \leq \kappa_c \leq 2$. Further a very good approximation for f_{λ_m} valid for $\kappa > \kappa_c$ is

$$f_{\lambda_m} \simeq \kappa^{\alpha_0/\lambda_m - 1} \tag{42}$$

- For the (integrated) structure function $F(\ell \equiv \ln(1/x), \kappa_Q \equiv \ln(Q^2))$ we then obtain, again as a good approximation for large ℓ, $(\lambda_m \ell > \alpha_0 \ln(\kappa_Q)/\lambda_m)$

$$F(\ell, \kappa_Q) \sim \mathit{const} \cdot \exp(\lambda_m \ell + \alpha_0 \ln(\kappa_Q)/\lambda_m) \tag{43}$$

which, as it is demonstrated in [3], corresponds to an interpolation between the BFKL and DGLAP mechanisms. For $\alpha_0 \ln(\kappa_Q)/\lambda_m > \lambda_m \ell$ the DGLAP mechanism dominates and there is evidently according to Eq (43) a smooth turnover to DGLAP when $\alpha_0 \ln(\kappa_Q)/\lambda_m = \lambda_m \ell$.

- The expected BFKL-diffusion in κ (with ℓ as the "time"-variable) is not noticeable in the model. For large values of ℓ we obtain in the center of phase space a saturating κ-distribution (valid at least for $\kappa > 2$)

$$\rho d\kappa \simeq d\kappa \kappa^{2\alpha_0/\lambda_m - 1} \exp\left[-(\lambda_m + 1)\kappa\right] \simeq \frac{dk_\perp^2}{k_\perp^{4+2\lambda_m}} \bar{\alpha} \cdot (\ln(k_\perp^2))^{2\alpha_0/\lambda_m} \tag{44}$$

which may be characterized as a kind of "renormalized Rutherford cross section".

A Numerical Method for Solving the Integral Equation

We will here briefly describe the method of using Chebyshev polynomials for solving the integral equation (14).

The Chebyshev polynomials are defined by

$$T_n(x) = \cos n(\arccos x), -1 < x < 1$$

and obey the orthogonality relation

$$\int_{-1}^{1} \frac{T_m(x)T_n(x)}{\sqrt{1-x^2}} = \begin{cases} 0, m \neq n \\ \frac{\pi}{2}, m = n \neq 0 \\ \pi, m = n = 0 \end{cases} \tag{45}$$

The eigenfunction and the kernel of the integral equation (times a factor $\sqrt{1-x'^2}$, because of the weight factor in the orthogonality relation) are expanded in Chebyshev polynomials, up to a certain degree N, thus converting the integral equation to an approximately equivalent matrix equation. Usually, we are interested in the largest eigenvalue and the corresponding eigenfunction.

For practical reasons, we must approximate the upper limit in the integral equation with a large number which we have set to $\kappa_{max} = 100$. No significant dependence on the value of $\kappa_{max} > 50$ has been noted.

Normally, the error in the largest eigenvalue λ is less than 1% for the number of polynomials $N > 50$ but we have used up to 320 polynomials to get a good description of the eigenfunctions for large κ-values.

In this work, we have used computer code from Numerical Recipes [13].

B Analytic Solution to the Approximated Integral Equation

In this appendix we will present an analytic solution to the integral equation:

$$\lambda f(\kappa) = \bar{\alpha} \int_{\kappa_{min}}^{\kappa} f(\kappa')d\kappa' + e^{(\lambda+1)\kappa} \int_{\kappa}^{\kappa_{max}} \bar{\alpha} f(\kappa') e^{-(\lambda+1)\kappa'} d\kappa', \tag{46}$$

with a running coupling $\bar{\alpha}(\kappa) = \alpha_0/\kappa$. This corresponds to approximation b') in section 3.2 where h is replaced by 1.

For finite κ_{min}, κ_{max} the integral equation is solved by rewriting it to a standard differential equation with solutions which are expressed in confluent hyper geometric functions. Using the boundary condition at κ_{max} and taking the limit $\kappa_{max} \to \infty$, we find that solutions to the integral equation have the asymptotic ($\kappa \to \infty$) behaviour $f(\kappa) \sim \kappa^{\frac{\alpha_0}{\lambda}-1}$. Using also the boundary condition at κ_{min}, the largest eigenvalue can be found as a function of κ_{min}. No simple relation for $\lambda(\kappa_{min})$ is found so it is evaluated numerically. The results are in agreement with the numerical solution of the integral equation.

We start by changing variables to $u = (\lambda + 1)\kappa$ to get rid of λ from the right hand side of the integral equation (46) which becomes

$$\frac{\lambda}{\alpha_0}\tilde{f}(u) = \frac{1}{u}\int_{u_{min}}^{u} \tilde{f}(u')du' + e^u \int_{u}^{u_{max}} \frac{e^{-u'}}{u'}\tilde{f}(u')du'. \tag{47}$$

This can be rewritten to the differential equation

$$\left(\frac{\tilde{f}' - \tilde{f}}{-\frac{1}{u^2} - \frac{1}{u}} \right)' = \frac{\alpha_0}{\lambda} \tilde{f}. \tag{48}$$

With

$$y(u) \equiv \frac{\tilde{f}' - \tilde{f}}{-\frac{1}{u^2} - \frac{1}{u}} \Rightarrow f(\kappa) = \tilde{f}(u) = \frac{\lambda}{\alpha_0} y'(u),$$

it can be rewritten to the following differential equation for $y(u)$

$$y'' - y' + \left(\frac{1}{u^2} + \frac{1}{u} \right) \frac{\alpha_0}{\lambda} y = 0. \tag{49}$$

Two linearly independent solutions are given by the real and imaginary part of the function (see e.g. Ref [14])

$$\tilde{M}(u) \equiv \frac{\Gamma\left(\frac{1}{4} - \nu^2 + i\nu\right)}{\Gamma\left(1 + i2\nu\right)} u^{\frac{1}{2}+i\nu} M\left(\frac{1}{4} - \nu^2 + i\nu, 1 + i2\nu; u \right),$$

where $\nu \equiv \sqrt{\frac{\alpha_0}{\lambda} - \frac{1}{4}}$ and M is the standard notation of the confluent hyper geometric function:

$$M(a, b; u) = \sum \frac{a(a+1)\cdots(a+n-1)}{b(b+1)\cdots(b+n-1)} \frac{u^n}{n!}.$$

The real and imaginary parts of $\tilde{M}$ have the asymptotic behaviour

$$\begin{aligned} y_1(u) \equiv \mathrm{Re}\left[\tilde{M}(u)\right] &\sim u^{-\frac{\alpha_0}{\lambda}} e^u \\ y_2(u) \equiv \mathrm{Im}\left[\tilde{M}(u)\right] &\sim u^{\frac{\alpha_0}{\lambda}} \end{aligned} \tag{50}$$

To find the boundary conditions from the integral equation we insert the differential operator in the left hand side of eq. (48) into the integral equation. The boundary conditions are

$$\begin{aligned} \left[\frac{\tilde{f}' - \tilde{f}}{-\frac{1}{u^2} - \frac{1}{u}} \right]_{u=u_{min}} &= 0 \\ \left[e^{-u} \frac{u\tilde{f}' + \tilde{f}}{1+u} \right]_{u=u_{max}} &= 0. \end{aligned} \tag{51}$$

From the second boundary condition, we see that the power solution (y_2 in Eqs. (50)) becomes more and more important as $u_{max} \to \infty$. This means that solutions to the integral equation have the asymptotic behaviour $f(\kappa) \sim \kappa^{\frac{\alpha_0}{\lambda}-1}$.

Having singled out y_2, we use the lower boundary condition, which simply means $y(u_{min}) = 0$, to find a relation between the largest eigenvalue λ and κ_{min}. For each λ, κ_{min} is given by the largest zero of the function $y_2(u)$.

Also in standard notations, the function $y_2(u)$ can be written (apart from a constant factor)

$$y_2(u) = u^{\frac{1}{2}+i\nu} U\left(\frac{1}{4} - \nu^2 + i\nu, 1 + i2\nu; u\right),$$

where U has the following definition:

$$U(a,b;u) \equiv \frac{\pi}{\sin \pi b}\left[\frac{M(a,b;u)}{(a-b)!(b-1)!} - \frac{u^{1-b}M(a+1-b, 2-b; u)}{(a-1)!(1-b)!}\right].$$

The solution $y_2(u)$, having a zero at $u = u_{min}$, is equivalent to requiring

$$\mathrm{Arg}\left[\tilde{M}(u_{min})\right] = -n\pi, \tag{52}$$

with n an integer. For very small u_{min} it is sufficient to include the leading term in an expansion of $\tilde{M}$. In this case eq. (52) can be approximated by the relation

$$\ln u_{min} = -\frac{n\pi}{\nu},$$

which means that $n = 1$ is relevant for the largest zero. A less severe approximation (for finite u_{min}) is given by using the first three terms in the expansion of $M(a,b;u)$ and evaluating $\mathrm{Arg}[\tilde{M}(u_{min})]$ numerically. This leads to an approximate relation between κ_{min} and the largest eigenvalue λ, which agrees well with the numerical solution discussed in appendix A.

C Random walk analogy

As mentioned in the main text, for a running coupling constant the chain has similarities with a random walk in a force field. Let us first study a simple example to show what happens if a stochastic process of the Brownian motion type contains a "force". Consider a set of discrete "space-locations" indexed $1, \ldots, j, \ldots$ and assume that at the discrete "times" $t = 1, \ldots, a, \ldots$ there is a number of "objects", $n(t = a, j)$ at the location indexed j. Assume further that there is a rule so that the number of objects changes with time according to

$$n(a+1, j) = \frac{1+\alpha}{2} n(a, j+1) + \frac{1-\alpha}{2} n(a, j-1) \tag{53}$$

Thus there is for a positive α a tendency for the sites with a larger space index to lose to the sites with a smaller index as the time goes by, i.e. the change in the distribution contain a "force" directed towards small space indices.

The equation can (by subtraction of $n(a,j)$ on both sides and a limiting procedure in space x and time t) be rewritten into (the space-size and time-size parameters are d and τ, respectively)

$$\frac{\partial n}{\partial t} = \frac{d^2}{2\tau}\frac{\partial^2 n}{\partial x^2} + \frac{\alpha d}{\tau}\frac{\partial n}{\partial x} \tag{54}$$

For $\alpha = 0$ we obtain the well-known diffusion equation for n, i.e. a Gaussian with an average and a width both increasing with time $\sim \sqrt{t}$. For $\alpha > 0$ we find, however, that starting with a narrow distribution at $t = 0$, the last term in Eq (54) becomes increasingly important when t increases. Thus the time derivative becomes reduced. For $t > \tau/\alpha^2$ the two terms on the right hand side become of equal magnitude in the dominating interval around $x = d\sqrt{t/\tau}$. This implies that the solution approaches the time-independent distribution

$$n \simeq \exp(-\alpha x/d) \tag{55}$$

This is just what happens for e.g. the atmospheric density of the earth.

This example is not totally a relevant one for the BFKL mechanism because the occurring weight distribution has no simple probabilistic interpretation (although positive definite it is non-normalized as the weight corresponds to a density). Nonetheless there are obvious similarities, all weights contain the notion of a "direction", in this case a preferred direction towards small κ-values in the cascade chains because of the running coupling, and the result is asymptotically an exponential distribution in κ.

References

[1] B. Andersson, G. Gustafson, J. Samuelsson, *Nucl. Phys.* **B463** (1996) 217.

[2] M. Ciafaloni, *Nucl. Phys.* **B269** (1988) 49;
S. Catani, F. Fiorani, G. Marchesini, *Phys. Lett.* **B234** (1990) 339, *Nucl. Phys.* **B336** (1990) 18.

[3] B. Andersson, G. Gustafson, H. Kharraziha and J. Samuelsson, *Z. Phys.* **C71** (1996) 613.

[4] E.A. Kuraev, L.N. Lipatov and V.S. Fadin, *Zh. Eksp. Teor. Fiz.* **72** (1977) 373, *Sov. Phys. JETP* **45** (1977) 199;
Ya.Ya. Balitsky and L.N. Lipatov, *Yad. Fiz.* **28** (1978) 1597, *Sov. J. Nucl. Phys.* **28** (1978) 822.

[5] J. Kwiecinski et al.,*Phys. Rev.* **D50** (1995) 217

[6] V.N. Gribov, L.N. Lipatov, *Sov. J. Nucl. Phys.* **15** (1972) 438 and 675;
G. Altarelli, G. Parisi, *Nucl. Phys.* **B126** (1977) 298;
Yu.L. Dokshitzer, *Sov. Phys. JETP* **46** (1977) 641.

[7] Yu.L. Dokshitzer, V.A. Khoze, A.H. Mueller and S.I. Troyan, Basics of Perturbative QCD (Editions Frontiéres, Gif-sur-Yvette, 1991)

[8] G. Gustafson, *Phys. Lett.* **B175** (1986) 453;
G. Gustafson, U. Petterson, *Nucl. Phys.* **B306** (1988) 746;
B. Andersson, G. Gustafson, L. Lönnblad, *Nucl. Phys.* **B339** (1990) 393.

[9] L. Lönnblad, *Comp. Phys. Comm.* **71** (1992) 15.

[10] H. Kharraziha, L. Lönnblad, LU-TP 97-21, H. Kharraziha, L. Lönnblad, LU-TP 97-34

[11] T. Sjöstrand, *Comp. Phys. Comm.* **82** (1994) 74

[12] J. Kwiecinski, A.D. Martin, P.J. Sutton, *Phys. Rev.* **D52** (1995) 1445

[13] W.H. Press, S.A. Teukolsky, W.T. Vetterling and B.P. Flannery, NUMERICAL RECIPES in C *The Art of Scientific Computing* 2:nd ed. (Cambridge University Press).

[14] M. Abramowitz and I.A. Stegun, Handbook of Mathematical Functions (DOVER PUBLICATIONS INC., NEW YORK).

Paper III

LU-TP 97-21
NORDITA-97/54 P
September 1997
Revised* December 1997

The Linked Dipole Chain Monte Carlo

Hamid Kharraziha
Dept. of Theoretical Physics
Sölvegatan 14a
S-223 62 Lund, Sweden
hamid@thep.lu.se

Leif Lönnblad
NORDITA
Blegdamsvej 17
DK-2100 København Ø, Denmark
leif@nordita.dk

Abstract

We present an implementation of the Linked Dipole Chain model for deeply inelastic ep scattering into the framework of the ARIADNE event generator. Using this implementation we obtain results both for the inclusive structure function as well as for exclusive properties of the hadronic final state.

*The original publication was based on results from an implementation containing an error. In this revised version this error has been corrected, some of the beyond leading-log assumptions have been revised and so have some of the results.

1 Introduction

With the HERA collider, a new kinematical regime has been opened up for studying deeply inelastic ep scattering (DIS) on partons carrying a very small momentum fraction x of the proton. Much theoretical and experimental effort has been made to increase our understanding of the dynamics of such small-x partons, and much progress has been made, although many problems still need to be solved. On the theoretical side, a major issue is how to handle the resummation of large logarithms of x and Q^2 in a consistent way, while a big obstacle for the experimental analysis has been the lack of theoretically well founded event generators which are able to describe the measurements made in this kinematical region.

The conventional way of describing the QCD evolution of the partons within a hadron, is to look at ladder diagrams where an incoming parton with large momentum and low virtuality undergo successive splittings, thus reducing its momentum and increasing its virtuality. The contributions from splittings where the parton retains only a small fraction $z \ll 1$ of its momentum or where its virtuality is increased by a large factor ν, are enhanced by large logarithms of $1/z$ or ν respectively, therefore such ladders need to be resummed to all orders.

The so-called DGLAP [1] evolution equations handles the resummation of logarithms of the virtuality by summing all ladder diagrams where the virtualities, or the transverse momenta $k_{\perp}$, are strongly ordered along the chain, while the BFKL [2] equations perform a $\ln(1/z)$ resummation, summing ladders with strongly ordered momentum fractions, but unordered in $k_{\perp}$. Looking only at the inclusive structure function F_2, both of these approaches are able to explain the steep rise with $1/x$ measured at HERA [3]. This is true also for the very small-x region where the DGLAP equations are thought to be unreliable. However, the prediction from these approximations rely heavily on the assumption of the input parton distributions from which the evolution is started, and the absence of a small-x enhancement in the evolution can be compensated with a steeply rising input distribution.

From the F_2 measurement alone it is therefore difficult to estimate the relative importance of the different resummation approaches, and several suggestions have been made to instead look at different details of the hadronic final state to get a better understanding of the dynamics of QCD evolution [4]. Neither the BFKL or DGLAP equations are, however, suitable for describing non-inclusive event properties since that may destroy cancellations between real and virtual diagrams which are essential for the different approaches. In contrast, the so-called CCFM [5] evolution equations are designed to explicitly describe exclusive final-state properties by very carefully handling interferences between initial- and final-state splittings in the ladder, based on an angular ordered description. It can be shown to reproduce both the BFKL and DGLAP equations in their respective regions of validity.

To properly analyze measured properties of the hadronic final states found at HERA, it is important to have event generators which reproduce these properties to a satisfactory level. Unfortunately this has not been the case. The conventional generators, such as HERWIG [6] and LEPTO [7], are based on leading-log initial state parton showers derived from the DGLAP equations, and predict much too small partonic activity in the direction of the incoming proton (hereafter also referred to as the forward direction) for small-x events [8,9]. This is expected, as the cascades are strongly ordered in transverse momenta, and are therefore limited by the smallness of Q^2 in these events. In contrast, the dipole cascade implemented in the ARIADNE [10] program, where the generated partons are unordered in transverse momenta, is able to describe the final-state properties in the proton direction quite well. From this one may suspect that the resummation in the BFKL equations indeed are important, but since there is no clear relationship between the semi-classical soft radiation model [11] in Ariadne and the BFKL equation besides the $k_\perp$ non-ordering, no firm statement can be made.

It is therefore important to construct an event generator implementing eg. the CCFM evolution, which can make reliable prediction about exclusive properties of the hadronic final state. Attempts has been made in this direction [12], but several difficulties have been encountered. A major obstacle with the CCFM equation is the presence of the so-called non-eikonal form factor which makes any implementation extremely inefficient.

Recently a reformulation of the CCFM equation has been proposed [13]. In this, the Linked Dipole Chain (LDC) model, the division between initial- and final-state radiation diagrams is redefined using the colour dipole cascade model (CDM). After this redefinition, the non-eikonal form factor drops out, which allows for a more simple implementation in an event generator.

A first attempt to construct such an event generator is presented in this paper. Although the LDC model is well suited for implementation in a Monte Carlo program there are a number of problems to be resolved. One problem is that both the CCFM and LDC models only deal with purely gluonic ladders while, to make a complete event generator, all types of ladders should be included. It is also important to handle energy-momentum conservation in a sensible way. Another important issue is the dependence on the input parton densities and the Sudakov form factors needed to regularize the poles in the splitting functions and to conserve the total momentum in the evolved parton density functions.

In section 2 we first recall the main ideas of the LDC model, then in section 3 we present the different issues involved in implementing the model in a Monte Carlo program. To obtain predictions for the hadronic final state we must first, as described in section 4, obtain input parton densities which together with the

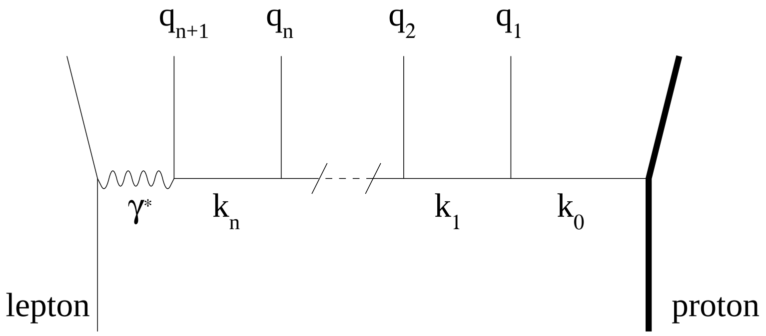

Figure 1: *Lepton proton scattering with n perturbative ISB emissions. The emitted ISB partons are denoted $\{q_i\}$ and the propagators are denoted $\{k_i\}$.*

LDC evolution will give a satisfactory description of the inclusive cross section. Some results for the hadronic final state are then presented in section 5. Finally, our conclusions can be found in section 6.

2 The Linked Dipole Chain model

It is well known that the cross section for DIS events is not describable only by the lowest order perturbative terms. Still, it is not necessary to consider all possible emissions. A large set of them can be summed over and do, in principle, not affect the cross section. In the LDC model [13], the emissions that are considered to contribute to the cross section are regarded as Initial State Bremsstrahlung (ISB). The description of these emissions is based on the CCFM [5] model which is a leading-log approximation of the structure function evolution in DIS. The CCFM model has been modified by redefining which emissions should be counted as ISB, resulting in a much simplified description.

To describe final state properties of DIS events, one must also consider Final State Bremsstrahlung (FSB). In the LDC model this is done within the framework of the Colour Dipole cascade Model (CDM) [14] which has previously proved to give a good description of parton cascades in hadronic e^+e^- events and DIS. The general picture is that the initial parton ladder builds a chain of linked colour dipoles and that the FSB is radiated from these dipoles.

Let $\{q_i\}$ denote the momenta of emitted partons, $\{k_i\}$ denote the momenta of the propagators (see fig. 1) and z_{+i} be the positive light-cone momentum fraction* of k_i in each emission: $k_{+i} = z_{+i}k_{+(i-1)}$. According to the CCFM model, the emissions that contribute to the cross section (ISB) are ordered

*Note that throughout this paper we work in the γ^*p centre of mass system with the in rapidity and energy. Furthermore, there is a restriction on the transverse momenta of the continuing propagator in each emission:

$$k_{\perp i}^2 > z_{+i} q_{\perp i}^2. \tag{1}$$

The weight distribution, dw, of the initial chains factorizes, with the factors dw_i given by the following expression ($\bar{\alpha} = 3\alpha_s/\pi$):

$$\begin{aligned} dw &= dw_1 dw_2 \cdots dw_n, \\ dw_i &= \bar{\alpha} \frac{dz_{+i}}{z_{+i}} \frac{d^2 q_{\perp i}}{\pi q_{\perp i}^2} \Delta_{ne}\left(z_{+i}, k_{\perp i}, q_{\perp i}\right). \end{aligned} \tag{2}$$

Δ_{ne} is the so called non-eikonal form factor, given by the expression:

$$\Delta_{ne}\left(z, k_\perp, q_\perp\right) = \exp\left[-\bar{\alpha} \log\left(\frac{1}{z}\right) \log\left(\frac{k_\perp^2}{z q_\perp^2}\right)\right]. \tag{3}$$

In the LDC model, the definition of the ISB is more restricted. Consequently, more emissions are summed over and the expression for the weight distribution, dw_i, is changed. The new restriction is that in each emission, the transverse momentum ($q_{\perp i}$) of the emitted parton must be larger than the lower one of the transverse momenta of the surrounding propagators

$$q_{\perp i} > \min\left(k_{\perp i}, k_{\perp(i-1)}\right). \tag{4}$$

In fig. 2 we show an example of an emission which belongs to the ISB according to the CCFM model but violates the restriction in eq. (4) and is regarded as FSB in the LDC model.

Summing over these emissions, the weight distribution of each allowed emission now becomes

$$dw_i = \bar{\alpha} \frac{dz_{+i}}{z_{+i}} \frac{d^2 q_{\perp i}}{\pi q_{\perp i}^2}. \tag{5}$$

This simplification of the expression for dw_i is due to the fact that one can interpret the non-eikonal form factor, Δ_{ne}, as a Sudakov form factor, that is, it is equal to the probability of not violating the restriction in eq. (4).

By changing variables to the propagator momenta and integrating dw_i over the azimuthal angle (in the transverse plane) it can be written approximately as:

$$dw_i = \bar{\alpha} \frac{dk_{\perp i}^2}{k_{\perp i}^2} \frac{dz_{+i}}{z_{+i}} \min\left(1, \frac{k_{\perp i}^2}{k_{\perp(i-1)}^2}\right). \tag{6}$$

---

proton along the positive z-axis, except in section 5 when comparing with experimental data, where the γ^* is along the positive z-axis.

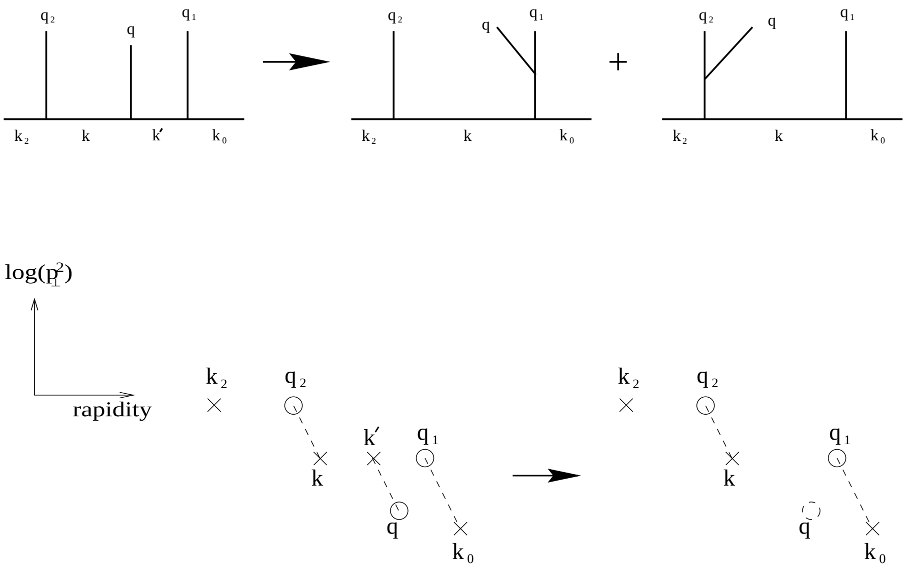

Figure 2: *CCFM $\rightarrow$ LDC: The emission q is regarded as ISB in the CCFM model but in LDC model it is regarded as FSB. This is illustrated (above) with fan diagrams and (below) in a $\log p_\perp^2$ −rapidity diagram. Rapidity here is defined as $\log(p_+/p_\perp)$ and the dashed lines indicate equal p_+.*

It is instructive to look at three different possibilities for two subsequent emissions, specified by different orderings of the transverse momenta of the propagators, numbered k_1, k_2 and k_3 (with the same order as in fig. 1):

- $k_{\perp 1} < k_{\perp 2} < k_{\perp 3}$: This is included in DGLAP and gives the same weight as there: $dw_2 dw_3 \propto \frac{1}{k_{\perp 2}^2}\frac{1}{k_{\perp 3}^2}$.
- $k_{\perp 1} < k_{\perp 2} > k_{\perp 3}$: This gives the weight $dw_2 dw_3 \propto \frac{1}{k_{\perp 2}^4}$ and resembles a hard sub-collision with a momentum transfer $\hat{t} \simeq k_{\perp 2}^2$.
- $k_{\perp 1} > k_{\perp 2} < k_{\perp 3}$: Here $dw_2 dw_3 \propto \frac{1}{k_{\perp 1}^2}\frac{1}{k_{\perp 3}^2}$, it has no factor $\frac{1}{k_{\perp 2}^2}$ and is thus infrared safe!

The LDC model, without corrections to the leading log approximation, has previously been studied and some qualitative results for the structure functions and final state properties in DIS have been presented in refs. [13, 15–17]. It is found that the LDC model, just as the CCFM model, interpolates smoothly between DGLAP and BFKL. The emissions along the rapidity axis can be separated in two phases: For rapidities closest to the proton (forward) direction,

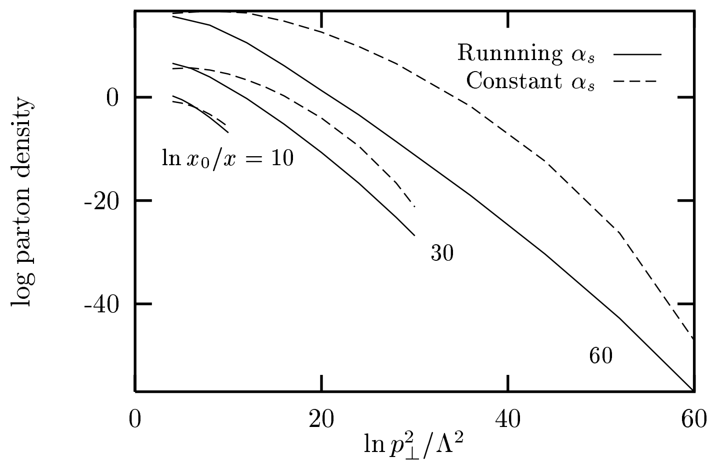

Figure 3: *The decrease of log of the parton density with* $\ln p_\perp^2$ *at a certain rapidity, for different* x*-values, for running (solid line) and constant (dashed line) coupling.*

the ISB chain performs a BFKL like motion with a constant mean $E_\perp$-flow. At a certain distance from the photon end, the transverse momentum of the emissions begins to rise to the photon virtuality, as expected by DGLAP. For the structure functions, a DGLAP behaviour ($\exp(\mathrm{const}\sqrt{-\log x})$) is shown for moderate values of x, but for small x-values it has the BFKL $x^{-\lambda}$ behaviour.

A prediction from the BFKL model is that $\log p_\perp$ of the emitted partons along the chain would be described by a Gaussian distribution with a growing width $\propto \log 1/x$. From the result of the LDC model, one can clearly see that this BFKL behaviour is indeed present for a constant coupling but not for a running coupling. This is illustrated in fig. 3 where the parton density at a certain rapidity is plotted as a function of $\log p_\perp$ for different values of x-Bjorken, for constant and running coupling. The Gaussian behaviour is observed for constant coupling, while for a running coupling it appears to decay exponentially. It seems though that the exponential decay is significant only for events with very small x-values and will probably not be visible in currently available data.

The dipole model [14] was originally developed for final-state parton cascades from a quark-anti quark system. The phase space for gluon emission from a $q-\bar{q}$ pair is approximately given by the triangular area in fig. 4a. The gluons are assumed to be radiated from a $q-\bar{q}$ colour dipole and after each emission, the dipole is split into smaller dipoles (fig. 4b), which continue to radiate

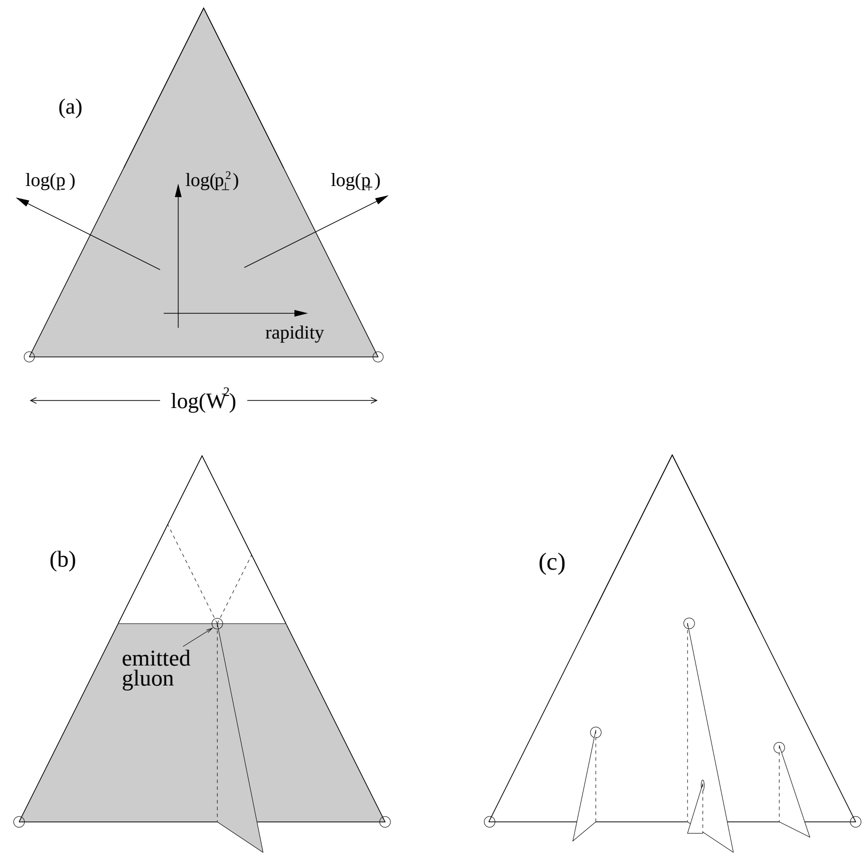

Figure 4: *(a) The phase space of parton emission from a $q-\bar{q}$ pair. (b) After the first emission, the phase space is split into two triangle which radiate gluons independently, but under a $p_\perp$-ordering condition. (c) An event with four emissions.*

independently under a $p_\perp$-ordering condition (shaded area). Also $g \to q+\bar{q}$ splittings have been included in this model. The size of the dipole triangle is determined by the total $q-\bar{q}$ invariant mass W.

The momenta $\{q_i\}$ of the emitted ISB partons in DIS are plotted in fig. 5a. Due to the ordering in positive and negative light cone momenta, one can insert the ISB into a dipole triangle with a size determined by the photon negative light cone momentum (left edge) and the positive light cone momentum of the incoming (non-perturbative) gluon (right edge). After doing this, the FSB partons can be emitted in a similar way as for the $q-\bar{q}$ parton shower (fig. 5b).

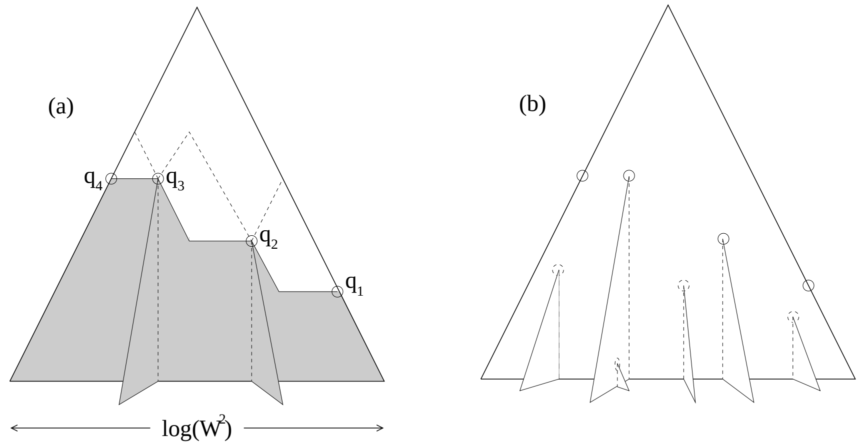

Figure 5: *(a) ISB emissions plotted in a dipole triangle. (b) The solid circles are ISB emissions and the dashed circles are FSB emissions.*

The phase space of the FSB is the shaded area in fig. 5a.

3 The Monte Carlo implementation

The LDC model has been implemented in a Monte Carlo program and some results within the leading log approximation have already been presented. Here we present a more complete implementation taking into account some non-leading corrections and generating complete events all the way down to the final state hadron level. What follows is a step-by-step description of the procedure.

The basic formula for the evolution of the parton densities is

$$xf_i(x,Q^2) = \sum_j \int_x^1 \frac{dx_0}{x_0} \Big[\; G_{ij}(x,Q^2,x_0,k_{\perp 0}^2) + S_j(Q^2,k_{\perp 0}^2)\delta_{ij}(\ln x - \ln x_0)\Big] \, x_0 f_{0j}(x_0,k_{\perp 0}^2), \tag{7}$$

Where $G_{ij}(x,Q^2,x_0,k_{\perp 0}^2)$ is the sum of the weights of all chains starting with a parton j at some low scale $k_{\perp 0}^2$ carrying a momentum fraction x_0, and ending up with a parton i carrying a momentum fraction x being hit by a photon with virtuality Q^2. The delta function corresponds to the case of no emissions. G is positive definite, and to conserve the total momentum, $\sum_j \int_0^1 xf_j(Q^2,x)dx = 1$, the delta function is multiplied by a Sudakov form factor, $S_j(Q^2,k_{\perp 0}^2)$, representing the probability that the parton j with with momentum fraction x_0 at $k_{\perp 0}^2$ has not split, and thus reduced its momentum, when probed at a higher scale Q^2. This form factor will be discussed in detail below.

The analytic approximate upper limiting function for G [15], given by

$$G_{ij}(x,Q^2,x_0,k_{\perp 0}^2) \lesssim G(Q^2/k_{\perp 0}^2, x/x_0) = \sqrt{\tfrac{a}{b}} I_1(2\sqrt{ab}) \tag{8}$$
$$a = \sqrt{\bar{\alpha}}(\ln Q^2/k_{\perp 0}^2 + \ln x_0/x), \quad b = \sqrt{\bar{\alpha}} \ln x_0/x$$

provides us with the starting point, and for each generated chain c a number of multiplicative weights are calculated $\omega_c = \Pi_l \omega_c^{(l)}$ so that the correct form of G_{ij} is obtained as

$$G_{ij}(x,Q^2,x_0,k_{\perp 0}^2) = \bar{\omega}_{ij}(x,Q^2,x_0,k_{\perp 0}^2) G(Q^2/k_{\perp 0}^2, x_0/x), \tag{9}$$

with the average weight

$$\bar{\omega} = \frac{1}{N}\sum_{c=1}^{N} \omega_c \tag{10}$$

This is how it is done:

1. First the x, Q^2 and the flavour i of the struck quark is chosen using evolved parton densities and the standard Born-level electro-weak matrix elements. This is currently done within the LEPTO program [7].

2. Then the x_0 and flavour of the incoming parton is chosen according to eqs. (7) and (8) with $k_{\perp 0}$ as a given parameter.

3. The number of emissions is chosen from

$$\sqrt{\frac{a}{b}} I_1(2\sqrt{ab}) = \sum_{n=1}^{\infty} \frac{a^n b^{n-1}}{n!(n-1)!} \tag{11}$$

4. The positive and negative light-cone momentum fractions, z_{j+} and z_{j-} which enters in each emission j is generated according to the ordered integral

$$\frac{a^n b^{n-1}}{n!(n-1)!} = \int \bar{\alpha}^n \Pi_j \frac{dz_{j+}}{z_{j+}} \frac{dz_{j-}}{z_{j-}} \delta(\ln x_0 + \sum_j \ln z_{j+} - \ln x) \tag{12}$$

5. At this point we need to choose the flavours of each link. To do this we introduce the standard Altarelli-Parisi splitting functions and preliminary we use their approximations, $\tilde{P}_{i\to j}(z)$, in the $z \to 0$ limit

$$\begin{aligned} P_{q\to q}(z) &= C_F \frac{1+z^2}{1-z} \approx C_F, \\ P_{g\to g}(z) &= 2N_C \frac{(1-z(1-z))^2}{z(1-z)} \approx 2N_C \frac{1}{z}, \\ P_{g\to q}(z) &= T_R(z^2+(1-z)^2) \approx T_R, \\ P_{q\to g}(z) &= C_F \frac{1+(1-z)^2}{z} \approx C_F \frac{2}{z}, \end{aligned} \tag{13}$$

We get the first weight factor as the approximated splitting functions summed over all possible flavour combinations,

$$\omega^{(0)} = \sum \Pi \frac{\tilde{P}_{i\to j}(z_+)}{\tilde{P}_{g\to g}(z_+)}. \tag{14}$$

6. We can then use eq. (14) to generate a specific flavour combination according to their individual weights.

7. Next, we generate the azimuthal angles of each emission and construct the exact kinematics. The delta function in eq. (12), which handles the conservation of positive light-cone momenta, does not take into account the transverse degrees of freedom. In particular it would give zero positive light-cone momentum for the struck quark, q_{n+1}, in the final-state. We therefore modify this delta function to exactly conserve the total energy and momentum, effectively setting z_{n+} by hand to the value needed. However, for some values of the azimuth angles this is not possible and we get a weight factor corresponding to the allowed integration area $\Delta\phi_j$:

$$\omega^{(1)} = \Pi_j \frac{1}{2\pi} \int_{\Delta\phi_j} d\phi_j. \tag{15}$$

8. Then we implement the condition that the transverse momenta (which is generalized to the transverse mass $m_\perp$ for massive partons) of an emitted parton must be larger than the smallest virtuality $v_{j\,\min}$ of the connecting links j and $j-1$, and that all virtualities must be above $k_{\perp 0}^2$, giving us the second weight factor

$$\omega^{(2)} = \Pi_j \Theta(m_{\perp j}^2 - v_{j\,\min})\Theta(v_{j\,\min} - k_{\perp 0}^2). \tag{16}$$

   We note that the weights are finite even if one of v_j and v_{j-1} goes to zero, and one could imagine replacing the second theta function in eq. (16) with $\Theta(v_{j\,\max} - k_{\perp 0}^2)$. This would reduce the dependency on $k_{\perp 0}$ and would allow for more unordered chains as discussed below.

9. Now we introduce the running of α_s, giving a fourth weight

$$\omega^{(3)} = \Pi_j \frac{1}{\ln(m_{\perp j}^2/\Lambda^2)} \tag{17}$$

10. Having obtained the virtualities of the links, we can now correct the splitting functions in eq. (14). We get the following cases:

   - $v_{j+1} > v_j > v_{j-1}$: Going upwards from the proton side we use $P_{f_{j-1}\to f_j}(z_{j+})$

- $v_{j+1} < v_j < v_{j-1}$: Going upwards from the photon side we use $P_{f_{j+1} \to f_j}(z_{j-})$
- $v_{j+1} < v_j > v_{j-1}$: Corresponds to a Rutherford scattering and $z_{j+} \approx z_{j-} \equiv z$. Here we use $2 \to 2$ matrix elements taking into account colour connections as explained in Appendix A.
- $v_{j+1} > v_j < v_{j-1}$: Here we use the $z \to 0$ limit, $\tilde{P}_{i \to j}(z)$ of the splitting functions, where $z = z_+$ if $v_{j+1} > v_{j-1}$ or else $z = z_-$.

Note that the colour factor is independent of the ordering of the virtualities. Therefor we have to correct for only the kinematical part of the splitting function by using reduced splitting functions $\not{P}$ where the colour factor is divided out. Here we also introduce the Sudakov form factor, to be discussed below and we can write the fourth weight factor

$$\omega^{(4)} = \Pi_j \frac{S_j(v_{j-1}, v_j, v_{j+1}) \not{P}^{v_{j-1} v_j v_{j+1}}_{f_{j-1} f_j f_{j+1}}(z_{j+}, z_{j-})}{\tilde{\not{P}}_{f_{j-1} \to f_j}(z_{j+})}, \tag{18}$$

where $S_j(v_{j-1}, v_j, v_{j+1})$ is $S_{f_{j-1}}(v_j, v_{j-1})$ or $S_{f_{j+1}}(v_j, v_{j+1})$ depending on whether the virtuality is going up or down.

$P_{q \to q}$ and $P_{g \to g}$ both have poles as $z \to 1$, corresponding to emission of low-energy gluons. Typically these should be counted as final-state emissions, but to be sure to avoid divergences we introduce a cutoff $z_{\text{cut}} = 0.5$. See also the discussion of double counting below.

Note also that we use mass less splitting functions, and the production of heavy quarks is only suppressed by the phase space. This should be improved in the future.

11. The final weight factor is introduced to correct the emission closest to the photon, in the cases where $v_n > v_{n-1}$, to reproduce the exact $\mathcal{O}(\alpha\alpha_s)$ matrix element as given eg. in ref. [18]:

$$\omega^{(5)} = \frac{\mathcal{M}(Q^2, x, z_{n+}, z_{n-})}{P^{v_{n-1} v_n Q^2}_{f_{n-1} f_n \gamma}(z_{n+}, z_{n-})} \tag{19}$$

12. The generated chain is now kept with a probability $\omega_c = \frac{1}{W} \Pi_l \omega_c^{(l)}$, where W is a scale factor to avoid probabilities larger than one. There is in principle nothing preventing weight larger than one, but they turn out to be very rare. Nevertheless, it may happen, and it is important to check that W is large enough so that the results are not influenced by this. Chains with $\omega > 1$ may optionally be saved and retrieved again when an event with the same flavour and similar x and Q^2 is requested. A

chain will then be used on the average ω_c times, each time with different final-state cascade and hadronization. Below we have used $W = 1$ giving less than 0.1% events with weight larger than one.

13. To prepare for the final-state dipole radiation the emitted partons must be connected together and form dipoles. In the case of quark links, this is straight forward, the incoming quark is simply connected to the first emitted gluon and so on until the struck quark. In the case of gluon links, there are two colour lines, and a radiated gluon can belong to either of these. This choice is done completely at random. The connection between the colour line of the incoming parton and the proton remnant is handled in the same way as in the default soft radiation model of ARIADNE [10].

    One could imagine using other methods for determining the colour-flow. One suggestion is to use the colour-flow which minimize the total string length†. One could also consider colour-**re**connections, following eg. the model already implemented in ARIADNE [20], possibly giving rise to large rapidity gaps among the final-state hadrons.

14. The constructed dipoles can then radiate more final-state gluons in the phase-space limited by the virtuality and the positive and negative light-cone momenta of the links in the chain as in fig. 5a. Note that also in the no-emission case corresponding to the delta function in eq. (7), some radiation is allowed within the triangular area defined by $q_+ < -Q_+$ and $q_- < Q_-$. In the Breit frame, this is just the area of allowed FSB in a $e^+e^- \to q\bar{q}$ event with centre of mass energy Q.

15. Finally the final state dipole chains are hadronized according to the Lund string fragmentation model as implemented in JETSET [21].

This concludes the description of the actual implementation. But before we can start producing events we have to fix the parameters involved. These are Λ, $k_{\perp 0}$, W, $z_{\rm cut}$ and the input parton densities $x_0 f_{0j}(x_0, k_{\perp 0}^2)$. W is not really a physical parameter, and should be set large enough so that the result no longer depend on it. It would be natural to take Λ and $k_{\perp 0}$ to be the values which have been tuned for the final state dipole cascade to reproduce LEP data, $\Lambda_{\rm LEP}$ and $k_{\perp 0 \rm LEP}$. One could, of course, use an increased cutoff $k_{\perp 0} > k_{\perp 0 \rm LEP}$ in the ISB. This would mean that more emissions would be moved from the initial to the final state, which would continue emitting down to $k_{\perp 0 \rm LEP}$. We therefore expect the final result to be fairly stable w.r.t. such variations as long as $k_{\perp 0}$ is not too large.

There is an additional complication with a large $k_{\perp 0}$ for the cases where the virtuality drops below $k_{\perp 0}$ somewhere along the chain, causing a zero weight in

†As defined eg. by the λ measure of ref. [19]

eq. (16). For the total cross section, this does not matter, as such fluctuations are included in the input parton densities at a lower x_0, corresponding to the momentum fraction of the link closest to the photon which is below the cutoff. For the final state, however, it means that we are excluding some radiation close to the direction of the incoming hadron.

As discussed above, one could replace the second theta function in eq. (16) with $\Theta(v_{j\,\max} - k_{\perp 0}^2)$ since the $m_\perp^2$ then would still be in the perturbative region. In this way the result would be less sensitive to variations of $k_{\perp 0}$, as the perturbative system on the proton side of the sub-cutoff link would still be generated. This would not, of course, solve the problem altogether as one can imagine chains where two or more consecutive links are below the cutoff.

In step 10 we have replaced the N_c/z pole, which is used in the emissions of the original leading log LDC model, with the standard Altarelli-Parisi splitting functions. This should be a sensible way of including some sub-leading effects, as long as the splitting functions are regularized in a correct way. In each emission, two particles are produced and one vanishes. For the parton distributions, this means we must subtract and add partons correspondingly.

A simple way of treating this double counting problem is to add only one of the produced partons assuming that the mother parton is not affected by the emission. The choice of which of the two partons to add is not trivial. One way is to introduce a cut-off $z_{cut} = 0.5$ allowing only $z < z_{cut}$. This is a good choice in the $g \to g$ splitting since the gluon with $z > 0.5$ is more similar to the mother gluon. For the other emissions, which involve both quarks and gluons, it is more important to make the choice which leads to a better approximation of the quark distributions. This can be done by allowing all $q \to g$ splittings, forbidding all $q \to q$ splittings and allowing $g \to q$ splittings only if the quark (or anti-quark) interacts directly with the photon.

In a more sophisticated treatment, the subtraction of a parton is done with Sudakov form factors corresponding to the probability for the partons not to vanish before the splitting can occur. In this way, we can take into account that e.g. the possibility for a gluon to split into a quark anti-quark pair with low virtuality reduces its contribution to emissions with higher virtualities. The suppression factor becomes an exponential of an integral over the splitting

$$S_g = \exp\left[-\int_0^1 P_{g\to q}(z)dz \int \frac{\alpha_s(q_\perp^2)}{2\pi}\frac{dq_\perp^2}{q_\perp^2}\right]. \tag{20}$$

The region of integration corresponds to the region of allowed emissions. Here we only use an approximate form. A more thorough investigation will be presented in a future paper.

The lower limit on $q_\perp^2$ is given by the lowest virtuality of an emission step multiplied by a fudge factor, e^δ, to account for the suppression of the emission probability for small $q_\perp$-values (eq. (4)). The value of $\delta = 0.4$ that is used

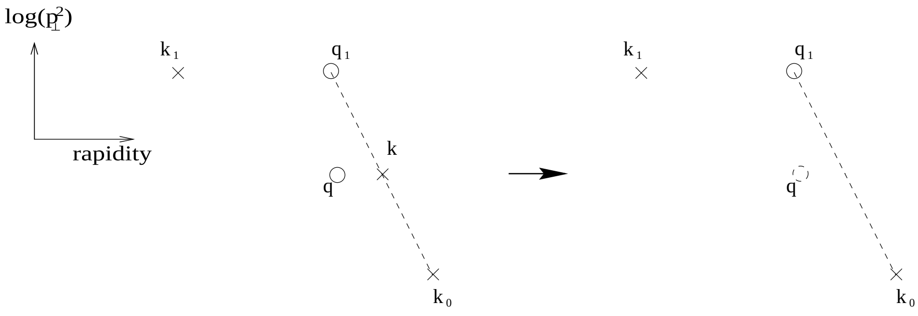

Figure 6: *In the case where the virtuality is increasing, a splitting with z larger than 0.5 corresponds to an emission of a gluon q which is inside the phase space where subsequent FSB emissions is allowed. Such splittings should therefore be removed from the ISB chains to avoid double counting.*

has proven to be an effective cut-off in the leading log treatment of the LDC model [15, 17]. The upper limit is set to the highest virtuality of an emission step. One could imagine having a higher, or a z dependent limit, but for simplicity we only use the virtuality in this publication.

The Sudakov factor due to the $g \to g$ splitting depends on the choice of z_{cut}. For $z_{cut} = 0.5$, there is no double counting to correct for and for larger z_{cut} the integration of the splitting function is in the region $0.5 < z < z_{cut}$. If $q \to q$ splittings are allowed, quarks are suppressed with a Sudakov factor where the integration region is given by $0 < z < z_{cut}$.

The situation is quite different when we are interested in the final state properties. Here, the Sudakov form factors are not as important since they for most events roughly give an overall factor $\prod_{j=1}^{n} S(v_{j-1}, v_j, v_{j+1}) \sim S(k_{\perp 0}^2, Q^2)$ which does not have an influence on the relative contributions of different final states. On the other hand, disallowing some of the initial state emissions to reduce double counting has a large effect on the final state properties since it reduces high $p_\perp$ emissions. This is a problem except for gluon emissions with $z > 0.5$ in regions with ordered virtuality, since these gluons can be treated as final state emissions as shown in fig. 6. Consequently, we would expect it to be a good approximation for the final state generation to skip the Sudakov form factors and to allow some of the splittings which lead to double counting.

It is clear that the result is very dependent on the non-perturbative input parton densities, which are basically unknown. If eg. the gluon

density is very divergent at small x, the x_0 chosen from eq. (7) will tend to be small, limiting the total phase space available for radiation $\Delta y \propto \ln x_0/x$. The input parton densities can, however, be constrained somewhat from the total cross section, and we can parametrize them and make a fit of the parameters to eg. F_2 data at different x and Q^2.

4 Fitting the input parton densities

From eq. (7) we can write the leading order expression for F_2 as

$$F_2 = \sum_{i\neq 0} e_i^2 \sum_j \int_x^1 \frac{dx_0}{x_0} \Big[\quad G_{ij}(x, Q^2, x_0, k_{\perp 0}^2) + \\ S_j(Q^2, k_{\perp 0}^2)\delta_{ij}(\ln x - \ln x_0) \Big] x_0 f_{0j}(x_0, k_{\perp 0}^2). \tag{21}$$

For given values of x, Q^2, x_0, $k_{\perp 0}^2$, i and j, we can calculate $G_{ij}(x, Q^2, x_0, k_{\perp 0}^2)$ from steps 3 through 11 in the previous section using eq. (9). For any given parametrization of the input densities it is then possible to calculate F_2 and compare with experimental data.

In principle one could also fit to other data, such as prompt photon and jet production in hadron-hadron collisions. This is not possible in our current implementation which only gives the evolved densities for quarks and anti-quarks. This means that the input gluon distribution is only constrained indirectly from the Q^2 dependence of F_2, and in this paper we only make a very crude fit using only four different parameters for $x_0 f_{0j}(x_0, k_{\perp 0}^2)$.

The input densities are parametrized as

$$x f_{0j}(x) = A_j x^{\alpha_j}(1-x)^{\beta_j}. \tag{22}$$

For the valence distributions $u_v(x)$ and $d_v(x)$ we use the same form, with $\beta_v = 3$ leaving α_v free and using the normalization

$$\int_0^1 u_v(x)dx = 2, \quad \int_0^1 d_v(x)dx = 1 \tag{23}$$

to fix A_{uv} and A_{dv}. For the gluon distribution, $\beta_g = 4$ while α_g and A_g are left free. All the sea-quarks distributions have the same form with $\beta_S = 4$, leaving α_S free and setting $2A_s = 2A_{\bar{s}} = A_u = A_{\bar{u}} = A_d = A_{\bar{d}}$ so that the total momentum

$$\int_0^1 dx \sum_j x f_{0j}(x) = 1 \tag{24}$$

is conserved.

We only use data from proton F_2 measurements from H1 [22], ZEUS [23], NMC [24] and E665 [25] without allowing for any normalization uncertainty factors. We use only data for $Q^2 > 1.5$ GeV and $x < 0.5$ to ensure a reasonable length of the evolution. We then make six sets of fits using different options in the generation of the G function:

A LDC default: $k_{\perp 0} = 0.6$ GeV, $\Lambda = 0.22$ GeV.

B DGLAP: As for A but only allow chains with monotonically increasing virtualities of the links from the proton side.

C DGLAP': As for B, but chains where the virtuality of the link closest to the virtual photon is larger than Q^2 are permitted. We use this as a kind of higher-order corrected DGLAP evolution although, of course, not equivalent to NLO evolution.

D As for A but $k_{\perp 0} = 1$ GeV, to check the sensitivity to this cutoff.

E As for A but without the Sudakov form factor. Instead $P_{q \to q}(z)$ is set to zero and $P_{g \to q}(z)$ is nonzero only in the splitting closest to the photon.

F As for A but $\beta_g = \beta_S = 5$ to check the sensitivity to the fit parameters.

G As for A but only fitting to F_2 data with $x < 0.1$, to reduce the sensitivity to the step size $\delta \ln x_0/x = 0.2$ used when integrating eq. (21), and to the high-x form of the input parametrization.

H As for A but allow the virtuality of some links to be below $k_{\perp 0}$ as long as the largest virtuality of two consecutive links always is above $k_{\perp 0}$.

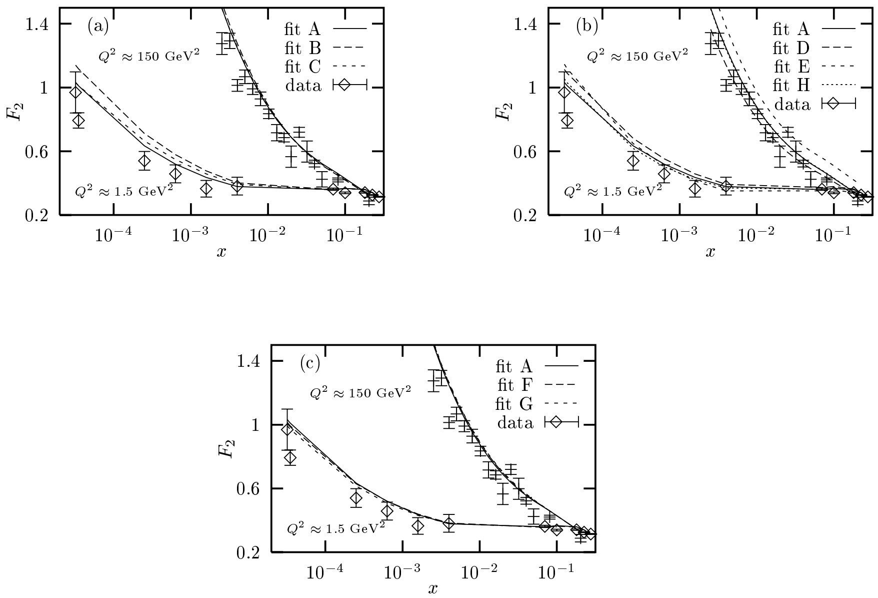

Figure 7: *The fitted F_2 as a function of x for different strategies and for two different values of Q^2, compared with data from [22–25].*

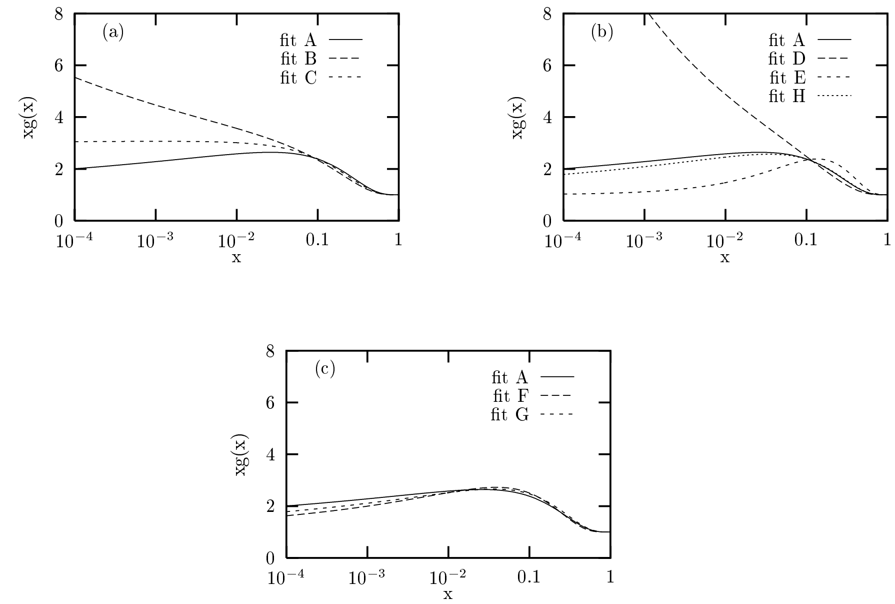

Figure 8: *The fitted input gluon density as a function of x for different strategies.*

The results of the fits are presented in figs. 7 and 8. For the default case, the fit is quite acceptable. We note in particular that the fitted input gluon density is slowly decreasing with $1/x$, although we must keep in mind that the gluon distribution is only indirectly constrained.

For the DGLAP case the fit is much worse. The number of allowed ISB emissions is here strongly restricted, especially for small Q^2 and x. This results in much slower evolution which forces the input densities to rise with $1/x$. In fit C, where the link closest to the virtual photon is allowed to be above Q^2, the fit is on the other hand again quite acceptable. The input gluon distribution is no longer rising with $1/x$, on the other hand it is as strongly decreasing as in fit A. It is known that F_2 can be fitted using conventional DGLAP evolution with a valence-like flat input distribution at small input scales, close to the one used here, as in the GRV parametrizations [26]. Such fits can, however, not be directly compared to this one, as we here have less parameters. But we can conclude that the ISB chains with unordered $k_\perp$ do play a rôle in our case, although most of the effect can be obtained allowing only for one 'stepping down', closest to the photon in the chain.

Increasing the input scale to 1 GeV in fit D makes a big difference particularly at small x as seen in figs. 7b and 8b. Also here the number of allowed ISB emissions is strongly restricted and again the input gluon is forced to increase strongly with $1/x$. This should come as no surprise. We expect, however, that when we below study the hadronic final states, the result should be less sensitive to the input scale used.

The importance of the Sudakov form factor is apparent in figs. 7b and 8b, comparing fits A and E, especially for the input gluon distribution. Also in figs. 7b and 8b we show the fit H, where some propagators below the cutoff is allowed. The reproduction of F_2 does not change much, but we see that the input gluon decreases slightly faster with $1/x$ than for the default fit A.

The fits F and G in figs. 7c and 8c show how sensitive the fit is to the input distribution is at large x. Changing β_g and β_S from 4 to 5 does not influence the fit very much and neither does the omission of the data points at high x, although in both cases the input gluon is shifted somewhat to higher x.

5 Results for the hadronic final states at HERA

The results for the hadronic final states will depend on the input densities used. If eg. the input densities are increasing with $1/x_0$, chains starting with low x_0 will be favoured and the length of the chains will be shorter resulting in fewer emissions and less activity in general due to the reduction of the available phase space, in particular close to the direction of the incoming hadron. Also a smaller input gluon density will result in fewer chains initiated with a gluon, which has higher charge than an incoming quark, and again the probability of emissions will become smaller. In addition, the non-perturbative hadronization is smaller if only one string is stretched between the perturbative system and the hadron remnant in the case of an incoming quark.

To study the hadronic final states we use the HZTOOL package [27] developed jointly by H1, ZEUS and theoreticians for comparison between event generators and published experimental data. We have selected six different distributions which have been shown to be sensitive to details in the models used in Monte Carlo event generators. The distributions presented in fig. 9, which are all measured in the hadronic centre of mass system, are as follows.

(a) The $E_\perp$-flow as a function of the pseudo rapidity for two bins in x and Q^2, one with low x and low Q^2, and one with moderate x and Q^2 in (b) [8]. The large amount of $E_\perp$ in the forward direction was previously claimed to be a good signal of $k_\perp$ non-ordering in the ISB, but it has been shown that this effect can also be obtained by the introduction of additional non-perturbative effects.

(c) The so-called seagull plot with the average $k_\perp^2$ as a function of Feynman-x [28], which at eg. EMC [29] was shown to be difficult to reproduce with event generators.

(d) The $k_\perp$-distribution of charged particles in a forward pseudo rapidity bin. This was recently proposed [9,31] as a new signal for perturbative activity in the forward region indicating $k_\perp$ non-ordering: a high-$k_\perp$ tail would be difficult to reproduce by non-perturbative models, where such tails would be exponentially suppressed.

(e) In [9] was also shown that the pseudo rapidity distribution of charged particles with $k_\perp > 1$ GeV also could be a good signal for $k_\perp$ non-ordering.

(f) Result for the two-jet ratio R_2 was recently reported [30] and showed large differences between the currently used event generators.

In fig. 9 we see the results from LDC with default settings and using fit A, labeled LDC A, compared with data and with the results for ARIADNE using the default soft radiation model, with LEPTO with and without the additional non-perturbative (soft colour interactions (SCI), and perturbative-like treatment of remnants in the case of sea quarks) assumptions presented in [32]. For the ARIADNE and LEPTO models we confirm previous results where ARIADNE, which until now was the only model implementing $k_\perp$ non-ordering, reproduces the data very well while the DGLAP-based LEPTO has difficulties, especially without the additional non-perturbative models. We find that the result for LDC is quite acceptable, although not reproducing data as well as ARIADNE.

To compare different LDC strategies, we show in fig. 10 only the number of charged particles with transverse momentum larger than 1 GeV as a function of pseudo rapidity for small x and Q^2 (fig. 10). The effects on the other distributions in fig. 9 are very similar.

In fig. 10a we see the results for LDC when restricting to DGLAP-like chains. In this case, corresponding to the lines marked LDC B, the result is very poor as expected. Allowing the virtuality of the link closest to the photon to be above Q^2 as for LDC C, makes things much better and only slightly worse than the default LDC A. Naïvely one may expect this to give the same result as LEPTO which uses the exact $\mathcal{O}(\alpha_s)$ Matrix Element for the emission closest to the photon, also allowing the first link to have a virtuality larger than Q^2, and which adds on parton-showers tabacckludge'a la DGLAP on such configurations. But in LDC, even though no ISB emissions are allowed between the highest virtuality link and the photon, there is still a resummation of diagrams which are then replaced by FSB emissions. LEPTO, however, uses the 'bare' matrix element and does not include any resummation.

For the line marked LDC D in fig. 10b, the cutoff in $k_\perp$ for the ISB is set to 1 GeV. In the previous section we saw that the parton density functions in this case became dramatically different. For the final state, however, the reduction

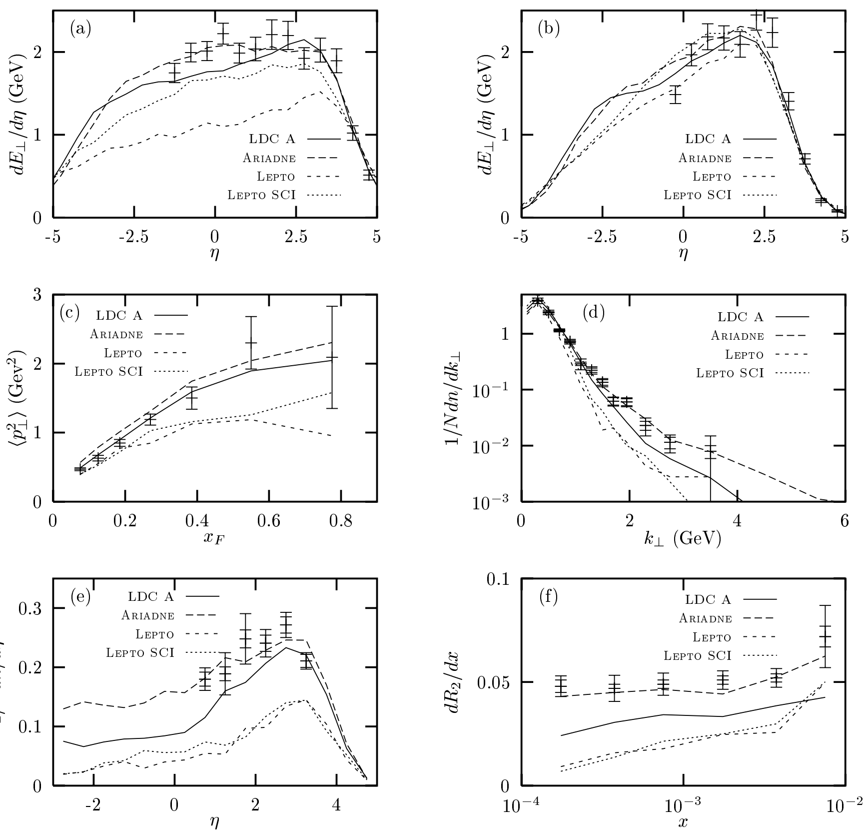

Figure 9: *Comparison of the default LDC A model with HERA data as given in [27] and other event generators. The distributions are as follows: (a) The transverse energy flow as a function of pseudo rapidity for events with* $0.0001 < x < 0.0002$, $5 < Q^2/GeV^2 < 10$ *[8]. (b) As (a) but for events with* $0.003 < x < 0.01$, $20 < Q^2/GeV^2 < 50$. *(c) The average squared transverse momentum of charged particles as a function of* x_F *[28]. (d) The transverse momentum distribution of charged particles in the pseudo rapidity bin* $0.5 < \eta < 1.5$ *for events with* $0.0002 < x < 0.0005$, $6 < Q^2/GeV^2 < 10$ *[9]. (e) The pseudo rapidity distribution of charged particles with a transverse momentum larger than 1 GeV for the same kinematical bin as in (d). (f) The two-jet ratio* $R_2(x)$ *as a function of x [30]. All measurements were made in the hadronic centre of mass system and only events without a large rapidity gap were included. The full line is LDC A, long-dashed is* Ariadne *4.08 with default parameter settings, dotted is* Lepto *6.4 with default parameter settings and short-dashed is the same but with SCI and the special sea-quark remnant treatment [32] switched off.*

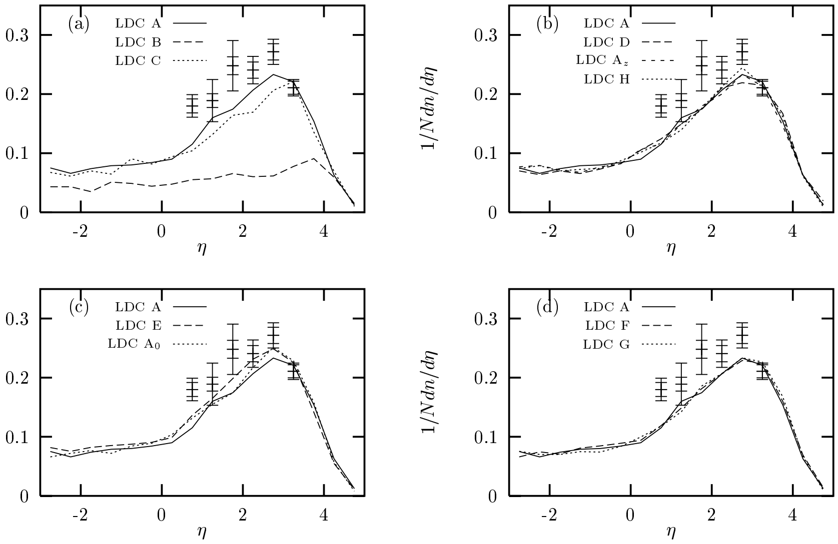

Figure 10: *Comparison between different LDC strategies and data corresponding to fig. 9e. In all cases the full line is the default LDC A strategy. In (a) the dashed line is LDC B using only DGLAP-like chains and dotted is LDC C, i.e. the same but allowing the virtuality of the link closest to the photon to be above* Q^2. *In (b) the long-dashed line is LDC D with* $k_{\perp 0} = 1$ *GeV, the short-dashed is LDC* A_z *with increased cutoff,* z_{cut}*, in the splitting functions and dotted is LDC H, allowing some propagators below the cutoff. In (c) the dashed line is LDC E without Sudakov form factors and disallowing all* $q \to q$ *and most* $g \to q$ *splittings in the parton density fit and the dotted, LDC* A_0*, is the same as LDC A but using Sudakov only in the parton density fit. Finally in (d) the dashed line is LDC F using a different form of the input densities at large* x *and the dotted is LDC G restricting the fit to* F_2 *data with* $x < 0.1$.

of ISB is compensated by final state dipole emissions, which are allowed in the whole rapidity range below $k_\perp = 1$ GeV down to the cutoff fitted to LEP data, $k_{\perp 0\mathrm{LEP}} = 0.6$. The effect of increasing z_{cut} is also shown in fig. 10b for the line LDC A_z. The dependence on this cutoff is small, which is expected as most of the emissions with $z > 0.5$ are counted as FSB as explained in fig. 6 above. Also in fig. 10b is shown the effects of allowing the virtuality of some links below the cutoff. Again the differences are small.

In fig. 10c we see the effect of different regularizations of the splitting functions. The line LDC E uses the fit E in the previous section, where all $q \to q$ and most of the $g \to q$ splittings are disallowed and all Sudakov form factors set to 1. For the final state generation, all splittings are again included, and we see a clear enhancement w.r.t. the default LDC A strategy which includes Sudakov form factors. The line LDC A_0 uses the same parton densities as the default strategy, but excludes the Sudakov form factors when generating the final states. The main effect of the form factor is to scale down all weights, and since in the total number of events is fixed, the effects on the final state is small. The fact that LDC E is as different is then mostly due to the difference in the input parton densities.

Finally in fig. 10d, we show the effects of using different fitting procedures for the input parton densities and we see that the differences are small.

6 Conclusions

We have here presented the first implementation of the Linked Dipole Chain model in an event generator. Being based on the CCFM formalism it represents one of the first attempts to correctly describe the details of the hadronic final states in small-x deep inelastic scattering to leading-log accuracy.

The LDC model was originally formulated only for $g \to g$ splittings in a strict leading-log approximation. Going from this to a full event generator is not trivial, and we have here described how we implement massive quarks splittings, sub-leading corrections, convolution with input parton densities, energy and momentum conservation, Sudakov form factors, final-state radiation and hadronization.

Our implementation still suffers from some uncertainties. One is the input parton densities which are poorly constrained because only F_2 data can be fitted, where the gluon only enters indirectly. Another issue is the uncertainty in how to deal with the final state of chains where a link drops below the cutoff, surrounded by one perturbative system on each side. But from the results in the previous sections, the main uncertainty is the regularization of the splitting functions and the conservation of total momentum in the evolved parton density functions. The correct way to treat this is with Sudakov form factors. But in the current implementation these are only treated in an approximate way and they need to be examined in more detail in the future.

Despite these uncertainties, the result presented here allows for some conclusions. Compared with the Lepto event generator, which is based on DGLAP evolution, LDC is clearly better in describing the hadronic activity in the forward region at HERA at small x. The description is not perfect, however, and it seems that LDC is still underestimating the perturbative activity in the forward region.

We have also shown the relative importance between DGLAP-like chains with monotonically increasing virtualities and the unordered chains in the full LDC model, and found that unordered chains indeed are very important, but that at HERA, most of the activity can be attributed to DGLAP-like chains where the link closest to the photon is allowed to be above Q^2.

The main goals for the future developments of the LDC generator is to investigate the exact form of the Sudakov form factors, and to include a treatment of hadron–hadron collisions, to get a better constraint on the input parton densities. Also further studies of the final state of chains with two or more perturbative systems connected with sub-cutoff links ought to be done. This is especially interesting in connection with the large fraction of rapidity-gap events found at HERA.

Despite the shortcomings of the current implementation, we feel that the LDC event generator may become a very important tool for understanding the small-x hadronic final states at HERA.

Acknowledgements

We would like to thank Bo Andersson and Gösta Gustafson for important contributions and discussions. We would also like to thank Hannes Jung for providing us with a preliminary HZTOOL implementation of the H1 results on di-jet production [30].

References

[1] V.N. Gribov, L.N. Lipatov, *Sov. J. Nucl. Phys.* **15** (1972) 438 and 675;
G. Altarelli, G. Parisi, *Nucl. Phys.* **B126** (1977) 298;
Yu.L. Dokshitzer, *Sov. Phys. JETP* **46** (1977) 641.

[2] E.A. Kuraev, L.N. Lipatov and V.S. Fadin, *Zh. Eksp. Teor. Fiz.* **72** (1977) 373, *Sov. Phys. JETP* **45** (1977) 199;
Ya.Ya. Balitsky and L.N. Lipatov, *Yad. Fiz.* **28** (1978) 1597, *Sov. J. Nucl. Phys.* **28** (1978) 822.

[3] See eg. J. Blümlein et al., Proceedings of the “Future Physics at HERA” workshop, Hamburg 1996, eds. G. Ingelman, A. De Roeck and R. Klanner, vol. 1, p. 3, hep-ph/9609425 and references therein.

[4] See eg. M. Erdmann et al., Proceedings of the “Future Physics at HERA” workshop, Hamburg 1996, eds. G. Ingelman, A. De Roeck and R. Klanner, vol. 1, p. 500, hep-ph/9610327 and references therein.

[5] M. Ciafaloni, *Nucl. Phys.* **B269** (1988) 49;
S. Catani, F. Fiorani, G. Machesini, *Phys. Lett.* **B234** (1990) 339, *Nucl. Phys.* **B336** (1990) 18.

[6] G. Marchesini et al., *Comput. Phys. Comm.* **67** (1992) 465.

[7] G. Ingelman, A. Edin and J. Rathsman, *Comput. Phys. Comm.* **101** (1997) 108, hep-ph/9605286.

[8] H1 Collaboration, S. Aid et al., *Phys. Lett.* **B356** (1995) 118, hep-ex/9506012.
[9] H1 Collaboration, C. Adloff et al., *Nucl. Phys.* **B485** (1997) 3, hep-ex/9610006.
[10] L. Lönnblad, *Comput. Phys. Comm.* **71** (1992) 15.
[11] B. Andersson et al., *Z. Phys.* **C43** (1989) 621.
[12] G. Marchesini, B. Webber, *Nucl. Phys.* **B386** (1992) 215.
[13] B. Andersson, G. Gustafson, J. Samuelsson, *Nucl. Phys.* **B463** (1996) 217.
[14] G. Gustafson, *Phys. Lett.* **B175** (1986) 453;
G. Gustafson, U. Petterson, *Nucl. Phys.* **B306** (1988) 746;
B. Andersson, G. Gustafson, L. Lönnblad, *Nucl. Phys.* **B339** (1990) 393.
[15] B. Andersson et al., *Z. Phys.* **C71** (1996) 613.
[16] H. Kharraziha, "The LDCMonte Carlo", talk presented at the DIS '97 conference, Chicago, April 1997, to be published in the proceedings.
[17] B. Andersson, G. Gustafson and H. Kharraziha,
LU-TP 97-29, aps1997nov19_001, hep-ph/9711403.
[18] R.D. Peccei, R. Rückl, *Nucl. Phys.* **B162** (1980) 125;
Ch. Rumpf, G. Kramer, J. Willrodt, *Z. Phys.* **C7** (1981) 337.
[19] B. Andersson, P. Dahlqvist and G. Gustafson, *Phys. Lett.* **B214** (1988) 604; *Z. Phys.* **C44** (1989) 455.
[20] L. Lönnblad, *Z. Phys.* **C70** (1996) 107.
[21] T. Sjöstrand, *Comput. Phys. Comm.* **82** (1994) 74
[22] H1 collaboration, S. Aid et al., *Nucl. Phys.* **B470** (1996) 3, hep-ex/9603004.
[23] ZEUS collaboration, M. Derrick et al., *Z. Phys.* **C72** (1996) 399, hep-ex/9607002.
[24] NMC collaboration, M. Arneodo et al., *Phys. Lett.* **B364** (1995) 107, hep-ph/9509406.
[25] E665 collaboration, M.R. Adams et al., *Phys. Rev.* **D54** (1996) 3006
[26] M. Glück, E. Reya and A. Vogt, *Z. Phys.* **C48** (1990) 471; *Z. Phys.* **C53** (1992) 127; *Z. Phys.* **C67** (1995) 433.
[27] J. Bromley et al., Proceedings of the "Future Physics at HERA" workshop, Hamburg 1996, eds. G. Ingelman, A. De Roeck and R. Klanner, vol. 1, p. 611.
[28] ZEUS Collaboration, M. Derrick et al., *Z. Phys.* **C70** (1996) 1, hep-ex/9511010.
[29] EMC Collaboration, M. Arneodo et al., *Z. Phys.* **C36** (1987) 527.
[30] H1 Collaboration, T. Ahmed et al., Contributed paper, Abstract 247, HEP97, Jerusalem, Israel, August 1997 (unpublished).
[31] M. Kuhlen, *Phys. Lett.* **B382** (1996) 441

[32] A. Edin, G. Ingelman, J. Rathsman, *Phys. Lett.* **B366** (1996) 371, hep-ph/9508386; *Z. Phys.* **C75** (1997) 57, hep-ph/9605281.

[33] H-U. Bengtsson, *Comput. Phys. Comm.* **31** (1984) 323.

[34] M.H. Seymour, *Nucl. Phys.* **B436** (1995) 443

Appendix A: Colour connected matrix element corrections

We will here describe the splitting functions that are used for the local sub-collisions (see point 10 in section 3). These are derived from the corresponding *colour connected* $2 \to 2$ QCD matrix elements presented in [33].

In order to use matrix elements for deriving splitting functions, it is necessary to take colour connections into account. We can illustrate this statement with the matrix element for the $g+g \to q+\bar{q}$ process. Suppose we are in a frame where the incoming gluons are moving head on and parallel to the longitudinal axis and let $\zeta_{+(-)}$ be the positive (negative) light-cone momentum fraction for the quark and $\bar{\zeta}_{+(-)}$ be the same for the anti-quark. Because of symmetry between the quark and the anti-quark it is clear that the matrix element must be symmetric in these variables: $|\mathcal{M}|^2(\zeta_{+(-)}, \bar{\zeta}_{+(-)}) = |\mathcal{M}|^2(\bar{\zeta}_{+(-)}, \zeta_{+(-)})$. In the program, the colours are connected randomly so that e.g. the quark has the same probability to be connected with the gluon coming in from either the proton or the photon side. This would mean that the two diagrams a′) and b′) in fig. 11 would be equally probable.

This is because the matrix element is calculated with an averaging of the colour states of the gluons. The corresponding colour connected matrix element, $|\mathcal{M}_{cc}|^2$ is on the other hand calculated with the assumption that the colour states of the incoming gluons are known. This means that we get two separate contributions, one from the case that the quark is colour connected with the gluon coming in from one side, say the proton side, and one contribution from the case that it is connected with the gluon from the photon side. Each of these contributions is non-symmetric with respect to the quark and anti-quark variables, while the sum of them still is symmetric.

A similar procedure is used in the $\mathcal{O}(\alpha\alpha_s)$ matrix element correction (see point 11 in section 3), to separate the γg matrix element into two contributions corresponding to quark and anti-quark scattering respectively as described in ref. [34].

For a colour connected matrix element $|\mathcal{M}_{cc}|^2(\hat{s}, \hat{t}, \hat{u})$, the corresponding splitting function is given by the formula

$$P(z) \propto z(1-z) \cdot |\mathcal{M}_{cc}|^2(1, z, 1-z) \quad \text{with} \quad z = z_+ \approx z_-. \tag{25}$$

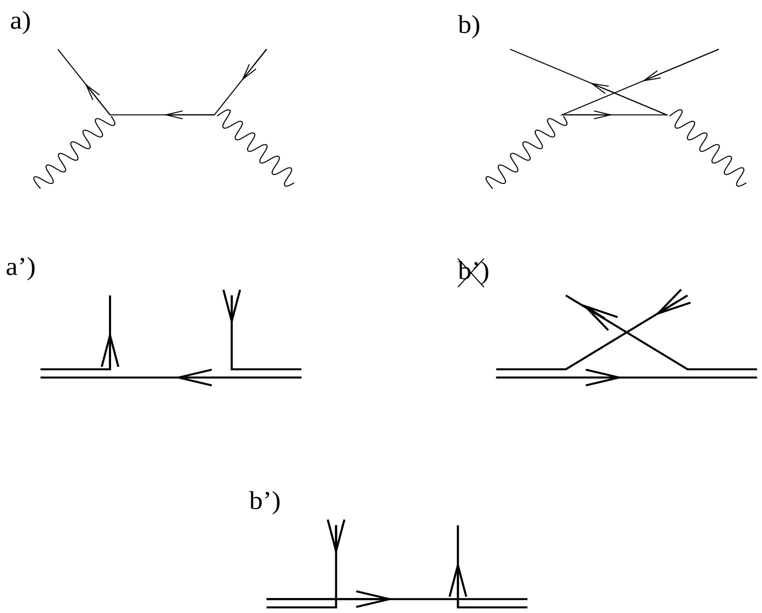

Figure 11: Feynman vs. colour connection diagrams for the $g + g \to q + q$ sub-process. If we do not average the colour states, the diagrams a') and b') give separate contributions. The contribution from diagram b') should be suppressed.

The splitting functions $\not{P}_{ijk}(z)$ where the colour factor is divided out and with the successive flavours ijk for the propagators, become

$$
\begin{aligned}
\not{P}_{qqq}(z) &= (1-z)^2\left[z^2+(1-z)^2\right] \\
\not{P}_{qqg}(z) = \not{P}_{gqq}(z) &= 0 \\
\not{P}_{qgq}(z) &= \frac{1-z}{z}\left[1+(1-z)^2\right] \\
\not{P}_{gqg}(z) &= (1-z)^2\left[z^2+(1-z)^2\right] \\
\not{P}_{qgg}(z) = \not{P}_{ggq}(z) &= \frac{1}{2z}\left[1+(1-z)^2\right]^2 \\
\not{P}_{ggg}(z) &= \frac{1}{3}\left\{\frac{\left[1-z(1-z)\right]^2}{z(1-z)}\cdot\theta(0.5-z)+2\frac{1-z}{z}\left[1-z+z^2\right]^2\right\}.
\end{aligned}
\tag{26}
$$

The θ-function in the first term of $\not{P}_{ggg}$ is a cut-off to prevent divergences. This is needed since the Sudakov form factors that are used regularize only regions with ordered virtualities. The splitting functions $\not{P}_{qqg}$ and $\not{P}_{gqq}$ are set to zero since they correspond to the same $(g+q \rightarrow g+q)$ scattering as the splitting functions $\not{P}_{qgg}$ and $\not{P}_{ggq}$ which have been chosen to take the whole contribution.

Here we have summed the contributions from different colour connections for each flavour combination. The choice of colour connections has an effect on the multiplicity and transverse momentum distributions at the hadronic level. Therefore, we will in the future use this information also to choose the colour connections for the local sub-collisions.

Paper IV

LU-TP 97-34
December 1997

LDCMC version 1.0

Hamid Kharraziha
Dept. of Theoretical Physics
Sölvegatan 14a
S-223 62 Lund, Sweden
hamid@thep.lu.se

Leif Lönnblad
NORDITA
Blegdamsvej 17
DK-2100 København Ø, Denmark
leif@nordita.dk

Abstract

We present the LDCMC program implementing the Linked Dipole Chain model for deeply inelastic ep scattering within the framework of the ARIADNE event generator.

1 Introduction

The large energies of the colliding positron and proton at the HERA accelerator enables a detailed study of the proton structure. Data is available for a wide kinematical region from very large virtualities Q^2 of the photon probe, to very small values of the Bjorken x-variable. We will here present a Monte Carlo event generator which covers the whole of this kinematical region and gives a theoretically well founded description of both the proton structure and the hadronic final state properties in the collision events.

Theoretical description of the proton structure has since long been available through the DGLAP evolution equations [1], valid for large values of Q^2, and the BFKL equations [2] which cover the very soft part of the proton structure (the $x \to 0$ limit). A third theoretical approach has been suggested by Ciafaloni, Catani, Fiorani and Marchesini and is referred to as the CCFM model [3]. This approach covers both the DGLAP and BFKL regions of validity and gives, unlike the DGLAP and BFKL equations, also a description of the final states produced in the collision process.

Recently, the CCFM model was reformulated into a new model, called the Linked Dipole Chain (LDC) model [4]. This reformulation leads to a considerable simplification of the formalism and provides a recipe for a Monte Carlo simulation. One assumes that some initial partons are produced with a weight distribution (given by the CCFM model) which provides the contribution to the total cross-section. These initial partons stretch up a chain of linked colour dipoles and more partons are emitted through a final-state Bremsstrahlung process which was initially developed for the description of parton cascades in hadronic e^+e^- events. The event generator presented here is based on the LDC model.

The CCFM model, and consequently also the LDC model, are approximate models valid to the leading log accuracy. One problem that was encountered in our development of the LDCMC event generator was to consistently include some sub leading effects into the formalism. Among these corrections are energy conservation and the description of quarks, both crucial for a realistic event generator. A set of assumptions has been made concerning these corrections, but the program provides some options to our default strategy, making it possible for the user to compare their effect on the results.

In section 2 we give a further description of the LDC model. The components of the program are presented in section 3 and finally a sample program is found in section 4.

You will find a more detailed description of the physics behind this event generator and some results in ref. [5]. The LDC model is presented in ref. [4] and some leading-log results and asymptotic solutions are described in refs. [6, 7]. For a full description of the CCFM model we refer to ref. [3], but a brief description of their results and the connection to the LDC model can be found

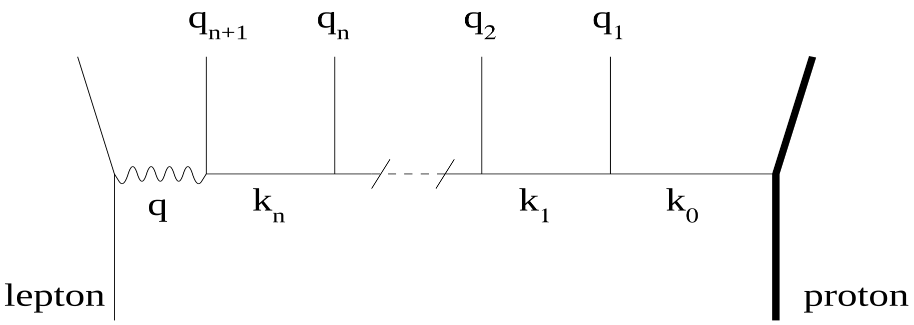

Figure 1: *Fan diagram for a DIS event with* n *initial emissions.* q_i *denote the emitted ISB partons,* k_i *denote the propagators.*

in ref. [4].

2 The LDC Model

The Linked Dipole Chain model is a reformulation of the CCFM model. Possible parton emissions in DIS are separated into two sets which are denoted Initial State Bremsstrahlung (ISB) and Final State Bremsstrahlung (FSB), respectively. The total cross-section or the structure function is evaluated by providing a weight distribution $d\omega_I$ for all possible ISB-chains:

$$F_2 = \left(\sum d\omega_I\right) \otimes f_0, \tag{1}$$

where f_0 denotes the input parton distribution. The requirement on the FSB is that recoils on the initial chain is negligible and also that their contribution to the cross-section is of Sudakov type, that is, these emissions can be added without affecting the total cross-section.

In the fan-diagram in fig. 1, describing a DIS-event with n emissions, the ISB partons are denoted $\{q_i\}$ and the propagators are denoted $\{k_i\}$. Let further $z_{i\pm}$ be the fraction of the positive/negative light-cone momentum (positive is defined in the proton direction) carried by the continuing propagator in each emission, $z_{i+} \equiv k_{i+}/k_{(i-1)+}$ and $z_{i-} \equiv k_{i-}/k_{(i+1)-}$.

In the CCFM model, the ISB set is defined by requiring that the emissions are ordered in rapidity (angular ordering) and energy. A further requirement is introduced in the LDC model by a constraint on the transverse momenta in each emission

$$q_{\perp i} > \min(\mathrm{k}_{\perp \mathrm{i}}, \mathrm{k}_{\perp \mathrm{i-1}}) \tag{2}$$

This means a redefinition of the ISB-FSB sets by moving ISB emissions which violates this constraint into the FSB set.

The ISB kinematical regions is then determined by the constraint in eq. (2) plus ordering in positive and negative light-cone momenta

$$q_- > q_{n-} > \cdots > q_{1-} \qquad q_{n+} < \cdots < q_{1+} < P_+ \tag{3}$$

with the outer limits set by the proton (P) and photon (q) momenta. The weight distribution for the ISB-chains factorizes into one factor for each emission and is given by

$$\begin{aligned} d\omega_I &= d\omega_1 d\omega_2 \cdots d\omega_n \\ d\omega_i &= \bar{\alpha} \frac{d^2\vec{q}_{\perp i}}{q_{\perp i}^2} \frac{dz_{i+}}{z_{i+}} \end{aligned} \tag{4}$$

with the effective coupling $\bar{\alpha} \equiv 3\alpha_s/\pi$.

This formalism is made symmetric with respect to the photon and proton directions and leads to evolution equations which work as a simultaneous evolution of the proton and the photon parton distributions. Consequently, it is within the LDC model, possible to, also describe resolved photon events in addition to normal DIS events where the probing photon is supposed to have the largest virtuality.

A further advantage with the reformulation of the ISB-FSB sets is that the FSB kinematical region, in the LDC model, is consistent with the colour Dipole model [8] for parton cascades. This means that, following the production of the ISB chain, the FSB partons can be emitted in a similar way as in e.g. hadronic e^+e^- events.

The emission phase space in the dipole model is usually plotted in a ($\ln p_\perp^2$, rapidity) plane and is given by a characteristic triangular area (see fig. 2a). In the LDC model one assumes that the initial ISB partons form a chain of linked colour dipoles which can radiate partons independently. For each dipole, the maximum possible transverse momentum is set by the virtuality of the corresponding propagator. The FSB kinematical region is then given by the shaded area in fig. 2b.

The CCFM model is correct only to leading log accuracy so some subleading corrections has been included in the event generator to be able to make more realistic predictions:

- Energy and momentum is conserved at every vertex.
- Quarks are introduced and some sub-leading terms are included by using standard Altarelli-Parisi splitting functions and full $2 \to 2$ matrix elements when appropriate.

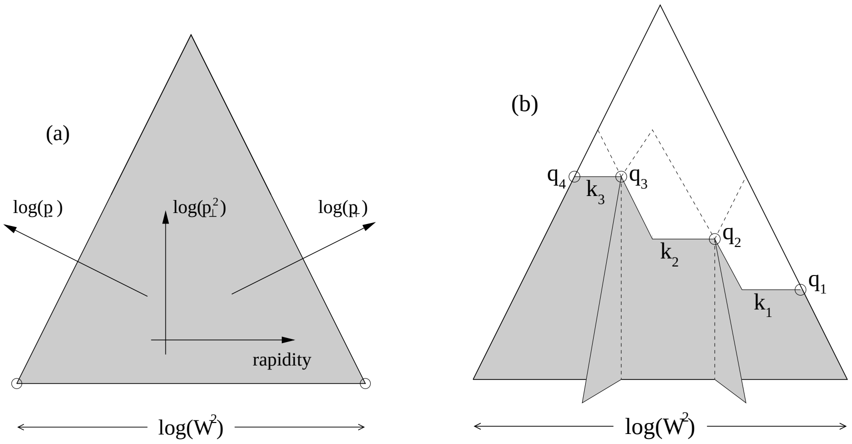

Figure 2: *(a) The dipole phase space for gluon emission from a $q-\bar{q}$ pair with central mass energy W. (b) The dipole phase space in a DIS event. The shaded are is the kinematical region for FSB.*

- The ISB emission closest to the electro-weak vertex is corrected with $\mathcal{O}(\alpha\alpha_s)$ matrix elements.

The momenta of the ISB partons $\{q_i\}$ are determined by generating the values of the positive $\{k_{i+}\}$ and negative $\{k_{i-}\}$ light-cone momenta for the propagators and the azimuthal angles $\{\phi_i\}$ of the emitted ISB partons. All other momentum components in the ISB chain are then determined by energy momentum conservation at each vertex.

The second correction is obtained by introducing generalised splitting functions $P^{k^2_{i+1},k^2_i,k^2_{i-1}}_{f_{i+1},f_i,f_{i-1}}(z)$. These are defined for every propagator link k_i and are determined by the flavours (f) and the ordering of the virtualities of the three successive propagators, k_{i-1}, k_i and k_{i+1}. The function variable is either $z = z_{i+}$ or $z = z_{i-}$.

In cases when the virtualities are uniformly ordered, $-k^2_{i-1} < -k^2_i < -k^2_{i+1}$ or $-k^2_{i-1} > -k^2_i > -k^2_{i+1}$, the generalised splitting functions are given by standard Altarelli- Parisi splitting functions with $z = z_{i+(-)}$ in the first (second) case. When the intermediate virtuality is larger than the others ($-k^2_{i-1} < -k^2_i > -k^2_{i+1}$), the process is viewed as a local sub-collision and the generalised splitting function is determined by the corresponding first order matrix element. Finally, if the intermediate virtuality is the smallest ($-k^2_{i-1} > -k^2_i < -k^2_{i+1}$), only the leading $1/z$ term of the standard Altarelli-Parisi splitting functions is used with $z = z_{i+}$ if $k^2_{i-1} < -k^2_{i+1}$ and $z = z_{i-}$ otherwise.

The colour factors are removed from the splitting functions. Instead, the colour factor for the whole ISB ladder is calculated separately, since it is (to leading order) independent of the kinematics.

The results of the CCFM model, as formulated in the LDC model, is intuitively quite easily comprehensible.

As we move in rapidity along the initial chain, the virtuality of the propagators can alternatively increase or decrease. In the DGLAP evolution formalism, the contribution to the total cross-section, or the structure function, is calculated with the assumption that the virtualities increase all the way to the photon end and that the photon has the largest virtuality. Unordered chains are shown to be suppressed. However, for events with very small x-values and moderately large Q^2, they are expected to have a significant contribution.

Generally one can subdivide the initial chain into regions with monotonically increasing or decreasing virtualities (see fig. 3). In ref. [7] it is shown that the structure function factorizes into one weight for each such region and that these weight factors are in principle given by the (leading order) DGLAP structure function. Regions with increasing virtuality, can be treated as an ordered (DGLAP) evolution of the proton parton distribution, while the regions with decreasing virtuality can be treated as ordered evolution of the photon parton distribution. These regions with ordered virtualities are then connected with propagators which have a virtuality which is either a local maximum, and can be treated as a local sub-collision, or a local minimum.

It then follows naturally that some sub-leading corrections can be included by using the Altarelli-Parisi splitting functions in the ordered regions and by using $2 \to 2$ matrix element for the local sub-collisions.

3 Program Components

The LDCMC program is logically divided into three parts. The first part generates chains to leading log accuracy given an x, Q^2, flavour of the struck quark and input parton density functions. The second part generates the exact kinematics taking into account quark masses and exact energy-momentum conservation in each branching. Finally, the third part handles the colour connections between partons and prepares the chains for subsequent final-state gluon emissions and hadronization. The detailed formulas used in the different parts are described in ref. [5], here we only describe some technical aspects of the implementation.

The first leading log part selects the flavour and x_0 of an input parton according to an approximate upper limit of the evolved parton density

$$\begin{aligned} xf_i(x,Q^2) \quad = \quad & \sum_j \int_x^1 \frac{dx_0}{x_0} \Big[\; G(Q^2/k_{\perp 0}^2, x/x_0) + \\ & \qquad S_j(Q^2,k_{\perp 0}^2)\delta_{ij}(\ln x - \ln x_0) \Big] \, x_0 f_{0j}(x_0,k_{\perp 0}^2), \end{aligned} \tag{5}$$

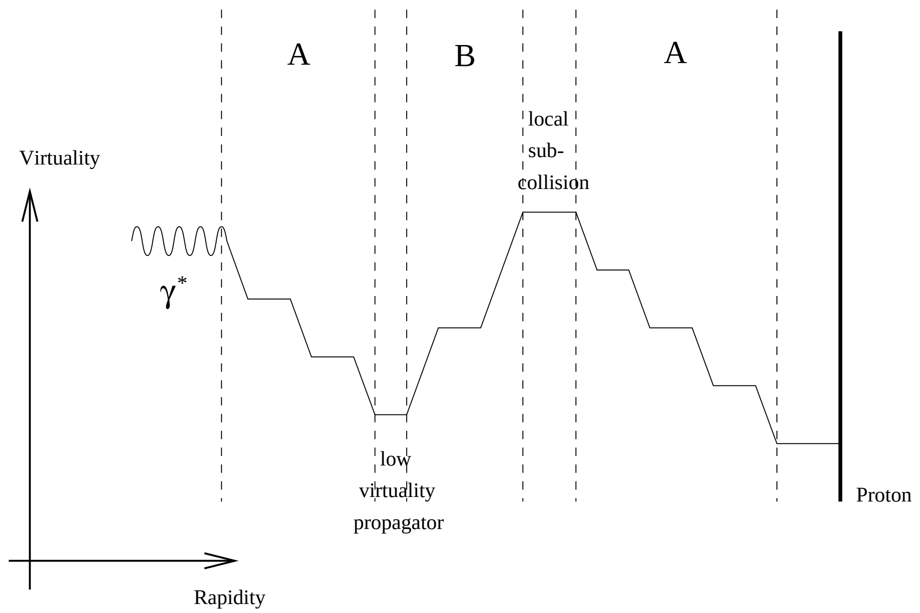

Figure 3: A general DIS-event can be separated into regions with ordered virtualities. These regions are connected either with a local sub-collision or a propagator with low virtuality. The weight factor for the regions A (B) is given by a DGLAP evolution of the proton (photon) parton distribution.

with

$$\begin{gathered} G(Q^2/k_{\perp 0}^2, x/x_0) = \sqrt{\tfrac{a}{b}} I_1(2\sqrt{ab}) \\ a = \sqrt{\bar{\alpha}}(\ln Q^2/k_{\perp 0}^2 + \ln x_0/x), \quad b = \sqrt{\bar{\alpha}} \ln x_0/x. \end{gathered} \tag{6}$$

This is done numerically, and for speed considerations the actual integration is done only once per struck flavour and per bin in x and Q^2. Then the number of emissions and the z_+ and z_- of each splitting is generated according to

$$\sqrt{\frac{a}{b}} I_1(2\sqrt{ab}) = \sum_{n=1}^{\infty} \frac{a^n b^{n-1}}{n!(n-1)!}, \tag{7}$$

and

$$\frac{a^n b^{n-1}}{n!(n-1)!} = \int \bar{\alpha}^n \Pi_j \frac{dz_{j+}}{z_{j+}} \frac{dz_{j-}}{z_{j-}} \delta(\ln x_0 + \sum_j \ln z_{j+} - \ln x). \tag{8}$$

After this, the flavour combination in all splittings is done according to simplified splitting functions.

In the second part, the exact kinematics of each splitting is performed, generating the azimuth angle in each splitting according to a flat distribution and taking into account quark masses and ensuring that the condition in eq. (2) is satisfied. Then it is checked that all virtualities and transverse momenta are above the cutoff and a number of corrections are calculated to obtain a running α_s, correct splitting functions, the relevant Sudakov form factors and a correct matching to the full $\mathcal{O}(\alpha\alpha_s)$ matrix elements.

The produced chain has now a weight, which normally is below one, and a veto algorithm is used to obtain unweighted events. Sometimes, however, the weight may be above one, and in that case the chain is saved and may be reused the next time an event with the same flavour is requested in the same x and Q^2 bin. Alternatively the weights can be rescaled with a common factor to avoid such situations. Finally, the partons along the chain is colour connected and limits for the subsequent FSB is determined and passed together with the chain back to the calling Fortran routine in ARIADNE.

The whole procedure for generating a complete event is then as follows:

- Generate x, Q^2 and the flavour of the struck quark using the electroweak matrix element and evolved structure functions in the LEPTO [9] program. The LDC distribution contains a replacement for the PYSTFU routine of PYTHIA [10] which is called from LEPTO to enable the usage of structure functions evolved with the LDC model.
- This information is passed to the ARIADNE [11] program which internally calls the LDCMC code to generate the the initial-state chains.
- ARIADNE then performs the final-state dipole cascade and optionally calls JETSET [10] to perform the subsequent hadronization.

There are a number of different options and parameters influencing the generation which are accessible to the user via Fortran common blocks. Most of these are in the `LDCDAT` common block defined as follows:

```
COMMON /LDCDAT/ MSTLDC(100),PARLDC(100)
```

`MSTLDC(1)` (Default = -1) Maximum number of flavours used in the generation. If negative, the corresponding ARIADNE number from `MSTA(15)` in common block `ARDAT1` is used.

`MSTLDC(2)` (D = -1) If positive, use running $\alpha_s(k_\perp^2) = \frac{\pi}{3}\bar{\alpha}/\log(k_\perp^2/\Lambda_{\text{QCD}}^2)$ otherwise use constant $\alpha_s = \frac{\pi}{3}\bar{\alpha}$. $\bar{\alpha}$ and Λ_{QCD} are given by `PARLDC(1)` and `PARLDC(3)` below. If negative, the corresponding ARIADNE switch `MSTA(12)` in common block `ARDAT1` is used.

`MSTLDC(3)` (D = 1) If positive, use full $\mathcal{O}(\alpha\alpha_s)$ matrix elements from [12] for the splitting closest to the virtual photon.

MSTLDC(4) (D = 0) If positive, only allow chains with monotonically increasing virtualities from the proton side.

MSTLDC(5) (D = 0) If positive, only allow chains with monotonically increasing virtualities from the proton side, except the link closest to the virtual photon may have a virtuality larger than Q^2.

MSTLDC(6) (D = 0) If positive, do not allow any links with virtuality above Q^2.

MSTLDC(7) (D = 5) Number of bins per unit in $\log^{10}(x)$.

MSTLDC(8) (D = 5) Number of bins per unit in $\log^{10}(Q^2)$.

MSTLDC(9) (D = 1) If zero, do not allow $q \to q$ or $g \to q$ splittings (except $g \to q$ closest to the photon) in the initial chain.

MSTLDC(11) (D = 0) If positive, allow some links with virtuality below cutoff, as long as both neighbouring links are above.

MSTLDC(12) (D = 1) Choice of Sudakov form factor. If zero, no form factor is used. If non-zero, use a form factor of the form

$$\ln S = -\int_0^{z_{\rm cut}} dz \int \frac{dq_\perp^2}{q_\perp^2}\frac{\alpha_s(q_\perp^2)}{2\pi}P_{g\to q}(z) \tag{9}$$

for quarks and

$$\ln S = -\int_{0.5}^{z_{\rm cut}} dz \int \frac{dq_\perp^2}{q_\perp^2}\frac{\alpha_s(q_\perp^2)}{2\pi}P_{g\to g}(z) - \int_0^1 dz \int \frac{dq_\perp^2}{q_\perp^2}\frac{\alpha_s(q_\perp^2)}{2\pi}P_{g\to q}(z) \tag{10}$$

for gluons. If negative, the lower limit in the $q_\perp^2$ integration is just the virtuality of the parton, while if MSTLDC(12) is positive, this virtuality is multiplied by a factor exp(0.4) to approximate the phase space constraint in eq. (2). In both cases the upper limit is given by the highest virtuality in an emission step.

MSTLDC(13) (D = 0) If positive, do not allow gluon emission with $z > 0.5$ if the virtuality is increasing also in next step, even if PARLDC(8) is larger than 0.5.

PARLDC(1) (D = -1.0) $\bar{\alpha}$. If negative, the value used is 36/23.

PARLDC(2) (D = -1.0) Cutoff in $k_\perp^2$. If negative, the value is taken from the corresponding ARIADNE parameter (PARA(3) in ARDAT1).

PARLDC(3) (D = -1.0) $\Lambda_{\rm QCD}$. If negative, the corresponding ARIADNE number from PARA(1) in common block ARDAT1 is used.

`PARLDC(4)` (D $= 1.0$) The factor dividing the generated weights to ensure that all weights are below one (to allow for unweighted events).

`PARLDC(6)` (D $= 0.2$) Effective $\bar{\alpha}$ used in the leading-log part of the generation for speed considerations. The actual $\bar{\alpha}$ used is the one in `PARLDC(1)`.

`PARLDC(8)` (D $= 0.5$) The upper cut in z used in the $q \to q$ and $g \to g$ splitting functions to avoid divergences as $z \to 1$.

The following switches in the ARIADNE common block `ARDAT1` are relevant also for the LDCMC:

`MSTA(12)` (D $= 1$) If positive, use running α_s. Cf. `MSTLDC(2)`.

`MSTA(15)` (D $= 1$) Maximum number of flavours used in the generation. Cf. `MSTLDC(1)`.

`MSTA(32)` (D $= 2$) Handling of DIS events in ARIADNE when run with LEPTO. If set to -32, LDCMC is used.

`PARA(1)` (D $= 0.22$ GeV) The Λ_{QCD} used in the running of α_s. Cf. `PARLDC(3)`.

`PARA(3)` (D $= 0.6$ GeV) The cutoff in $k_\perp$. Cf. `PARLDC(2)`.

4 Sample Program

The main part of the LDCMC is written in C++ and therefore special care has to be taken when installing the program to ensure that the interface between the C++ and Fortran code is working properly. In the distribution there are detailed instructions on how to install the program in the `README` file and here we will only discuss the main points.

The C++ code relies heavily on the *Standard Template Library* so the installation requires a C++ compiler which supports this. The C++/Fortran interface assumes that the Fortran compiler appends an underscore to all external symbols and converts them to lower-case characters, ie. a Fortran subroutine declared as `SUBROUTINE HERA` will be declared as `void hera_()` in the C++ code. The file `f77hack.h` contains *typedefs* for `Fint`, `Fdouble` and `Ffloat` and the user must ensure that these types corresponds to the Fortran equivalents `INTEGER`, `DOUBLE PRECISION` and `REAL` respectively.

The distribution includes a sample program to check that the installation was successful, and to serve as a template for user customized runs. It consists of a C++ main program which must be linked together with the Fortran steering routines and the LDCMC, LEPTO, PYTHIA, ARIADNE and JETSET libraries (in that order) as well as with the Fortran runtime libraries.

The C++ main program looks like this:

```
#include <fstream.h>
#include "EvolvedDensities.h"

// Declare the F77 subroutine as extern.
extern "C" {
  void hera_();
}

int main() {

  // First read in structure function parametrization from file.
  ifstream evolved("xf-LDC-97.A");
  EvolvedDensities::readInputFrom(evolved);
  EvolvedDensities::readFrom(evolved);
  evolved.close();

  // Call F77 subroutine.
  hera_();

  // Done.
  return 0;
}
```

and the corresponding Fortran steering routines looks like this:

```
      SUBROUTINE HERA

C...Initialize parameters in Ariadne and Jetset
      CALL ARTUNE('4.08')

C...Call a user supplied routine setting
C...the parameters and switches in LEPTO
      CALL LEPSET

C...Call a user supplied routine setting
C...the parameters and switches in Ariadne
      CALL ARISET

C...Initialize Ariadne to run with LEPTO
      CALL ARINIT('LEPTO')

C...Initialize LEPTO for HERA
      CALL LINIT(0,11,-26.5,820.0,4)

C...Loop over a number of events
      DO 100 IEVE=1,10

C...Call generate an event with LEPTO
        CALL LEPTO

C...Apply the Dipole Cascade
        CALL AREXEC

C...Call a user supplied analysis routine
        CALL HERANA

 100  CONTINUE

      END

      SUBROUTINE LEPSET

      COMMON /LEPTOU/ CUT(14),LST(40),PARL(30),X,Y,W2,XQ2,U
```

```
      SAVE /LEPTOU/
      COMMON /PYPARS/ MSTP(200),PARP(200),MSTI(200),PARI(200)
      SAVE /PYPARS/

C...Use structure functions from Pythia
      LST(15)=0

C...Or rather use the LDC version of pystfu giving the structure
C...functions evolved with LDC as read from the file in the C++
C...main program (Make a dummy call to pystfu to ensure correct
C...version of pystfu is linked.)
      IF (MSTP(51).EQ.940801) CALL PYSTFU
      MSTP(51)=0

C...Switch off hadronization
      LST(7)=0

C...Suppress printouts from LEPTO
      LST(3)=0

C...Set x, Q2 and W2 ranges in Lepto
      CUT(1) = 0.00008
      CUT(2) = 0.5
      CUT(5) = 5.0
      CUT(6) = 1280.0
      CUT(7) = 1000.0

      RETURN
      END

      SUBROUTINE ARISET

      COMMON /ARDAT1/ PARA(40),MSTA(40)
      SAVE /ARDAT1/
      COMMON /ARHIDE/ PHAR(400),MHAR(400)
      SAVE /ARHIDE/
      COMMON /LDCDAT/ MSTLDC(100),PARLDC(100)

C...Master switch for using LDC in Ariadne
      MSTA(32)=-32

C...Some parameters in LDCMC
      PARLDC(4)=1.0
      PARLDC(6)=0.2


      RETURN
      END

      SUBROUTINE HERANA

C...Trivial analysis - print the event
      CALL LULIST(1)

      RETURN
      END
```

If the installation was successful, running this program should print ten reasonable HERA events on the parton level (rather than producing a core dump).

The distribution also contains a selection of sample parton density function files containing input parton density parametrizations and tabulated densities evolved with the LDC model. The files are named `xf-LDC-97.A` to `xf-LDC-97.H`, where the last letter indicates the strategy used in the fitting in [5]:

A LDC default.

B DGLAP: As for A but only allow chains with monotonically increasing virtualities of the links from the proton side. `MSTLDC(4)=1`.

C DGLAP': As for B, but chains where the virtuality of the link closest to the virtual photon is larger than Q^2 are permitted. `MSTLDC(4)=0`, `MSTLDC(5)=1`.

D As for A but $k_{\perp 0} = 1$ GeV. `PARLDC(2)=1`.

E As for A but without the Sudakov form factors. Instead $P_{q\to q}(z)$ is set to zero and $P_{g\to q}(z)$ nonzero only in the splitting closest to the photon. `MSTLDC(9)=0`, `MSTLDC(12)=0`.

F As for A but $\beta_g = \beta_S = 5$ in the input density parametrization.

G As for A but only fitted to F_2 data with $x < 0.1$.

H As for A but allow the virtuality of some links to be below $k_{\perp 0}$ as long as the largest virtuality of two consecutive links always is above $k_{\perp 0}$. `MSTLDC(11)=1`.

The LDCMC program is available as a part of the ARIADNE program from the ARIADNE web pages `http://www.nordita.dk/~leif/ariadne/`.

References

[1] V.N. Gribov, L.N. Lipatov, *Sov. J. Nucl. Phys.* **15** (1972) 438 and 675;
G. Altarelli, G. Parisi, *Nucl. Phys.* **B126** (1977) 298;
Yu.L. Dokshitzer, *Sov. Phys. JETP* **46** (1977) 641.

[2] E.A. Kuraev, L.N. Lipatov and V.S. Fadin, *Zh. Eksp. Teor. Fiz.* **72** (1977) 373, *Sov. Phys. JETP* **45** (1977) 199;
Ya.Ya. Balitsky and L.N. Lipatov, *Yad. Fiz.* **28** (1978) 1597, *Sov. J. Nucl. Phys.* **28** (1978) 822.

[3] M. Ciafaloni, *Nucl. Phys.* **B269** (1988) 49;
S. Catani, F. Fiorani, G. Machesini, *Phys. Lett.* **B234** (1990) 339, *Nucl. Phys.* **B336** (1990) 18.

[4] B. Andersson, G. Gustafson, J. Samuelsson, *Nucl. Phys.* **B463** (1996) 217.

[5] H. Kharraziha, L. Lönnblad, LU-TP 97-21, NORDITA-97/54 P, hep-ph/9709424.
[6] B. Andersson et al., *Z. Phys.* **C71** (1996) 613.
[7] B. Andersson, G. Gustafson and H. Kharraziha, LU-TP 97-29, aps1997nov19_001, hep-ph/9711403.
[8] G. Gustafson, *Phys. Lett.* **B175** (1986) 453;
G. Gustafson, U. Petterson, *Nucl. Phys.* **B306** (1988) 746;
B. Andersson, G. Gustafson, L. Lönnblad, *Nucl. Phys.* **B339** (1990) 393.
[9] G. Ingelman, A. Edin and J. Rathsman, *Comput. Phys. Comm.* **101** (1997) 108, hep-ph/9605286.
[10] T. Sjöstrand, *Comput. Phys. Comm.* **82** (1994) 74
[11] L. Lönnblad, *Comput. Phys. Comm.* **71** (1992) 15.
[12] R.D. Peccei, R. Rückl, *Nucl. Phys.* **B162** (1980) 125.

Paper V

LU TP 96-8
February 1996
Revised in September 1996

Colour: A Computer Program for QCD Colour Factor Calculations

Jari Häkkinen, Hamid Kharraziha*
Department of Theoretical Physics, Lund University,
Sölvegatan 14A, SE-223 62 Lund, Sweden

Computer Physics Communications **100**, 311-321 (1997)

Abstract:
A computer program for evaluating colour factors of QCD Feynman diagrams is presented, and illustrative examples on how to use the program to calculate non trivial colour factors are given. The program and the discussion in this paper is based on a diagrammatic approach to colour factors.

*jari@thep.lu.se, hamid@thep.lu.se

Program Summary

Title of program: colour

Program obtainable from: http://www.thep.lu.se/tf2/hep
or ftp:thep.lu.se/pub/LundPrograms/Misc/colour.tar.Z

Computer for which program is designed: Computers with an ANSI C compiler.

Program language used: C

Peripherals used: terminal and mass storage for input, terminal for output

Number of lines in combined program: ≈1000

Keywords: Feynman diagrams, QCD colour factors

Nature of the physical problem: In many QCD Feynman diagrams there is a need to calculate the colour factor. This program calculates colour factors fast and accurately.

Method of solution: QCD Feynman diagrams, with no four-gluon vertices, factorize into a colour (group) factor and a kinematical factor. The colour part of any closed QCD Feynman diagram can be transformed into a sum of diagrams including only closed quark (colour) lines. In each such term, the number of quark (colour) loops is counted, giving factors of 3 (or N_c). The sum of these terms is then the desired colour factor.
To perform the translation, we need to have rules to interpret gluons and vertices into quark lines. There is in principle only need for three equalities to be able to calculate any closed QCD diagram (not containing four gluon vertices). To achieve good computing performance further equalities have been introduced. The most essential ones are listed in Appendix A.

Restriction of complexity of the problem: Four gluon vertices cannot be included directly in diagrams to be calculated. The number of gluons in diagrams to be calculated are limited to 200, but can easily be changed prior to compiling.

Typical running time: For typical diagrams, fractions of a second. Complicated diagrams - a few seconds to hours.

1 Introduction

There are several programs available to perform momentum Feynman diagram calculations, either symbolically or numerically [1]. Some of these perform QCD calculations with the QCD colour factors inlcuded, but the calculation of colour factors is not in focus. In this paper we present a program, *colour*, which is more suitable and efficient for studying problems where the colour properties are of main interest. *colour* uses the rules and equalities derived in [2, 3] for calculating the colour factors of QCD diagrams. A similar approach [4] has been implemented in the REDUCE computer algebra system [5]. Our program, which is written in C, has the advantage that it does not require a third party vendor computer algebra system. Furthermore, it is easy to use, and with some modifications the program can be used as a function to be called from a user defined main program.

We also give an introduction on how to use the program and what results can be obtained. Using a set of projection operators non trivial results can be achieved, such as how the interaction probability between two gluons depend on their common colour state. Only closed Feynman diagrams (vacuum QCD diagrams, i.e. diagrams with no external legs) can be calculated, but this is not a real problem since this restriction can be easily circumvented as will be shown. We also present a short introduction to the group theory part of the calculations.

2 Theory in brief

The program presented here is based on the results in [2] and [3]. These results has been further developed and explained to us by Yuri Dokshitzer and Bo Söderberg [6]. In this section and the appendices we give a brief presentation of the main results.

The existence of colour factors in QCD originates from the invariance of the Lagrangian under colour transformations. For a certain interaction, with incoming and outgoing particles, intermediate propagators and different kinds of vertices, one has to sum over all possible colours, if they are not explicitly specified. Since the kinematical factor in the interaction probability is equal for all these diagrams (excluding diagrams containing four-gluon vertices), we therefore have a multiplicative factor to the probability, which we get by counting the colours.

Two preliminary remarks. When we discuss colours and anti-colours we often use quarks and anti-quarks, respectively, to describe the colour flow. In most expressions we keep N_c as a free variable in order to be general. Whenever the number of colours is specified, $N_c = 3$ has been used.

Every $3^m \otimes \bar{3}^n$ space can be divided into a set of irreducible subspaces.

In the simplest example of a quark and an anti-quark system, the irreducible representation is the singlet and the octet state, i.e. $3 \otimes \bar{3} = 1 \oplus 8$, where the octet state corresponds to the gluons. The equation

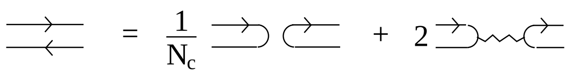

(1)

states this fact in equation form. (The factor of 2 in the second term is due to the Gell-Mann normalization of gluons, see discussion in Appendix B. We have adopted Gell-Mann normalization in all calculations in this paper.) In the LHS of Eq (1) a colour and an anti-colour state, $3 \otimes \bar{3}$, are divided into irreducible singlet and octet states on the RHS. The degeneracy (multiplicity) of a state is given by taking the trace of the representation of the state. Calculating the trace in this diagrammatic representation corresponds to connecting the incoming legs and the outgoing colour flow. For the LHS we find

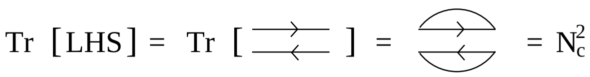

as expected, and for the RHS

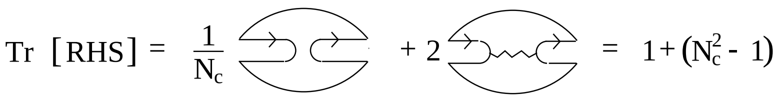

Another observation is that the two diagrams, P_1 and P_2, in the RHS of Eq (1) are disjoint projection operators since the terms satisfy $P_i^2 = P_i$ and $P_i P_j = 0, P_j P_i = 0$. These can be used to split any quark–anti-quark diagram into an irreducible representation

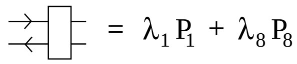

The projection operators can be used to ask specific questions about the colour states particles are in, e.g. what is the probability to find two free gluons in an anti-symmetric octet state. This is easily solved by calculating colour states. The two gluons are in a $8 \otimes 8$ state with degeneracy 64, and the irreducible representation of the $8 \otimes 8$ space contains an anti-symmetric octet (with degeneracy 8), i.e. the answer is 8/64 since the probability is equal for all states. In the next section we will give a few other examples on these issues and describe how to perform the calculations using the program.

Given a problem concerning colour states, the problem of finding solutions boils down to finding the projection operators for reduced representations. Once this is done all interesting numbers can be calculated using the program.

In Appendix B we have listed the (irreducible representation) projection operators for a few states.

The triple gluon coupling is anti-symmetric in colour. We have generalized the program to include also a symmetric coupling between three colour octets ("gluons").

3 Using the program

A straight forward use of the program is to calculate QCD vacuum diagrams. This might not be too exciting. Using projection operators more interesting results can be obtained. A few illustrative examples will be given below.

The program interacts with the user through input files. The diagram to be calculated is defined in one input file which is read by the program, the diagram is calculated and the result is written on the screen. No interaction with the user is needed after the program has been started.

The command line syntax to start the program is:

colour [-df file | -h | -help]

where

-df Changes the input file name. The default name is *colour.in*.

-h or **-help** Prints a small description of the program and a list of valid options.

There are few rules for defining a qcd diagram in the input file.

- Every gluon line is assigned a unique number.
- Triple anti-symmetric gluon vertices are represented by a letter f followed by the three incoming gluon numbers.
- Symmetric triple vertices[†] are represented in the same way as the anti-symmetric vertices but with the letter d.
- Quark loops are represented by a letter t, followed by all gluons connected to the quark loop.
- Four-gluon vertices cannot be directly included in the program since the colour and the kinematical parts of the cross section do not factorize. This can, however, be taken care of by separating the four-gluon vertex in factorizable terms, as discussed further in Appendix A.
- Ghosts can also be included since these couple to gluons with the same colour factor as gluons themselves. Thus ghost vertices can be represented with a letter f.

[†]As mentioned above these are not physical QCD gluon vertices, but are included for generality. The vertex is also used in projection operators.

- For the quark loops and the anti-symmetric gluon vertex the order of the gluons are important since $f_{abc} = -f_{bac}$. So when translating a diagram into a file all loops and f vertices must be written down in the same order (clockwise or anti-clockwise).
- Composite objects, d, f, and t, must be separated with a newline character, while gluon numbers are separated with a space. All other separation characters are invalid and will stop the execution of the program.

For example, the diagram

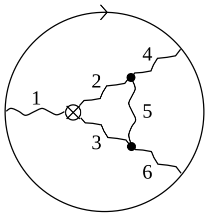

would transform to a file like

```
d 1 2 3
f 2 4 5
f 3 5 6
t 1 4 6
```

The numbers assigned to every gluon are arbitrary and occur twice in the file since every gluon is connected to two vertices in the diagram. If you run this file, the answer will be: $\frac{1}{2^3}(N_c^4 - 5N_c^2 + 4)$ and is equal to 5 using $N_c = 3$.

3.1 Example 1: Colour factor for gluon emission from quarks

Let us start with the problem of calculating the colour factor, often denoted $\mathrm{C_F}$, for emission of a gluon from a quark line. This can be easily done by hand, but it is a nice example to demonstrate how the program can be used.

We will study a transition matrix T, defined in Fig 1. A colour singlet comes in, a quark–anti-quark pair is created and a gluon is emitted from one of the quark legs. We have chosen to use a singlet state since the program can only handle closed diagrams‡. By definition, $\mathrm{C_F}$ is a multiplicative factor to the transition probability, due to the emission of a gluon from the quark leg. For the transition probability, we have to square the matrix by multiplying it with its conjugate (reversing the colour flow and using the mirror image). The

‡There are obviously other diagrams which would enable us to calculate C_F, but these involve obscuring technicalities.

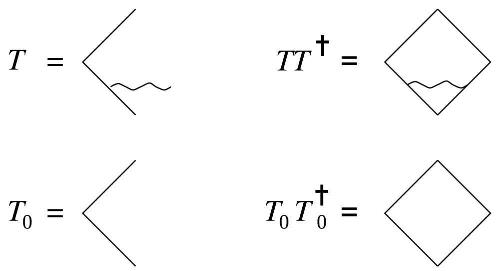

Figure 1: *Diagrams used to calculate C_F.*

result then must be normalized by dividing by the squared amplitude of just creating the quark–anti-quark pair.

Consequently, to obtain C_F we have to run the program twice, one time with the diagram $TT^\dagger$ and once with the diagram $T_0T_0^\dagger$.

In order to use the program we have to translate the diagrams into an input file. This can be done as

Diagram	Input file	Result
$TT^\dagger$	t 1 1	$\frac{1}{2}\left[N_c^2-1\right]$
$T_0T_0^\dagger$	t	N_c

Thus, we get that

$$C_F = \frac{N_c^2-1}{2N_c} = \frac{4}{3}.$$

3.2 Example 2: Partitioning into irreducible representations

Any diagram in the $8 \otimes 8$ space can be written as a sum of the projection operators described in Appendix B (and crossing operators which are built from operators of the same multiplicity). Consider e.g. the gluon-gluon scattering matrix T in Fig 2. This matrix can be written as a sum of projection operators solely, that is without any crossing operators,

$$T = \sum \lambda_i P_i.$$

The eigenvalues can easily be found. To be concrete we will determine λ_1 corresponding to the singlet state, and the other eigenvalues are derived in the same way. To calculate this, we apply the operator to the matrix T, thus projecting out the singlet part of the diagram. Then we take the trace of PT

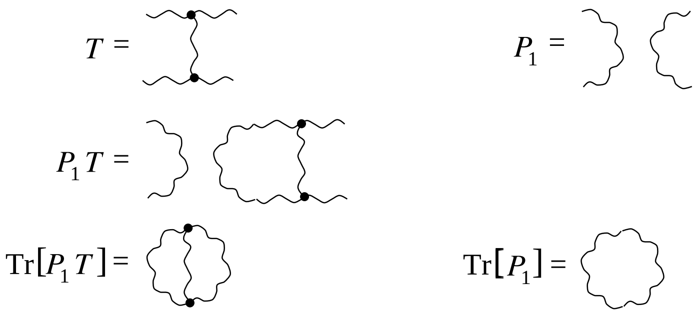

Figure 2: *Diagrams used to calculate the singlet eigenvalue, λ_1, for the state T.*

and divide the result with the trace of just the operator,

$$TP_1 = \lambda_1 P_1, \qquad \lambda_1 = \frac{\mathrm{Tr}(P_1 T)}{\mathrm{Tr}(P_1)}.$$

The translation into a file looks like

Diagram	Input file	Result
$\mathrm{Tr}(P_1 T)$	f 1 2 3	
	f 1 3 2	$N_c \left[N_c^2 - 1\right]$
$\mathrm{Tr}(P_1)$	See Sec 3.4	$N_c^2 - 1$

Running the program we find that $\lambda_1 = N_c$.[§]

3.3 Example 3: Probability of an octet state

The question here is: If we have a transition matrix of some kind containing two gluons, what is the probability that the two gluons are in any of the colour states described in Fig 6 in Appendix B. Take for example the transition matrix T in Fig 3. If two incoming gluons are interacting in this way, what is the conditional probability that they were in an anti-symmetric octet state P_{8a}?

To solve this problem, the first step is to square the matrix, thus getting the symmetric matrix $TT^\dagger$ which correspond to the probability. Then the antisymmetric octet part of the amplitude is projected out, by applying the operator. The probability is given by the multiplicity of the projected part,

[§]Note that the eigenvalues depend on the normalization of the gluon, see Appendix B.

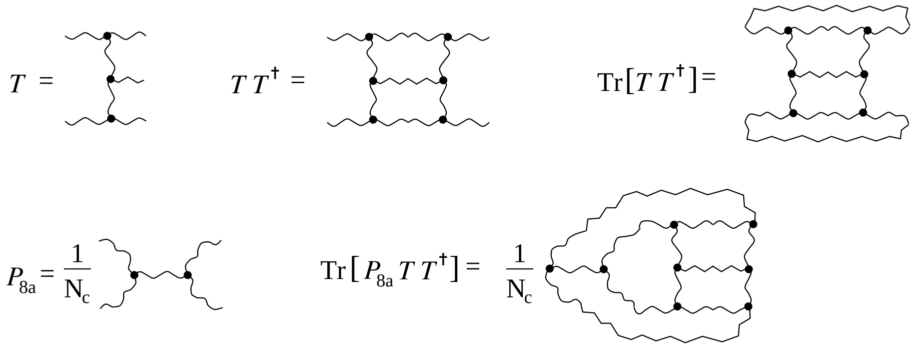

Figure 3: *Diagrams used in Example 3.3.*

divided by the total multiplicity of the amplitude,

$$Prob(P_{8a}|T) = \frac{Tr(P_{8a}TT^\dagger)}{Tr(TT^\dagger)}.$$

For this we have to run the program twice, once with the diagram $Tr(TT^\dagger)$ and once with the diagram $Tr(P_{8a}TT^\dagger)$.

The translation into a file looks like

Diagram	Input file	Result
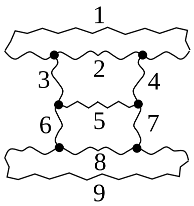	f 1 4 2 f 4 7 5 f 7 9 8 f 6 8 9 f 3 5 6 f 1 2 3	$N_c^3\left[N_c^2-1\right]$
$N_c\,\mathrm{Tr}(P_{8a}TT^\dagger)$	f 1 4 2 f 4 7 5 f 7 9 8 f 6 8 12 f 3 5 6 f 11 2 3 f 1 10 9 f 10 11 12	$\frac{1}{8}\left[N_c^6+11N_c^4-12N_c^2\right]$

Putting it all together gives a probability of 7/24 (with $N_c = 3$) to find the two incoming gluons in an anti-symmetric octet state before the transition.

3.4 Limitations

There are some limits in the program. First, the physics limitations. Four-gluon vertices are not included and therefore diagrams containing these vertices cannot be calculated directly. The four-gluon vertex must be replaced with three other diagrams, which have to be calculated separately (see Appendix A). There is also one specific diagram that the program cannot evaluate, a gluon ring, but the colour factor for this diagram is simply the number of different gluons, $N_c^2 - 1$. This is purely technical and the diagram could in principle be implemented into the program as a special case, but the gain is not worth the effort.
Secondly, local implementation limits. There is a limit on the number of gluons which can be included in the program. This is set to 200 but can easily be changed by the user before compiling. There is also a limit to which power in N_c calculations can be done, the default range is N_c^{-100} – N_c^{99}, this can also easily be changed prior to compiling the program. A warning message will appear if over- or underflow occurs.

4 Acknowledgments

We would like to thank Yuri Dokshitzer and Bo Söderberg for introducing us into the world of colour factors.

References

[1] H. Strubbe, *Comp. Phys. Comm.* **8** 1 (1974)
J. Kühlbeck, M. Böhm, A. Denner, *Comp. Phys. Comm.* **60** 165 (1990)
R. Mertig, M. Böhm, A. Denner, *Comp. Phys. Comm.* **64** 345 (1991)
E.E.Boos *et al.*, CompHEP, preprint HEP-PH/9503280, SNUTP 94-116, INP MSU-94-36/358

[2] Yu.L. Dokshitzer, S.I. Manaenkov, Quantum Chromodynamics for Beginners. Color Algebra, Leningrad Nuclear Physics Inst. Preprint 1103, Leningrad, September 1985

[3] P. Cvitanović, Group Theory, Nordita Classics Illustrated, 1984

[4] A.P. Kryukov, A.Ya. Rodionov, *Comp. Phys. Comm.* **48** 327 (1988)

[5] A.C. Hearn, REDUCE User's Manual, Version 3.6, RAND Publication CP 78, July 1995

[6] Yu.L. Dokshitzer, Introduction to Colour Dynamics, Seminars based on [2], given at Department of Theoretical Physics, Lund University, Spring 1992.
B. Söderberg, Private communications

A Colour Rules

The set of rules in Fig 4, taken from [2], are implemented in the program with the exception of the gluon loop C1b. The equation numbers are the ones to be found in [2], and as indicated we do not list all of them. We note that in principle it is enough to use equations C11 and C19 to translate any diagram without four-gluon vertices to diagrams containing only quark loops. The other equalities are implemented in order to increase the computing performance.

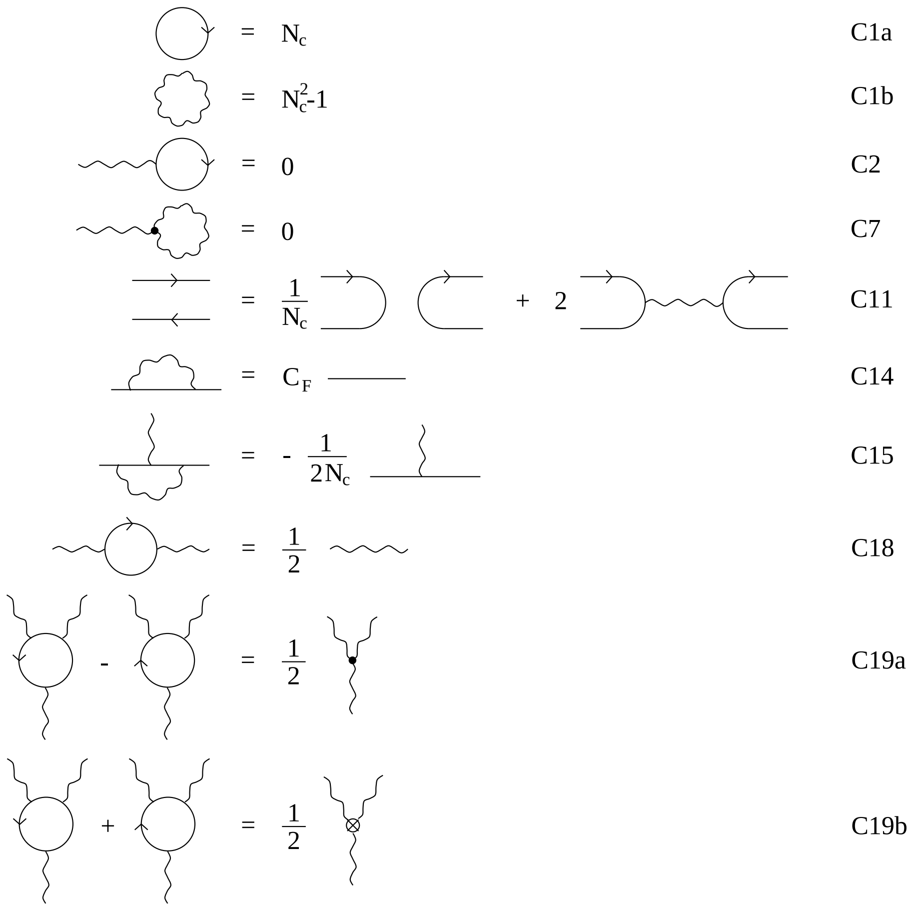

Figure 4: *Rules for diagram manipulations.*

The four-gluon vertex has not been included in the program since QCD diagrams containing four-gluon vertices do not factorize into a colour (group theoretical) part and a kinematical part. The four-gluon vertex,

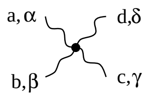

has the form

$$f_{abn}f_{ncd}[g^{\alpha\gamma}g^{\beta\delta}-g^{\alpha\delta}g^{\beta\gamma}]+f_{and}f_{bcn}[g^{\alpha\gamma}g^{\beta\delta}-g^{\alpha\beta}g^{\gamma\delta}]+f_{anc}f_{bdn}[g^{\alpha\delta}g^{\beta\gamma}-g^{\alpha\beta}g^{\gamma\delta}].$$

Thus a diagram with such a vertex can be split into three pieces, each of which has a factorized form (this separation is not unique). Each piece has a colour factor corresponding to a diagram where the four-gluon vertex is replaced by two three-gluon vertices, as symbolically shown in Fig 5.

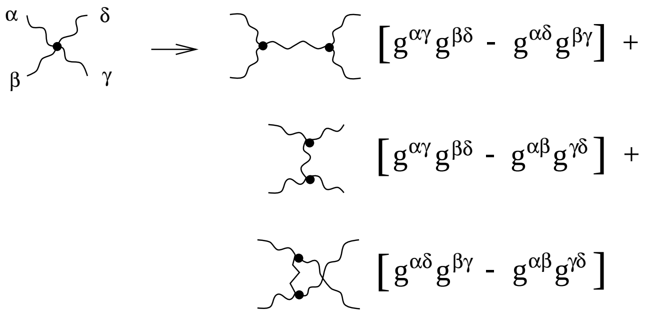

Figure 5: *Symbolic representation of the colour factors in a four-gluon vertex.*

B Projection Operators

In Figs 6–9 we present the set of projection operators needed to obtain irreducible representations of the $8\otimes 8$, $3\otimes\bar{3}$, $3\otimes 3$, and $3\otimes 3\otimes 3$ spaces, respectively. For the derivation of these operators we refer to Cvitanović [3].

There are different normalizations adopted for gluons and the coupling constant α_s. A difference in the overall normalization of the projection operators is not a problem as long as it is used consistently. The overall normalization is factorized out in most cases, as in the Examples 3.2 and 3.3. In Example 3.1 we have adopted the Gell-Mann (conventional) normalization of the gluons.

The difference in normalization, lies in how we interpret the curly lines, representing the gluons, and also in the interpretation of the triple vertices. With the Gell-Mann normalization, the gluon is interpreted as the octet projection in the $3\otimes\bar{3}$ space together with a factor $1/2$ (compare Eq C11 of Appendix A).

This factor originates from the conventional QCD normalization of the generators of the SU(3) group, i.e.

$$t^a = \frac{1}{2}\lambda^a. \tag{2}$$

A more convenient way to normalize the gluon is to let the factor of $\frac{1}{2}$ in Eq 2 go into α_s, i.e. to let the gluon represent just the octet projection, without any factors. In the same spirit, the triple gluon vertices (symmetric and anti-symmetric) can be defined without any factors.

The program output comes with both normalizations. The answer which is expressed as a polynomial in N_c, is normalized with the second convention. If you use the polynomial ignoring the overall factor (and the numerical answer), you should replace the factors within parenthesis, in the operators in Figures 6 and 7, by a factor 1. If you prefer to use the Gell-Mann normalization, you must make use of the factors within parenthesis.

The projection operator, P_0, has the multiplicity 0 when the number of colours is 3. This subspace exists e.g. in SU(2) where it has multiplicity 3 and corresponds to a real state.

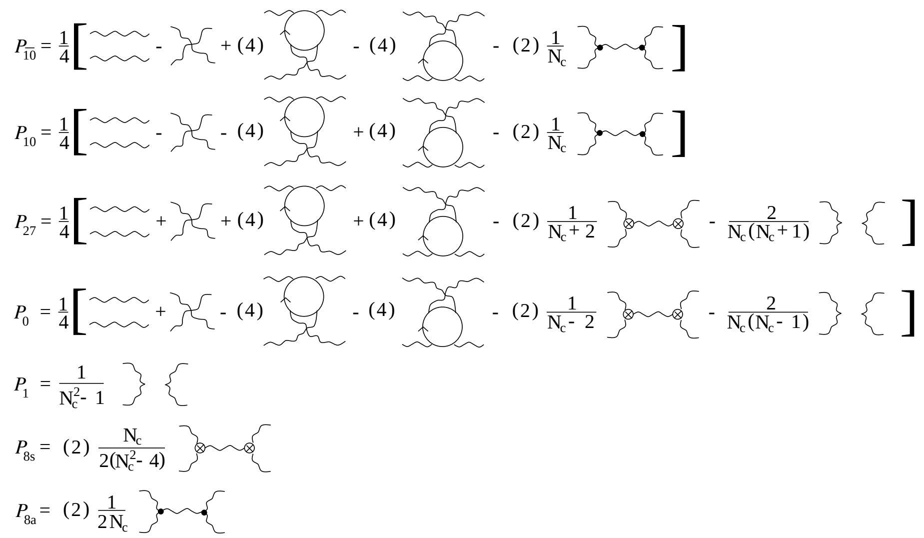

Figure 6: *Projection operators needed to obtain the irreducible representations of the* $8 \otimes 8 = 0 \oplus 1 \oplus 8_a \oplus 8_s \oplus 10 \oplus \overline{10} \oplus 27$ *space.*

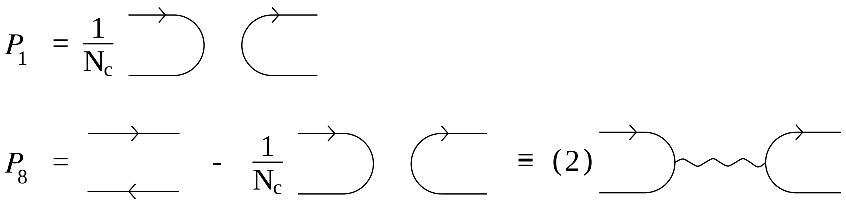

Figure 7: *Projection operators needed to obtain the irreducible representations of the* $3 \otimes \bar{3} = 1 \oplus 8$ *space.*

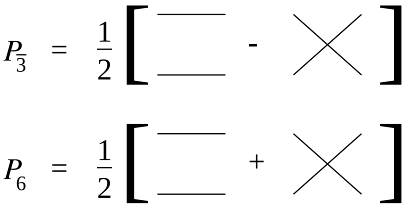

Figure 8: *Projection operators needed to obtain the irreducible representations of the* $3 \otimes 3 = \bar{3} \oplus 6$ *space.*

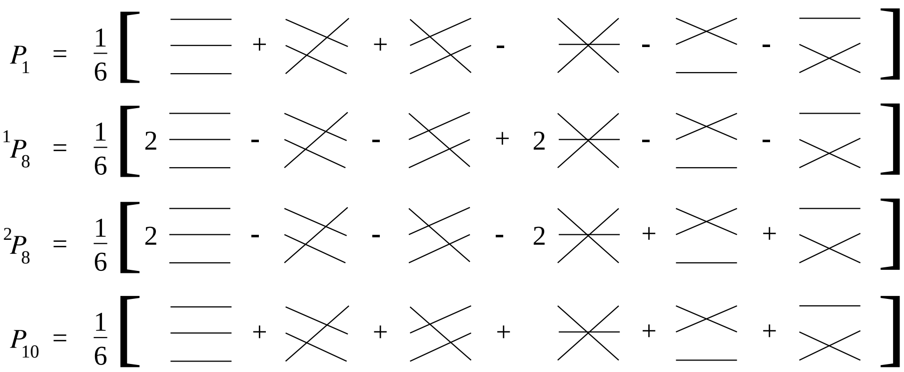

Figure 9: *Projection operators needed to obtain the irreducible representations of the* $3 \otimes 3 \otimes 3 = 1 \oplus 8 \oplus 8 \oplus 10$ *space.*